

JAERI - M  
87-131

PROGRESS REPORT ON SAFETY RESEARCH  
OF HIGH-LEVEL WASTE MANAGEMENT FOR  
THE PERIOD APRIL 1986 TO MARCH 1987

August 1987

(Eds.) Haruto NAKAMURA and Shingo TASHIRO

JAERI-Mレポートは、日本原子力研究所が不定期に公刊している研究報告書です。  
入手の間合わせは、日本原子力研究所技術情報部情報資料課（〒319-11茨城県那珂郡東海村）  
あて、お申しこしください。なお、このほかに財団法人原子力弘済会資料センター（〒319-11茨城  
県那珂郡東海村日本原子力研究所内）で複写による実費頒布をおこなっております。

JAERI-M reports are issued irregularly.

Inquiries about availability of the reports should be addressed to Information Division, Department  
of Technical Information, Japan Atomic Energy Research Institute, Tokai-mura, Naka-gun,  
Ibaraki-ken 319-11, Japan.

© Japan Atomic Energy Research Institute, 1987

---

編集兼発行	日本原子力研究所
印刷	日立高速印刷株式会社

Progress Report on Safety Research of High-Level Waste  
Management for the Period April 1986 to March 1987

(Eds.) Haruto NAKAMURA and Shingo TASHIRO  
Department of Environmental Safety Research  
Tokai Research Establishment  
Japan Atomic Energy Research Institute  
Tokai-mura, Naka-gun, Ibaraki-ken

(Received July 30, 1987)

Researches on high-level waste management at the High Level Waste Management Laboratory and the Waste Safety Testing Facility Operation Division of the Japan Atomic Energy Research Institute in the fiscal year of 1986 are reviewed in the report.

Topics in the three sections are as follows:

- 1) Non-radioactive research has been continued on Synroc irradiation and modellings of waste form leaching.
- 2) Research results are described in the section of Safety Evaluation for Geological Disposal on engineered barriers, field tests, safety assessment models, migration, natural analogue, seabed disposal and conceptual design of a repository.
- 3) Adsorption behaviour of plutonium on leach-containers and migration of leached cesium in a rock column are described in the section of Safety Examination of Vitrified Forms in the Hot Cells of WASTE-F.

Keywords: High-level Radioactive Waste, Waste Management, Safety Study, Glass Form, Geologic Disposal, Natural Analogue, Seabed Disposal, WASTE-F, Hot Examination, Synroc

高レベル廃棄物処理処分の安全性研究に関する昭和61年度報告書

日本原子力研究所東海研究所環境安全研究部

(編) 中村 治人・田村 晋吾

(1987 年 7 月 30 日 受理)

高レベル廃棄物処理処分研究室とWASTE F管理において昭和61年度に実施した高レベル廃棄物処理処分に関する研究を報告書にまとめた。

主要点は次の通り。

- 1) シンロック照射及び廃棄物固化体浸出のモデル化が継続された。
- 2) 地層処分の安全性評価では、人工バリア、フィールド試験、安全性評価モデル、移行、ナチュラルアナログ、海洋底処分及び処分場の概念設計が記載されている。
- 3) WASTE Fでのホットセルにおけるガラス固化体の安全性試験では、浸出容器へのプルトニウムの汚染挙動及び岩石カラム中での浸出セシウムの移行が記載されている。

## Contents

Introduction .....	1
1. Waste Forms Examination .....	2
1.1 The leaching model of nuclear waste glasses .....	2
1.2 Irradiation test of Synroc .....	10
1.3 Program for analysis of electron diffraction patterns .....	14
2. Safety Evaluation for Geological Disposal .....	16
2.1 Engineered barrier .....	16
(1) Buffer material test .....	16
(2) Stress corrosion cracking of austenitic stainless steel in a granite groundwater at elevated temperature under gamma-ray irradiation .....	22
(3) Slow strain rate stress-corrosion test under gamma-ray irradiation for container materials .....	25
2.2 Field test .....	30
(1) Buffer material test .....	30
(2) In-situ corrosion test .....	37
2.3 Nuclide migration experiment .....	40
(1) Diffusion of "non-sorbing" ions in rock pores .....	40
2.4 Natural analogue .....	44
(1) Red coloration of a granitic rock along fractures .....	44
2.5 Subseabed disposal .....	50
(1) Distribution of redox-sensitive elements in undisturbed and disturbed sea floor sediments at Antibes site, France taken during HOCUS project .....	50
2.6 Model for safety assessment .....	55
(1) Numerical model of radionuclide migration .....	55
(2) HYDROCOIN study .....	56
2.7 Conceptual design of repository for safety assessment in the preclosure period .....	59

3. Safety Examination of Vitrified Forms in the Hot Cells	
of WASTE	62
3.1 Preparedness for the actual waste treatment	63
3.2 Cold tests with MCC-4 type low flow-rate leaching test	
apparatus	66
3.3 In-cell Synroc solidification apparatus	69
3.4 Contamination and decontamination behaviour of volatilized	
cesium from glass onto container materials	75
3.5 Adsorption of plutonium and curium leached from waste	
glass on various materials for leach-container	79
3.6 Cs migration by column test	82

## 目 次

まえがき .....	1
1 廃棄物固化体の試験 .....	2
1.1 核廃棄物ガラス固化体の浸出モデル .....	2
1.2 SYNROCの照射試験 .....	10
1.3 電子回折パターン解析用プログラム .....	14
2 地層処分の安全評価 .....	16
2.1 工学バリア .....	16
(1) 緩衝材の試験 .....	16
(2) 花崗岩地下水における高温下, $\gamma$ 線照射下でのステンレス鋼の応力 腐食割れ .....	22
(3) 容器材の $\gamma$ 線照射下の低歪応力腐食割れ試験 .....	25
2.2 フィールド実験 .....	30
(1) 緩衝材の試験 .....	30
(2) 原位置腐食実験 .....	37
2.3 核種移行試験 .....	40
(1) 岩石空降中の“非吸着”イオンの拡散 .....	40
2.4 天然相似現象 .....	44
(1) フラクチャーに沿った花崗岩中の紅色化現象 .....	44
2.5 海洋底下処分 .....	50
(1) HOCUS計画で採取されたフランスアンチーブサイトの海底土中の酸 化還元に敏感な元素の分布 .....	50
2.6 安全評価モデル .....	55
(1) 核種移行の数値解モデル .....	55
(2) HYDROCOINでの比較研究 .....	56
2.7 処分場閉鎖前の安全評価の為の処分施設の概念設計 .....	59
3 WASTEFのホットセルでのガラス固化体の安全性試験 .....	62
3.1 実固化体取扱いの為の準備 .....	63
3.2 MCC-4型低流速浸出試験装置によるコールド試験 .....	66
3.3 インセルSYNROC固化体製作装置 .....	69
3.4 ガラスより容器材料に揮発付着したセシウムの汚染及び除染挙動 .....	75
3.5 廃棄物ガラスより浸出したプルトニウム, キュリウムの浸出試験容器 への吸着 .....	79
3.6 カラム試験によるセシウムの移行 .....	82

## Introduction

As the high-level radioactive waste management in Japan has become a realistic time schedule, needs have been raised for safety data of the related techniques to the management. The High Level Radioactive Waste Management Laboratory and the WASTEF (Waste Safety Testing Facility) Operation Division of the Japan Atomic Energy Research Institute have conducted studies on safety evaluation of the management technology and development of future techniques to meet the needs.

This report is divided into three sections; waste form examination, safety evaluation for geological disposal and safety examination of vitrified forms in the hot cells of WASTEF.

The waste form examination has continued to compile source term data for a long term safety assessment of the waste management.

The studies on the geological disposal contain labo-scale examination of buffer materials and host rocks, nuclide migration, natural analogue, etc.

In WASTEF hot experiments have been performed using radioactive sources on the performance and durability of materials to be used for the management to obtain radioactive data, especially of transuranic elements, precise data using radio tracers and demonstrative data using radiation source and actual waste.

The annual progress reports have been pressed in the following numbers; JAERI-M 82-145, 83-076, 84-133, 85-090 and 86-131.



## 1. Waste Forms Examination

T. Banba

Examinations of glass waste forms have been carried out in order to elucidate the leaching mechanisms of them. In the past year, we set about developing a leaching model for a long-term prediction of leach rates, in which the growth of surface layers is taken account of.

A SYNROC waste form is one of the most favorable alternatives because of its stability assurance for a long time. Cooperation between Japan and Australia on development of SYNROC waste forms has progressed favorably. The irradiation tests of SYNROC waste forms were carried out by using the oxygen ion beam of a Van de Graaff accelerator.

Besides, a program for analysis of electron diffraction patterns obtained by the transmission electron microscope (TEM) was developed in order to identify easily the crystals of various waste forms such as SYNROCs.

## 1.1 A leaching model of nuclear waste glasses

T. Banba

The present work was undertaken to develop the three dimensional spherical mathematical leaching model which emphasized the surface layer growth and element immobilization reaction inside the layers. To determine the growth rate of the surface layers, especially, two simple models were examined.

## [Leaching Model]

The model adopts the following assumptions for the foundation of the mathematical representation of each species transport. 1) Glass specimen considered here is a sphere, so diffusion occurs in a spherical geometry. 2) The surface layer-solution interface remains at the original position. 3) The position coordinate of the bulk glass-surface layer interface is expressed as a function of time. 4) Immobilization reaction in the surface layers is an irreversible first-order reaction. 5) A fictitious film exists at the solution-surface layer interface. There are many discussions about the processes occurring at the solution-surface layer interface (see, for example, Ref. 1), but there is no consensus about them yet. Therefore, we adopt here the fifth assumption<sup>2</sup> which is applicable for any process. The concept of this model is shown in Fig. 1, schematically.

These assumptions give the following equations for diffusion of a given element A in the bulk glass,

$$\frac{\partial c_{A1}}{\partial t} = \frac{D_{Ab}}{r^2} \frac{\partial}{\partial r} \left( r^2 \frac{\partial c_{A1}}{\partial r} \right), \quad r_c > r \geq 0 \quad (1)$$

and in the surface layers,

$$\frac{\partial c_{A1}}{\partial t} = \frac{D_{As}}{r^2} \frac{\partial}{\partial r} \left( r^2 \frac{\partial c_{A1}}{\partial r} \right) - k_{A1} c_{A1}, \quad R > r > r_c \quad (2)$$

where the immobilization reaction is represented by

$$\frac{\partial c_{A2}}{\partial t} = k_{A1} c_{A1}. \quad R > r > r_c \quad (3)$$

The glass-surface layer interface position  $r_c$  is given by

$$r_c = f(t). \quad (4)$$

The initial conditions are

$$c_{A1} = c_{A0}, \quad c_{A2} = 0.0, \quad 0 \leq r \leq R, \quad t = 0 \quad (5)$$

The boundary conditions are

$$-D_{As} \frac{\partial c_{A1}}{\partial r} \bigg|_{r=R} = K_A (c_{A1} \big|_{r=R} - c_A), \quad r = R \quad (6)$$

$$D_{As} \frac{\partial c_{A1}}{\partial r} \bigg|_{r=r_c} = D_{Ab} \frac{\partial c_{A1}}{\partial r} \bigg|_{r=r_c}, \quad r = r_c \quad (7)$$

$$D_{Ab} \frac{\partial c_{A1}}{\partial r} \bigg|_{r=0} = 0. \quad r = 0 \quad (8)$$

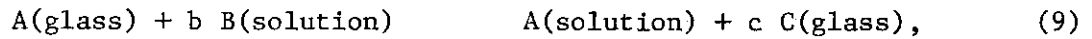
The equations obtained by using the Crank-Nicholson implicit method are implemented in a computer code, named "LEACH-2".

## [Examples of Determination of the Moving Boundary Location]

Two simple models are presented here to determine the location of moving boundary.

## 1) Reaction Controlled Model

Fig. 2(a) shows the concentration distribution of species A in the glass under the reaction controlled mechanisms. This distribution is similar to that of sodium in the glass. Therefore, assuming that the following chemical reaction occurs in the glass,



the concentration distribution of species B is shown in Fig. 2(b). This reaction has been proposed as the relationship of alkali ion(A) to hydrogen ion(B) by Boksay et al.<sup>3</sup>. If the reaction yield of B is defined by  $dN_B$ , that of A becomes  $dN_B/b$ . So, the reaction between reaction yields and the change of specimen shape is

$$-dN_A = -dN_B/b = -c_A dV = -4\pi c_A r_c^2 dr_c \quad (10)$$

Also, as the reaction yield is proportional to the surface area of the bulk glass, the reaction rate per unit surface area becomes

$$\begin{aligned} -\frac{1}{4\pi r_c^2} \frac{dN_A}{dt} &= -\frac{1}{4\pi r_c^2} \frac{1}{b} \frac{dN_B}{dt} \\ &= (1/b) k_s c_{Bf} \end{aligned} \quad (11)$$

Substitution of eq. (10) into eq. (11) gives

$$-c_A \frac{dr_c}{dt} = \frac{k_s}{b} c_{Bf} \quad (12)$$

And integration of eq. (12) gives

$$t = \frac{bc_A}{k_s c_{Bf}} (R - r_c) \quad (13)$$

The time required until the reaction is completed is obtained by setting  $r_c = 0$ :

$$t_0 = \frac{bc_A R}{k_s c_{Bf}} \quad (14)$$

By using eq. (14) the position of moving boundary becomes

$$t/t_0 = 1 - (r_c/R) . \quad (15)$$

## 2) Diffusion Controlled Model

Fig. 3(a) and (b) show the concentration distributions of species A and B in the glass, respectively, under the diffusion controlled mechanisms. These distributions imply that the diffusion of species B in the surface layers controls the chemical reaction of these species. In this reaction, both species B and bulk glass-surface layer interface move to the center of specimen. However, since the latter moves much slower than the former does, it can be assumed that the distance from the center to the bulk glass-surface layer interface is constant as against the concentration change of B in the surface layers. Namely, we assume that the diffusion of A is quasi-steady state as against the moving of that interface.

The amount of diffusing species B through the surface layers (i.e. the range from  $R$  to  $r_c$ ) is constant. Hence, defining the amount of conversion of B into the different product at the bulk glass-surface layer interface,  $N_B$ , we get

$$-dN_B/dt = 4\pi r^2 F_B = 4\pi R^2 F_{Bs} = \text{constant}, \quad (16)$$

where  $F_B$  is the diffusion flux of B and subscript s represents the original glass surface. Substitution of Fick's first law,  $F_B = D_B (dc_B/dr)$ , into eq. (16) gives

$$-dN_B/dt = 4\pi r^2 D_B (dc_B/dr) = \text{constant}, \quad (17)$$

The integrated form of eq. (17) is as follows:

$$-\frac{dN_B}{dt} \left( \frac{1}{r_c} - \frac{1}{R} \right) = 4\pi D_B c_{Bg}, \quad (18)$$

where  $c_{Bg} = \int_{r_c}^R dc_B$ . Substitution of eq.(10) into eq. (18) gives

$$-c_A \left( \frac{1}{r_c} - \frac{1}{R} \right) r_c^2 dr_c = \frac{D_B c_{Bg}}{b} dt . \quad (19)$$

And by integration of eq. (19) we get

$$t = \frac{bc_A R^2}{6D_B c_{Bg}} \left\{ 1 - 3\left(\frac{r_c}{R}\right)^2 + 2\left(\frac{r_c}{R}\right)^3 \right\} . \quad (20)$$

By setting  $r_c = 0$ ,

$$t_0 = \frac{bc_A R^2}{6D_B c_{Bg}} . \quad (21)$$

Substituting eq. (21) into eq. (20), we get the following objective formula of the position of moving boundary:

$$\frac{t}{t_0} = 1 - 3\left(\frac{r_c}{R}\right)^2 + 2\left(\frac{r_c}{R}\right)^3 . \quad (22)$$

These examples will provide useful clues for the future formulation of the moving boundary location of waste glass.

#### NOMENCLATURE

- $c_{A0}$  = initial concentration of A in the glass.
- $c_{A1}$  = concentration of a diffusing element A.
- $c_{A2}$  = concentration of a immobilized element A.
- $c_{A1}$  = surface concentration of A.
- $c_A$  = concentration of A in the solution.
- $c_{Bf}$  = concentration of B in the solution.
- $D_{Ab}$  = diffusion coefficient of A in the bulk glass.
- $D_{As}$  = diffusion coefficient of A in the surface layers.
- $D_B$  = diffusion coefficient of B in the surface layers.
- $F_B$  = diffusion flux of B.
- $k_A$  = reaction rate constant in the surface layers.
- $k_s$  = reaction rate constant per unit surface area.

- $K_A$  = film mass transfer coefficient of A.  
 $r$  = space coordinate measured from the center of a spherical specimen.  
 $r_c$  = position coordinate of the bulk glass-surface layer interface.  
 $R$  = radius of a specimen.  
 $t$  = time.  
 $t_0$  = time required until  $r_c = 0$ .

## REFERENCES

1. J. F. Flintoff and A. B. Harker, Scientific Basis for Nuclear Waste Management VIII, p.147, C. M. Jantzen, J. A. Stone, and R. C. Ewing, Eds., Materials Research Society, Pittsburgh (1985).
2. R. B. Bird, W. E. Stewart, and E. N. Lightfoot, Transport Phenomena, P.522, John Wiley & Sons, Inc., New York (1960).
3. Z. Boksay, G. Bouquet, and S. Dobos, Phys. Chem. Glasses, 9, 69 (1968).

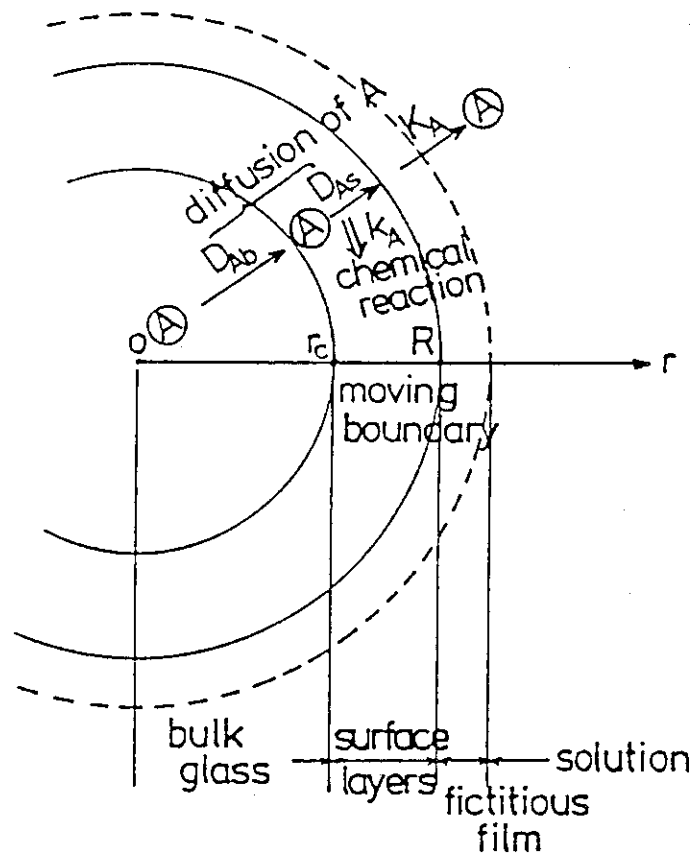


**Fig. 1** Schematic representation of spherical leaching model

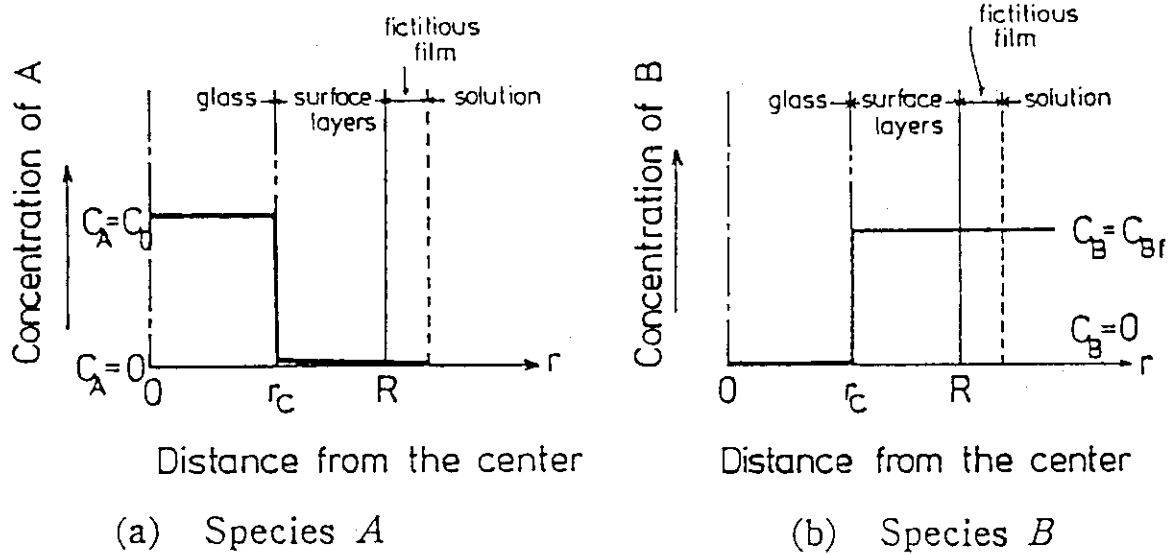


Fig. 2(a), (b) Concentration distribution of species A and B in glass under reaction controlled model

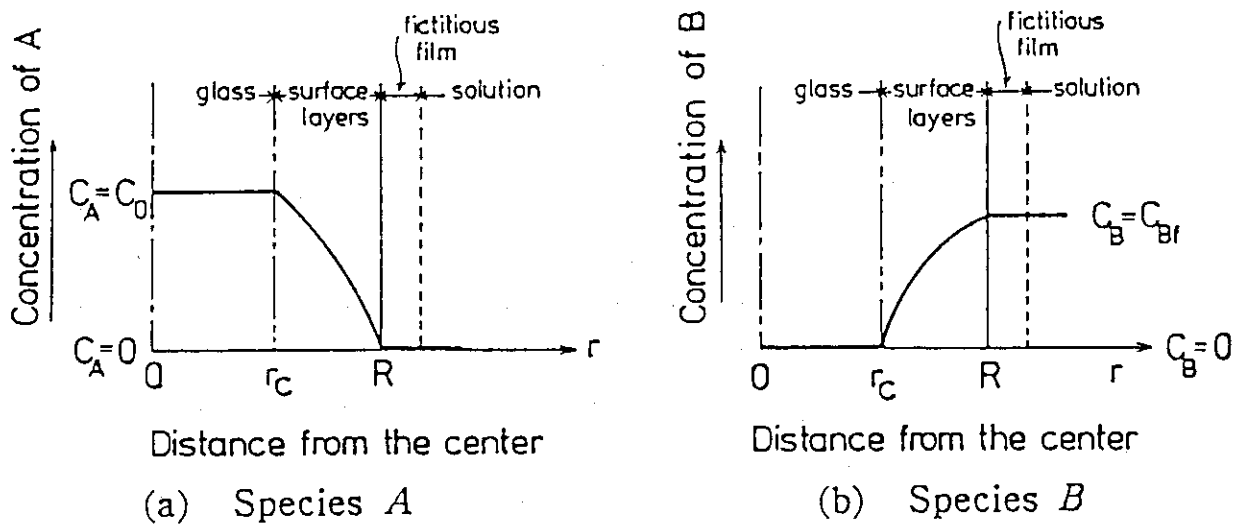


Fig. 3(a), (b) Concentration distribution of species A and B in glass under diffusion controlled model



## 1.2 Irradiation test of Synroc

H. Mitamura and T. Murakami

## [Introduction]

Synroc<sup>(1)</sup> incorporates the various radwaste elements as dilute solid solutions in three main constituent minerals, namely hollandite ( $\text{BaAl}_2\text{Ti}_6\text{O}_{16}$ ), perovskite ( $\text{CaTiO}_3$ ) and zirconolite ( $\text{CaZrTi}_2\text{O}_7$ ). Since the actinide elements are incorporated especially in perovskite and zirconolite, these crystalline phases are to be subjected to significant radiation damage for a disposal time. For simulation of the knock-on damage, irradiation test using oxygen ions was conducted at room temperature on thin disks of Synroc containing 10 wt% of a simulated high level nuclear waste.

## [Experimental]

Before irradiation, both sides of Synroc specimens<sup>(2)</sup> of 3 mm in diameter and 0.2 mm thick were ion-milled using 6 kV argon ions to electron transparency for observation by transmission electron microscopy. The specimens were irradiated on one side with 0.4 MeV of oxygen ions accelerated by a Van de Graaff generator at a dose rate of  $1.4 \times 10^{12} \text{ ions.cm}^{-2}.\text{s}^{-1}$  to the total dose of  $2.2 \times 10^{16} \text{ ions.cm}^{-2}$ . Some of the specimens were covered with a 150-mesh copper grid of 30  $\mu\text{m}$  thick to compare irradiated and unirradiated parts in the same observation condition.

## [Results and Discussion]

Calculated values of displacement per atom are two and seven at the surface and at the peak, respectively, and calculated irradiation depth is up to approximately 0.8  $\mu\text{m}$  for the total dose. Figure 1 shows a transmission electron micrograph of an irradiated Synroc specimen covered with a mesh copper grid. Since edges in the irradiated part ("I") appears to keep its original features, the obscurity may be not due to heat damage, but due to real radiation damage. A selected area electron diffraction pattern in this figure was obtained from the irradiated part indicated by a black arrow. The pattern contains amorphous halos and diffraction spots. This means that the irradiated part becomes electron-diffraction amorphous.

Energy dispersive X-ray analysis was carried out to examine changes in composition after irradiation. Since areas between  $2\mu\text{m} \times 2\mu\text{m}$  and  $6\mu\text{m} \times 6\mu\text{m}$  were selected at random to conduct the area analysis, these

rectangles contained at least several grains which are mostly submicron in size. This area analysis can therefore give the mean compositions of the masked and the irradiated parts to some extent. Figures 2 and 3 are typical X-ray spectra of the masked and the irradiated areas, respectively. Comparison of these figures implies that irradiation altered composition of the thin specimen.

[References]

1. RINGWOOD, A. E., KESSON, S. E., WARE, N. G., HIBBERSON, W., and MAJOR, A., "Immobilisation of high level nuclear reactor waste in Synroc", *Nature*, 278 (1979) pp. 219-223.
2. MITAMURA, H., AMAYA, T., MURAKAMI, T., NAKAMURA, H., NAGANO, T., and BANBA, T., "A new method using titanium hydride for fabrication of Synroc", *Ceram. International* (in press).

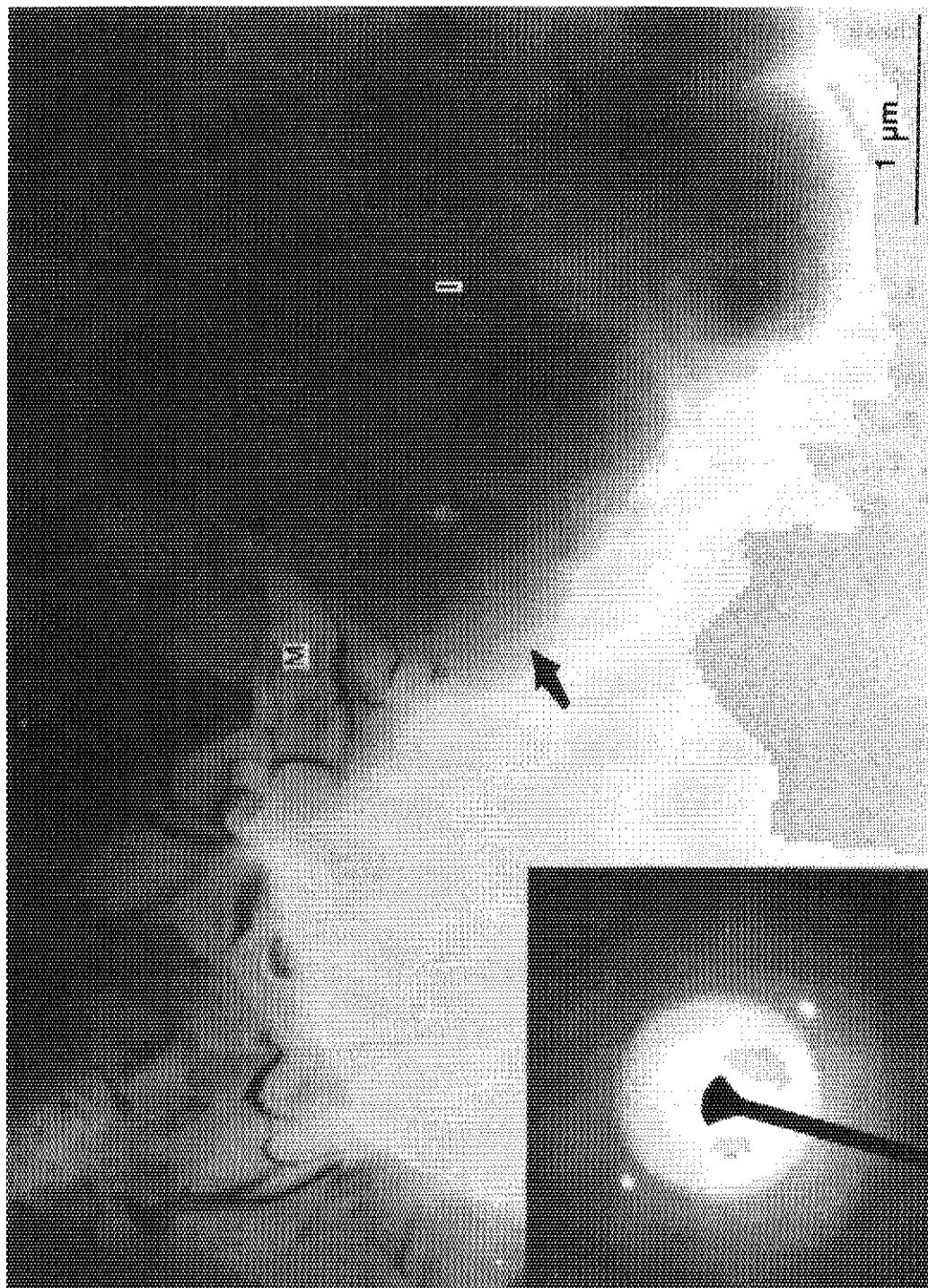


Fig. 1 Transmission electron micrograph of a Synroc specimen after irradiation with 0.4 MeV oxygen ions to a total dose of  $2.2 \times 10^{16}$  ions.cm<sup>-2</sup>. Masked and irradiated parts are shown by "M" and "I", respectively. A selected area diffraction pattern in the lower left hand corner corresponds to the irradiated part shown by the black arrow. A black bar is 1 μm.

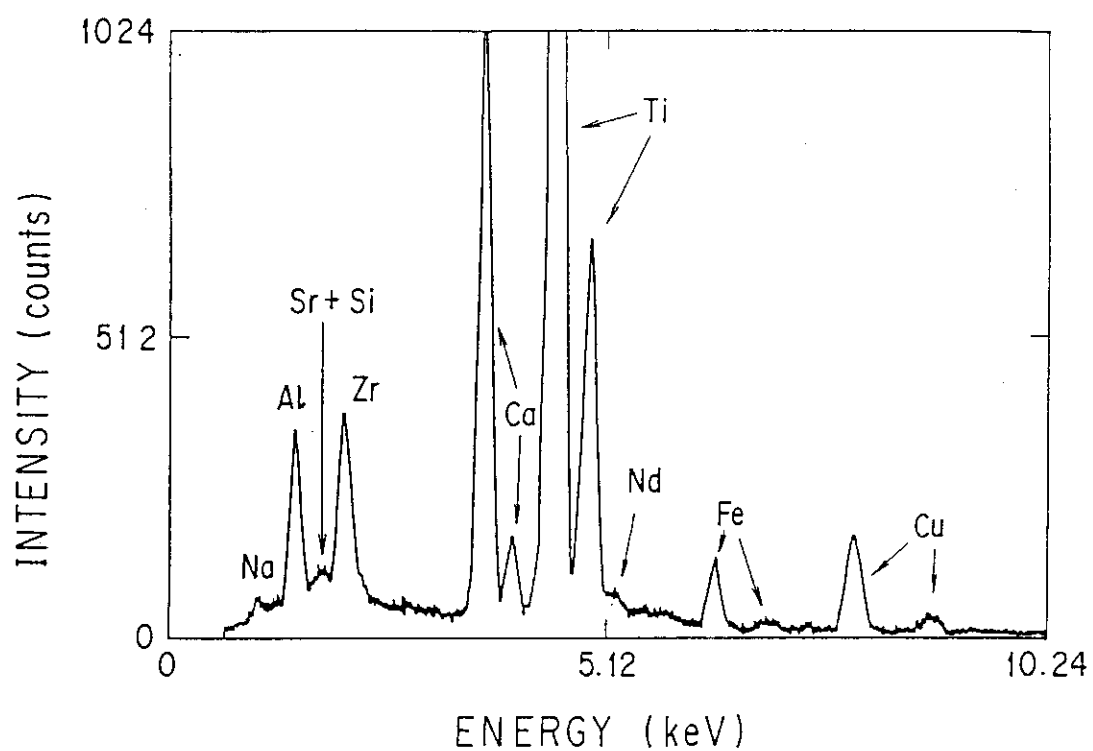


Fig. 2 Typical energy dispersive X-ray spectrum of a masked area ( $6\ \mu\text{m} \times 6\ \mu\text{m}$ ).

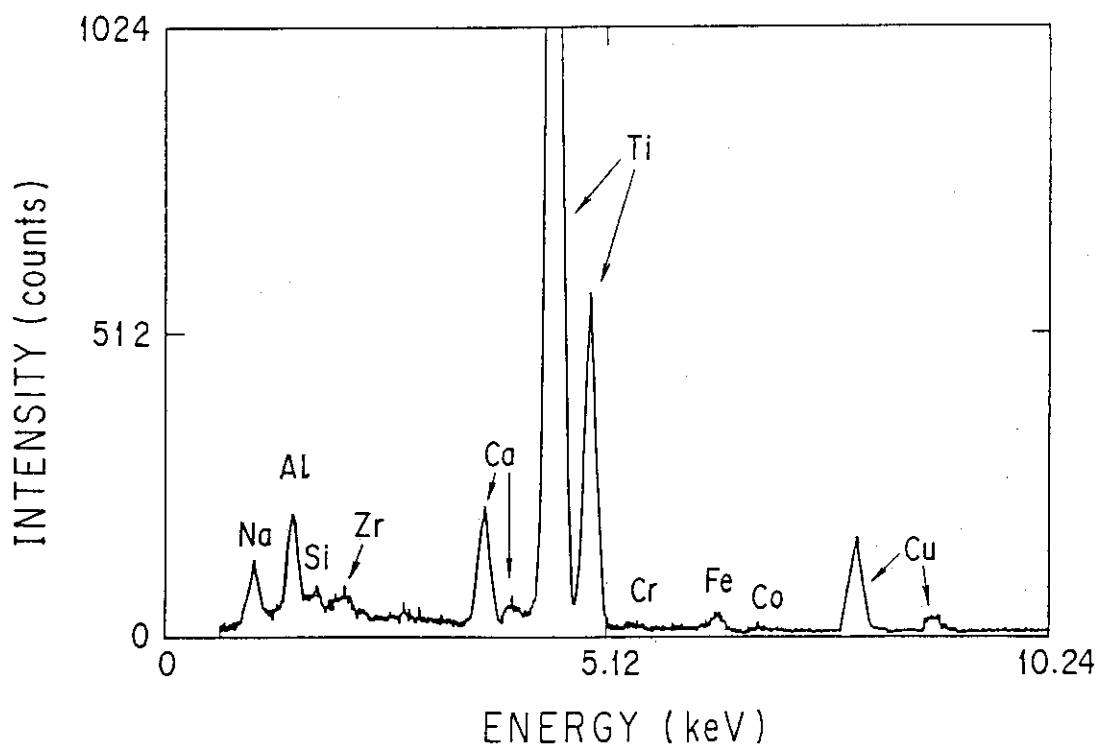


Fig. 3 Typical energy dispersive X-ray spectrum of an irradiated area ( $2\ \mu\text{m} \times 2\ \mu\text{m}$ ).

### 1.3 Program for analysis of electron diffraction patterns

T. Nagano

Synroc is a nuclear waste form and is composed of micro crystals of three major mineral phases, namely hollandite, perovskite and zirconolite. For characterization of Synroc, the transmission electron microscopy is one of the most favorable methods since it supplies the information about microscope images and electron diffraction patterns of a sample specimen. These diffraction patterns can be used for identification of crystals because they reflect the crystal structures. In the interpretation of the electron diffraction patterns, indexing of each diffraction spot is indispensable and it is required to list d-spacings equivalent to Miller's indices with each diffraction spot by trial and error. Therefore, the work of identification of various diffraction patterns is complicated and timeconsuming. In order to identify the diffraction patterns rapidly and efficiently the following programs were developed using a personal computer. These programs are (1) program for listing d-spacings equivalent to Miller's indices and (2) program for drawing electron diffraction patterns along given zone axes.

In order to verify the propriety of the present program, electron diffraction patterns of two crystals, gold and molybdenum oxide, drawn by the program were compared with those obtained from the TEM observation. Fig. 1 and Photo. 1 show electron diffraction patterns of gold along zone axis[100] obtained by the calculation and by TEM observation, respectively. As can be seen, there is close agreement between both results. The electron diffraction patterns of molybdenum oxide along zone axis[010] by the calculation (Fig. 2) also agrees with that by TEM observation (Photo. 2). Although actual pattern (Photo. 2) shows a difference of intensity between the different spots, the present program takes no account of intensity of each diffraction spot.

The present program can apply to all fundamental crystalline phases and all zone axes. Therefore it is very useful in interpreting electron diffraction patterns about crystalline phases produced in Synroc and also in surface layers of high-level waste glasses and natural mineral phase assemblages such as granite.



Fig.1 Electron diffraction pattern of gold (Au) along zone axis  $[100]$  obtained from the program.

Fig.2 Electron diffraction pattern of molybdenum oxide ( $\text{MoO}_3$ ) along zone axis  $[010]$  obtained from the program.

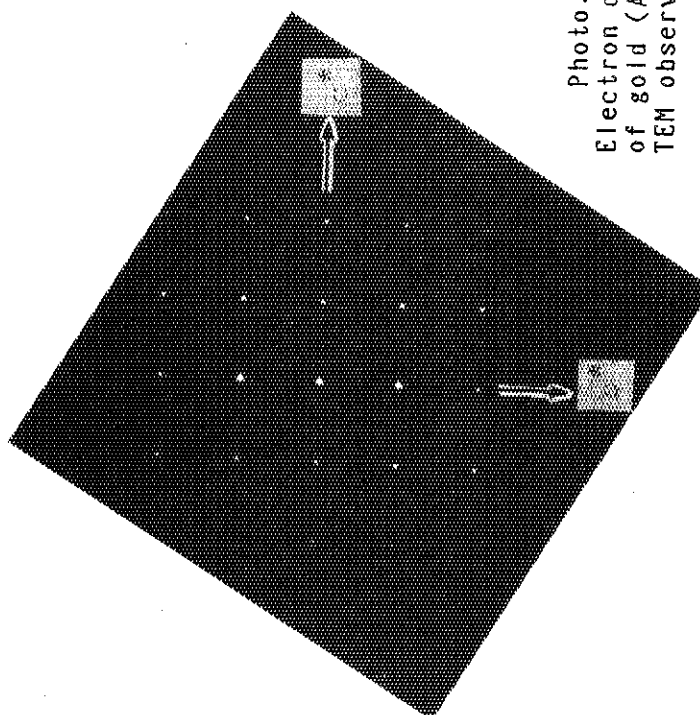


Photo.1  
Electron diffraction pattern of gold (Au) obtained from the TEM observation.

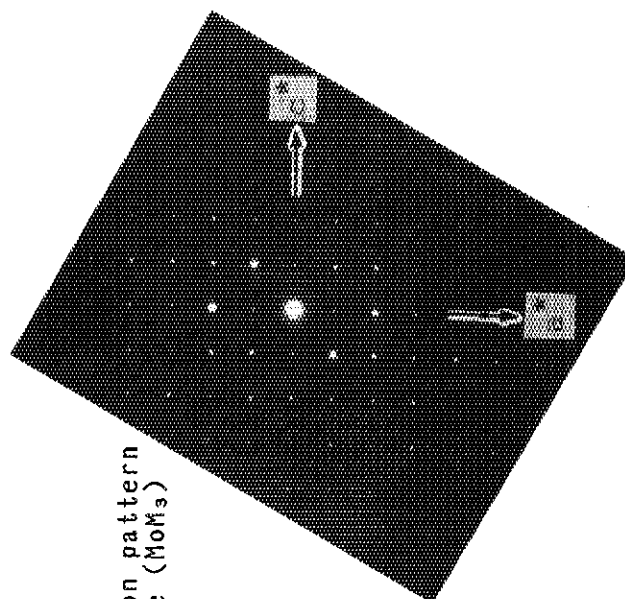


Photo.2  
Electron diffraction pattern of molybdenum oxide ( $\text{MoO}_3$ ) obtained from the TEM observation.

## 2. Safety Evaluation for Geological Disposal

S. Muraoka

An extensive R and D has been carried out for the long term assessment of the geological disposal of high-level waste. The research activities for the present period are as follows;

By analysing the results of heating tests both in laboratory and in the field, thermal characteristics of buffer materials were evaluated.

Corrosion tests were carried out to study the durability of the container materials under a simulated disposal condition.

Diffusion of non-sorbing iodide ions in granite and tuff was studied.

As a natural analogue study, fixation of groundwater elements around a fracture of a granitic rock has been studied to get fundamental information of groundwater-rock interactions.

By participating in the HOCUS project of the safety evaluation of subseabed disposal organized by OECD/NEA, vertical distributions of elements were investigated on sea floor sediment cores.

The computer code MIG2DF was developed to estimate the radionuclide migration in geosphere and HYDROCOIN level-2 problems were tackled by using 2D-SEEP and 3D-SEEP.

From this year we have initiated the conceptual design study of a repository system in the safety assessment point of view for the preclosure period.

### 2.1 Engineered barrier

#### (1) Buffer material test

T. Suzuki and S. Amagai

##### [Introduction]

The results of heater test were reported in the previous progress report JAERI-M 86-131 last year. By analyzing the results, the thermal conductivities of the buffer material has been calculated by using 2D-SEEP code [1].

In addition, the radial distribution of water contents in some areas was measured in order to analyze the relationship between water content and thermal conductivities of the buffer material.

## [Equipment and experiment]

The testing equipment is shown in Fig. 1. In order to simulate the heat generation from HLW, an electric heater was set in the center of the equipment. The simulated buffer material which were the mixtures of bentonite (8wt%) and zircon sand (92wt%), were filled up in a vessel around the heater. The moisture content of the buffer material was 2.82 wt% before the test. The density of the material was  $3.18 \text{ g/cm}^3$ . The vessel containing heater and the buffer material was made of steel, and was set in a water tank to keep the equipment at a constant temperature during the experiment. For the thermal conductivity measurement, five thermocouples were installed in the buffer material and connected to a data acquisition system. The buffer material in the vessel were heated at an electric power of 1.0 Kw/h. In order to measure the radial distribution of water contents in the buffer material, three holes were bored on the wall of the equipment as shown in Fig. 2. Through the each hole, the buffer materials have been sampled as crumbled powder every 20 mm by a drill. Water contents were measured for the samples by using a gravimetric method and the radial distribution of water contents was determined.

## [Results and discussion]

In a homogeneous cylindrical medium, the distribution of temperature is given by the following equation (1);

$$t = t_1 - (t_1 - t_2) * \ln(r/r_1) / \ln(r_2/r_1) \dots\dots (1)$$

where

$r_1, r, r_2$  : radial distance from axis

$t_1, t, t_2$  : temperature

There is a discrepancy between the observed temperature and the calculated one by using equation (1) as shown in Fig. 3. It means that,



in the buffer material, thermal conductivity became not homogeneous in the course of heating and the equipment became too complex to regard it as a simple cylindrical model.

The 2D-SEEP finite element code was used to calculate the thermal conductivity. The finite element grids used in the calculation is shown in Fig. 4. Buffer material was divided into four areas by using the grids as shown in Fig. 5. A thermal conductivity of vessel  $\lambda_5$  was equal to 53.5 [W/m.k] in the test. Each variable  $\lambda_1$ ,  $\lambda_2$ ,  $\lambda_3$ , and  $\lambda_4$  was assumed to be the average thermal conductivity in each area. A series of calculations was carried out to find the best fit curve and the distribution of thermal conductivities was determined as shown in Fig. 6.

Generally, a thermal conductivity of mixtures of coarse-grained and fine-grained materials is influenced by their composition, density, temperature, and moisture content. In this test, the composition and the density were fixed through the test, and the temperature was kept under 200[°C], and it is difficult to assume that the thermal conductivity of the buffer material changed under the influence of these conditions. On the other hand, as reported by Radhakrishna[2], the moisture content has the great influence on the thermal conductivities of clay based materials at the value of moisture content from 0 % to 4 %. The radial moisture content distribution in the buffer material after the heater test determined by the gravimetric method is shown in Fig. 7. The thermal conductivities at the inner part were lower than those at the outer part, and these results can be explained by the fact that the evaporation of moisture within the buffer material occurred to a greater degree at the inner part than at the outer part. And it should also be noted that, in this test, thermal conductivities were considered to be overestimated because of a heat loss from the electric heater through the buffer material.

#### [References]

- [1] Private communication
- [2] H.S. Radhakrishna and K.K. Tsui,  
 "Proceedings of the workshop on near-field phenomena in geologic repositories for radioactive waste",  
 Nuclear Energy Agency, Paris, France. OECD. (1981) p.329-344

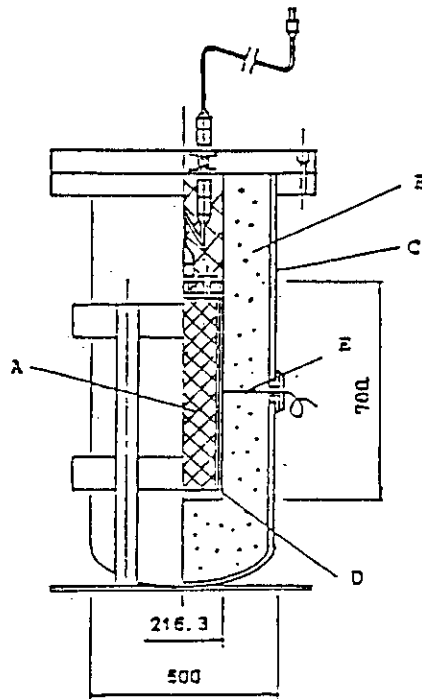


Fig. 1 The equipment of engineered barrier performances test  
 A; electric heater. B; buffer materials  
 C; outer vessel D; inner vessel E; thermo couples

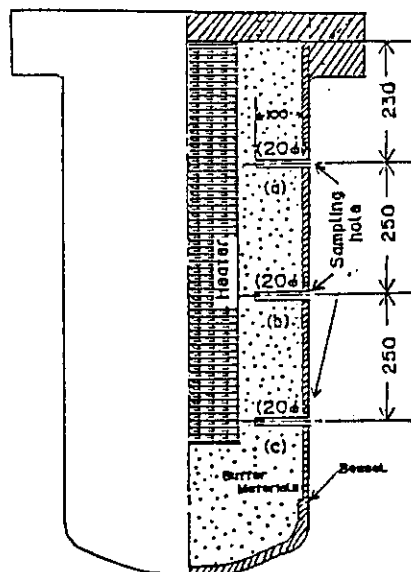


Fig. 2 Positions of sampling holes for measuring water content.

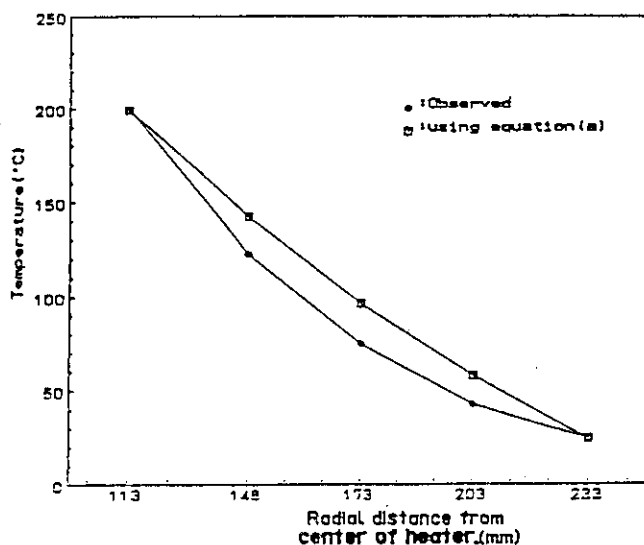


Fig.3  
Observed temperature and calculated one using equation (a).

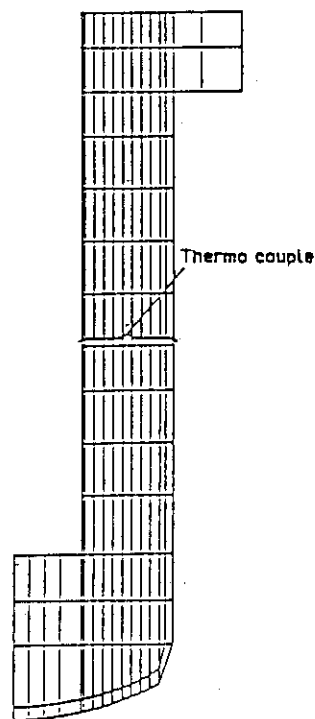


Fig.4  
The finite element grid.

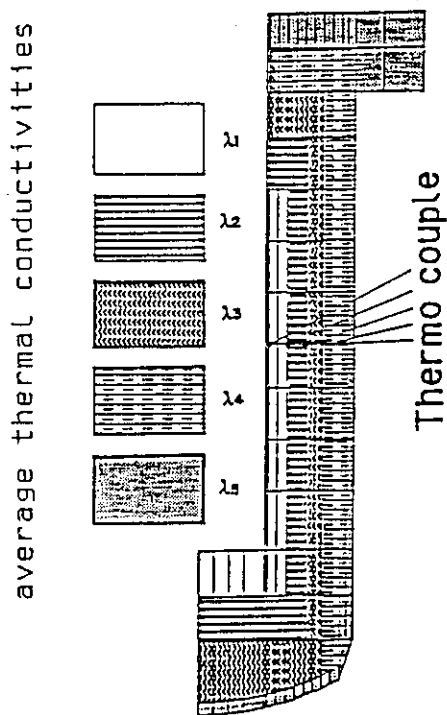


Fig.5  
Arrangement of averaged thermal conductivities in calculation using 2D-SEEP.

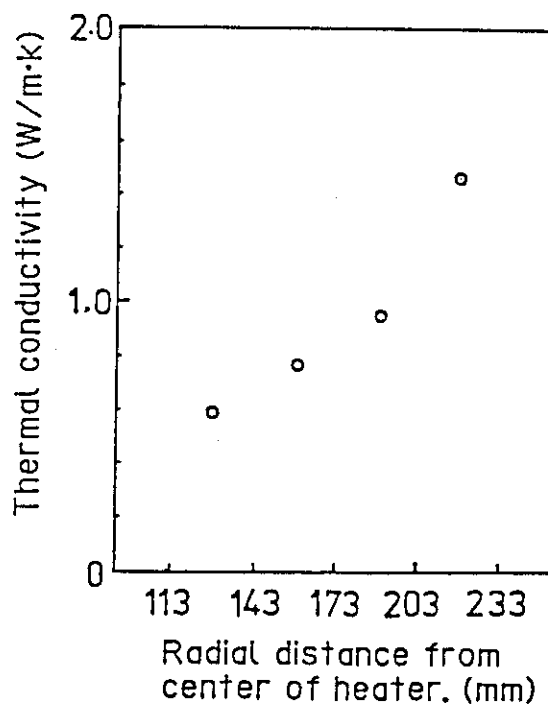


Fig.6  
Determined average thermal conductivities in each area using 2D-SEEP.

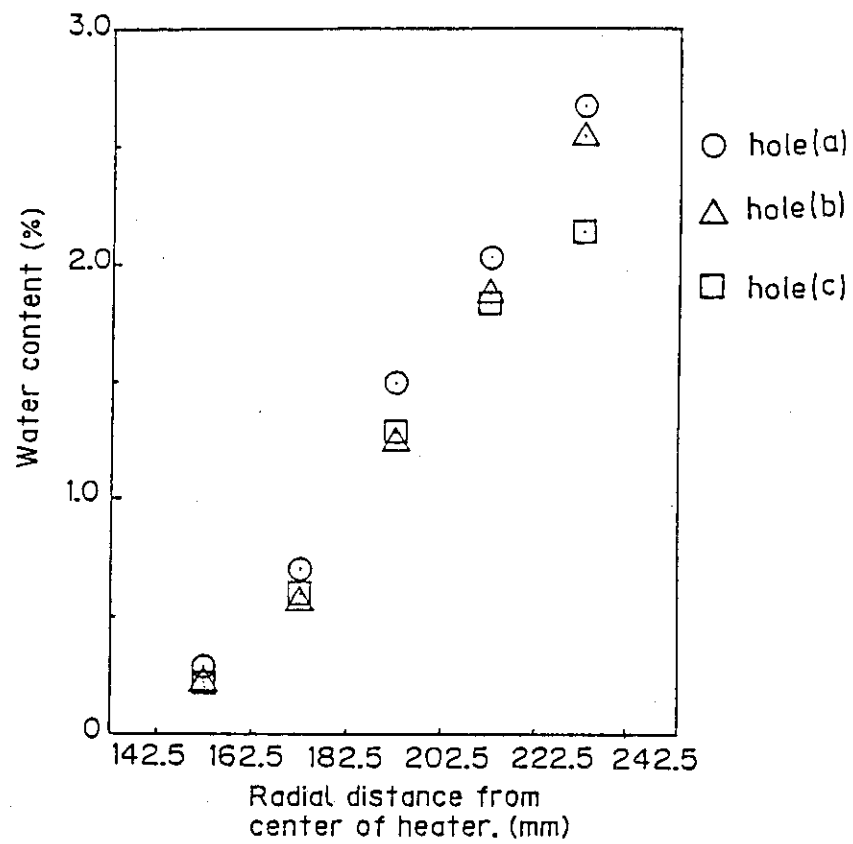


Fig. 7  
Radial distribution of  
water content.

- (2) Stress corrosion cracking of austenitic stainless steels in a granite groundwater at an elevated temperature under gamma-ray irradiation

M. Kumata

[Introduction]

Austenitic stainless steels have been considered as a canister material for vitrified high level radioactive wastes (HLW). The canister would be exposed under gamma-ray radiation and high temperature conditions caused by the decay heat of vitrified HLW for long time periods. For the purpose of evaluation of canister materials under near-field condition, the stress corrosion cracking (SCC) test was carried out. C-ring and double U-bent specimens of the sensitized austenitic stainless steels have been exposed in a granite groundwater at a high temperature under gamma-ray irradiation for 30 days.

[Experimental]

Test Materials and Specimen; The stainless steels tested were commercial Type 304 ss and Type 309s ss, whose chemical compositions are given in Table 1. In order to simulate the thermal history of the canister during HLW vitrification, sensitization heat treatments shown in Table 1 were carried out. In the case of Type 309s ss, a part of samples was water quenched as shown in Table 1, to examine the heat treatment effect on stress corrosion cracking under gamma-ray irradiation. Stress was applied in three ways, one was by bending two coupon specimens along their longitudinal direction into a double U-bent type, and the second into a notched double U-bent type, the third was by tightening a nut on a bolt across the legs of the C-ring. The C-ring specimens were made by cutting 1.5 cm wide ring from the heat-treated, 0.2 cm wall tubing and then notched in the center of the top. Three or six specimens were used for each test.

SCC test with Gamma-ray Irradiation; Type 304 ss and Type 309s ss specimens were immersed into a granite groundwater in a autoclave with small granite disks to insulate samples each other. The autoclave was set up in front of  $^{60}\text{Co}$  source in a cave of the Takasaki Establishment of JAERI. Temperature and pressure of the autoclave was maintained at 250°C and 4.3 MPa (about saturated water vapor pressure) for 30 days. The dose rate was kept at  $0.92 \times 10^5$  R/h and  $1.74 \times 10^5$  R/h by varying the

distance from the  $^{60}\text{Co}$  source to each specimen. Cold experiments without gamma-ray irradiation were also carried out for comparison.

[Results]

For Type 304 ss, all specimens exposed under gamma-ray irradiation showed no SCC susceptibility with the naked eye, in the case of three stress conditions and for the total dose ranging from  $0.99 \times 10^8$  R to  $1.20 \times 10^8$  R. For Type 309s ss all specimens exposed under gamma-ray irradiation showed no SCC susceptibility with the naked eye, in the case of two types of heat treatment and for the total dose ranging from  $0.62 \times 10^8$  R to  $0.94 \times 10^8$  R. In the cold experiments for both steels, all specimens showed no SCC susceptibility either. It was concluded that Type 304 ss and Type 309 s ss showed soundness in granite groundwater at 250°C with total gamma-ray irradiation dose up to about  $10^8$  R.

Table 1 Chemical composition and heat treatment of test materials

Steel	Chemical Composition						Heat Treatment *
	C	Si	Mn	P	S	Cr	
Type 304 ss	0.048	0.44	1.30	0.034	0.021	8.55	17.72
	0.08	0.43	0.86	0.030	0.006	8.42	18.06
Type 309s ss	0.14	0.56	1.53	0.023	<0.005	14.3	23.76
							700°C x 100 min → Air cooling + 500°C x 24 hr → Air cooling

\* A part fo Type 309s ss was heat treated as 1050°C x 30 min + water quenching

(3) Slow Strain Rate Stress-corrosion Test under Gamma-ray irradiation for container materials

S. Amagai and S. Muraoka

[Introduction]

In the safety assessment of geological disposal of high-level waste the performance of the container material must be evaluated.

This study aimed to evaluate the influence of gamma-ray irradiation on stress corrosion cracking (SCC) of candidate alloys for canister and over pack materials. In this study, stress corrosion cracking test was carried out for Type 304 stainless steel and 1020 low carbon steel.

[Experimental]

The stress corrosion susceptibility was studied by the Slow Strain Rate techniques (SSRT). The test equipment is shown in Fig. 1. Round tension specimens were machined from rods of Type 304 stainless steel and 1020 carbon steel. In order to clarify the influence of the gamma-ray irradiation on SCC, specimens were thermally treated. About 240 ml of a test solution was poured into the test cell. The test solution was a simulated basalt ground water, and its synthetic composition is shown in Table 1. Test temperature was kept at 90°C during the test run. The surface of the solution in the cell was swept by Ar gas to keep the initial electro-chemical condition. Gamma-ray irradiation test was carried out in the hot cave with a Co-60 source (about 2.9 kCi). Irradiation dose rate was  $2.8 \times 10^4$  R/hr at the specimen.

[Results and discussion]

Fig. 2 shows the stress-strain curves of Type 304 stainless steel and 1020 carbon steel under gamma-ray irradiation and non-irradiation respectively. In the case of Type 304 stainless steel, maximum stress under gamma-ray irradiation is larger than under non-irradiation. In the case of 1020 carbon steel, no obvious difference was observed under both gamma-ray irradiation and non-irradiation. Photo 1 and photo 2 show microphotograph of the fracture surface of Type 304 stainless steel and 1020 carbon steel for the purpose of comparison. Type 304 stainless steel shows the susceptibility of stress corrosion cracking under both gamma-ray irradiation and non-irradiation. On the other hand, in the case of 1020 carbon steel, stress corrosion cracking was not observed under both conditions.



The index of stress corrosion cracking [1] was applied to our results to analyse the susceptibility of SCC. The results indicated that Type 304 stainless steel was more susceptible to stress corrosion cracking under gamma-ray irradiation than under non-irradiation, but 1020 carbon steel was not susceptible to stress corrosion cracking under both conditions.

The number of tests must be increased to clarify the influence of gamma-ray irradiation, because the phenomena of SCC is a rather statistical one. And also electro-chemical approach should be applied to understand the effect of gamma-ray irradiation to SCC susceptibility.

[Reference]

- [1] Hideya Okada, Yuzo Hosoi, Seizaburo Abe and Shuichi Yamamoto, "A Rapid Testing Method of Stress Corrosion Cracking of Austenitic Stainless Steels." JOURNAL OF THE JAPAN INSTITUTE OF METALS, Vol. 38, 646-653 (1974)

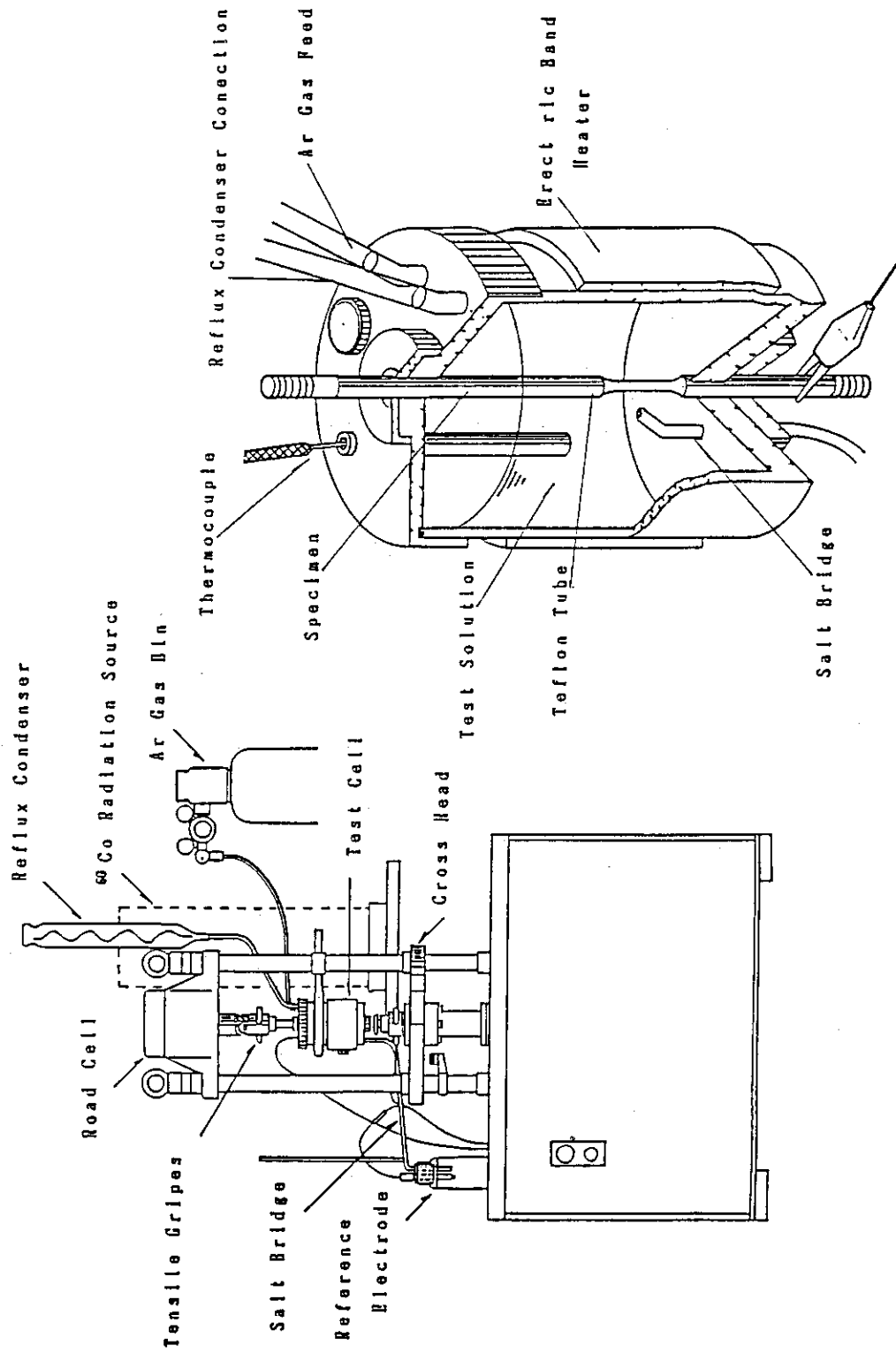


Fig. 1 Slow Strain Rate Test Equipment

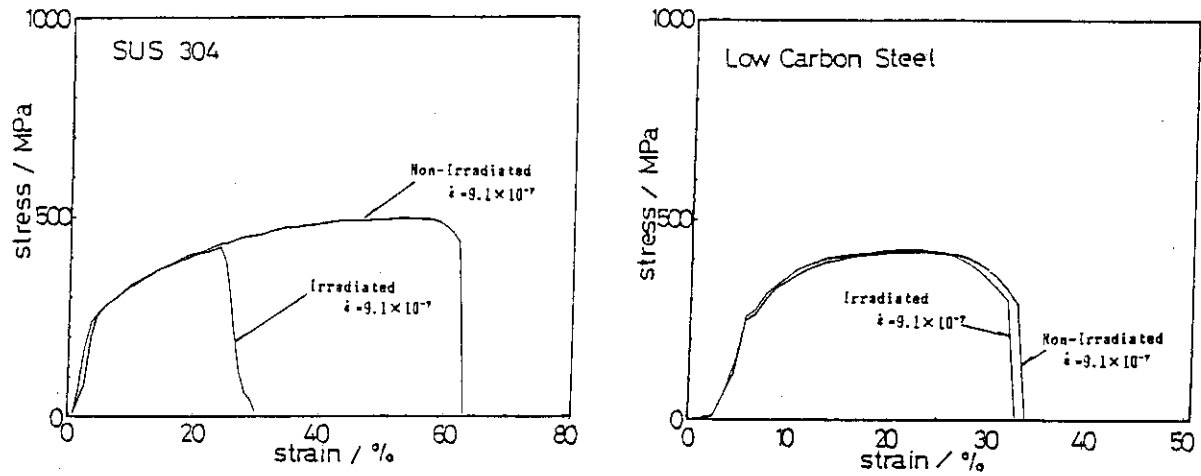
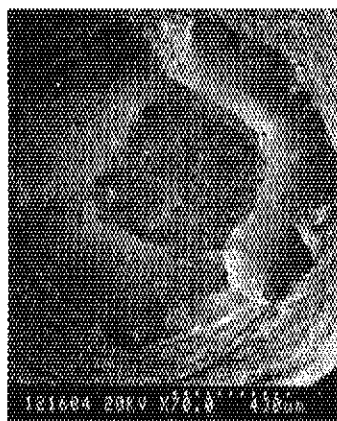


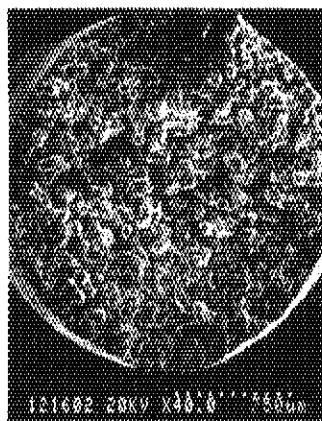
Fig. 2 Stress-strain curves of Type 304 stainless steel and 1020 carbon steel

Table 1 Composition of Synthetic Basalt ground water

Cemical Species	mg/L
N a	393
K	4.14
C a	0.26
M g	0.009
F	38.7
C l	389
S O <sub>4</sub>	160



A i r

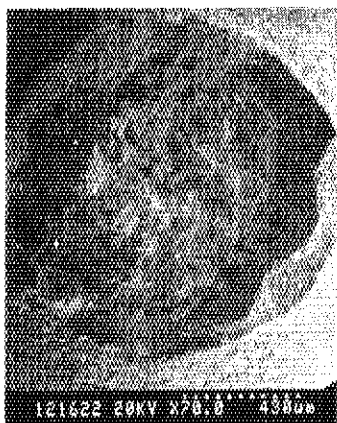


Irradiated

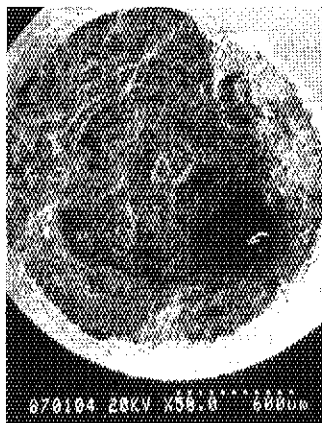


Non-irradiated

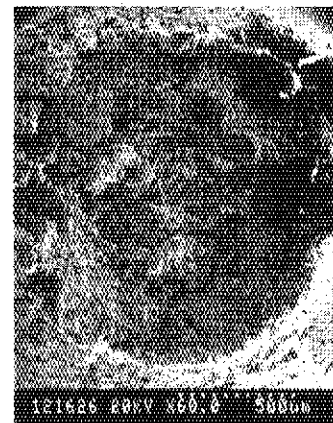
Photo 1 Fracture surface of Type 304 stainless steel



A i r



Irradiated



Non-irradiated

Photo 2 Fracture surface of 1020 carbon steel

## 2.2 Field Test

### (1) Buffer Material Test

M. Kumata

#### [Introduction]

Compacted sand/bentonite mixtures are being considered for use as buffer materials, an engineered barrier component of a vitrified high level radioactive waste (HLW) package, in the concept for geological disposal of HLW<sup>1,2)</sup>. In order to test these characteristics in situ, a heater test with the buffer material was carried out at a field experimental room which was constructed at 40 m depth below surface in a granite rock mass at the Inada quarry<sup>3)</sup>. At first, as a preliminary experiment, in the case of no groundwater flow, the thermal characteristics of the buffer material was examined with a large electric heater in a test hole.

#### [Experimental]

Materials: The buffer material used in this study was prepared by compaction of a mixture of air-dry bentonite powder and quartz sand under a pressure of approximately 200 kg/cm<sup>2</sup> with a small amount of tap water. The bentonite used in the study was a commercially available material, "Volclay MX 80", composed mainly of sodium montmorillonite. Chemical composition of the bentonite is shown in Table 1. The quartz sand consisted of particles about 0.15-2.3 mm in diameter. The bentonite and the quartz sand were mixed in a weight ratio of 7:3. The mixture was milled in a soil mixer then pressed with about 165-270 kg/cm<sup>2</sup> in a molding box. Through this operation the test blocks of the buffer material were obtained with a bulk density of 2.015 to 2.026 g/cm<sup>3</sup> and a water content ranging between 15.1 and 17.0 %. Buffer material blocks were tightly arranged around the heater (Fig. 1). Shape of a buffer material block is a 45° part of a 15 cm thick ring, with an inner and outer diameters of 52.8 cm and 90 cm. Some basic physical data of the buffer material are given in Table 2.

Test hole: A hole for the experiment was drilled in the granite from the test room floor with 1 m diameter and 5 m depth. A large steel can was fitted in the hole to be obstruct groundwater into the hole from the wall and bottom of the hole.

Heater: The size of the heater is 0.4 m in diameter and 1.5 m in length. Thirty-two (32) heater elements were set in a SUS 304 stainless

steel capsule. This large heater was set in the center of the test hole at the depth of 3.75 m. The heater was operated initially at 4 kw power and later at 3 kw during 1800 hours by the output controller.

The major objective of the test was to record the development of temperature fields and moisture change in the buffer material. The test blocks of the buffer material were set up in the hole around the heater from the bottom up to the test room floor (Fig. 2). In order to measure the temperature change, 60 sheathed thermocouples were used in the buffer material, and 45 thermocouples were used in the granite rock mass. At the excavation of the hole 36 samples were taken to obtain a detailed picture of the water content distribution.

#### [Results]

1) The temperature distribution in the hole and surrounding granite after the heating of 1800 hours are shown in Fig. 3. The maximum temperature in the hole was about 208°C after 1800 hours at the nearest part of the buffer material to the heater.

2) There was a heat-induced redistribution of the original water content through which partial drying took place close to the heater, while water was accumulated at the outside of the dry area (Fig. 4). In the dry area up to 200°C, the minimum water content of the buffer material block was about 2 %. Some blocks of the buffer material in the area of over 100°C were taken into several pieces because of a shrinkage of the buffer material itself resulting from an evaporation of an initial moisture.

3) Comparing with the observed temperature distribution and the calculated one which was obtained by FEM-based calculation using analytical program "MARC"<sup>4)</sup>, it was revealed that the thermal conductivity of the buffer material changed depending on the temperature and moisture during the heater experiment.

## References

- 1) Wood, M.I. et al. (1981) : RHO-BWI-SA 80.
- 2) Nuttall, K. et al. (1986) : Proc. Int. Symp. Siting, Design and Construction of Underground Repositories for Radioactive Wastes, IAEA, pp.431-448.
- 3) Kumata, M. et al. (1986) : Proc. 2nd. Int. Conf. Radioactive Waste Management, Canadian Nucl. Soc., pp.326-331.
- 4) Structure analysis with MARC-CDC, "Course note", vol. IV, MARC Analysis Research Co.

Table 1 Chemical composition of the bentonite

SiO <sub>2</sub>	Al <sub>2</sub> O <sub>3</sub>	Fe <sub>2</sub> O <sub>3</sub>	Mg O	CaO	Na <sub>2</sub> O	K <sub>2</sub> O	Fe O	TiO <sub>2</sub>	other	H <sub>2</sub> O
58.0	18.0	2.5	2.5	0.1	1.5	0.2	0.2	0.1	0.5	5.0
}	}	}	}	}	}	}	}	}	}	}
64.0	21.0	2.8	3.2	1.0	2.7	0.4	0.4	0.2	0.8	6.0

Table 2 Properties of the buffer material \*

Bulk density	Water content	Heat conductivity	Heat capacity
g/cm <sup>3</sup>	%	cal/m.s.°C	cal/g.°C
2.02	15.9	0.227	0.197

\*Average for room temperature



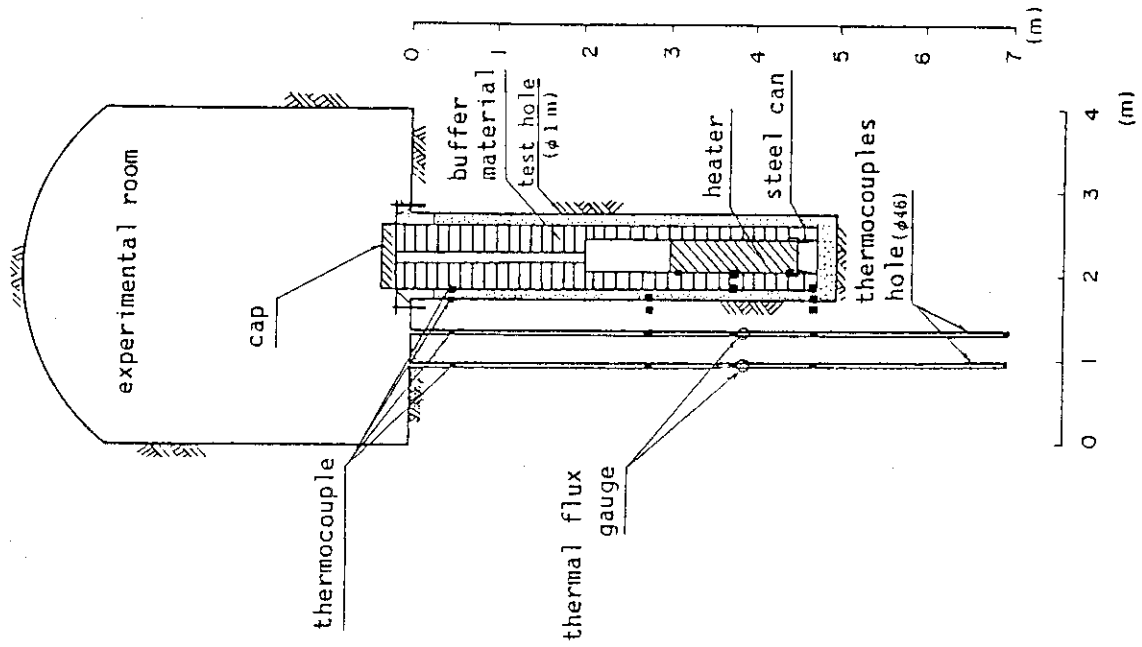


Fig. 2 Main features of the buffer material test

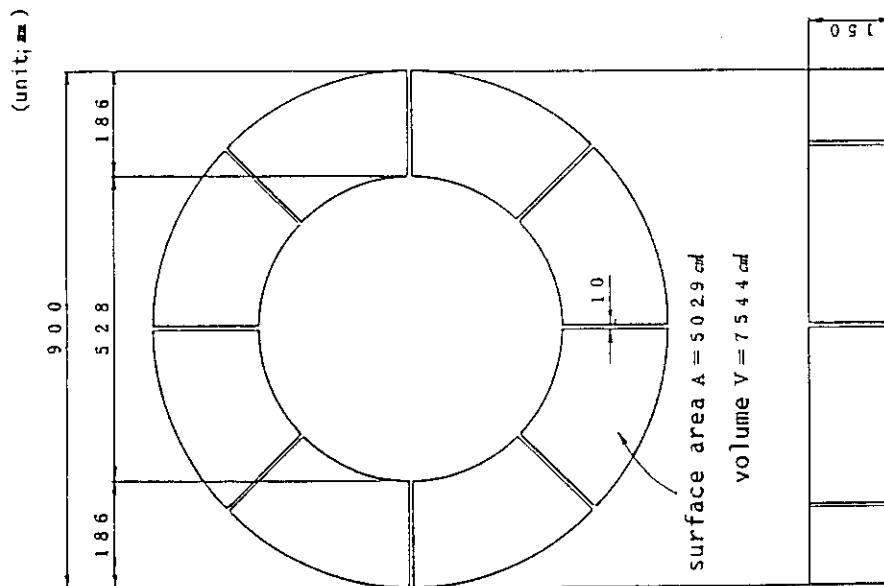


Fig. 1 Example of trimmed blocks of compacted bentonite/sand mixture for use in a heater hole

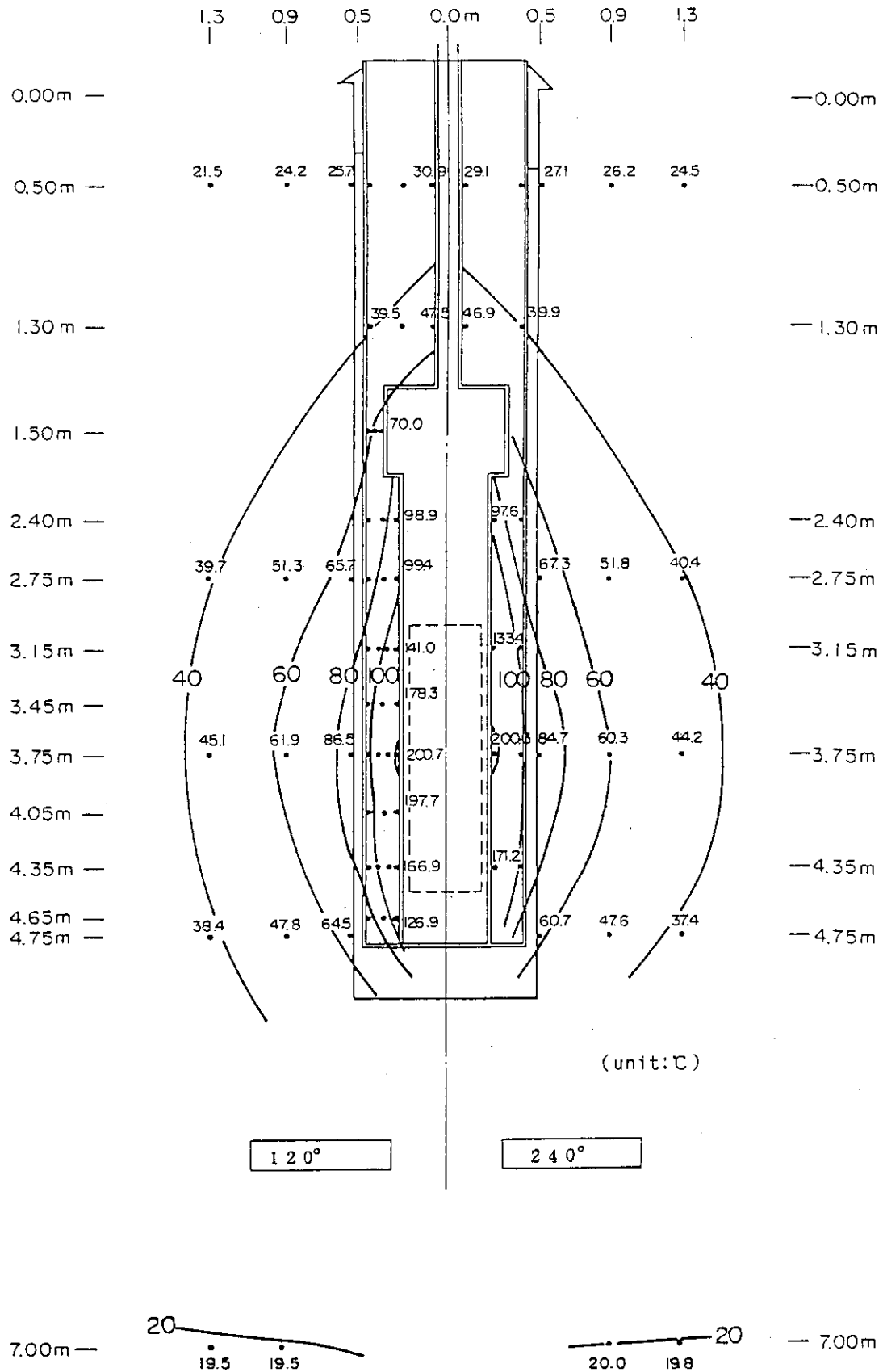


Fig. 3 Temperature distribution and isothermal curves in the hole and surrounding granite

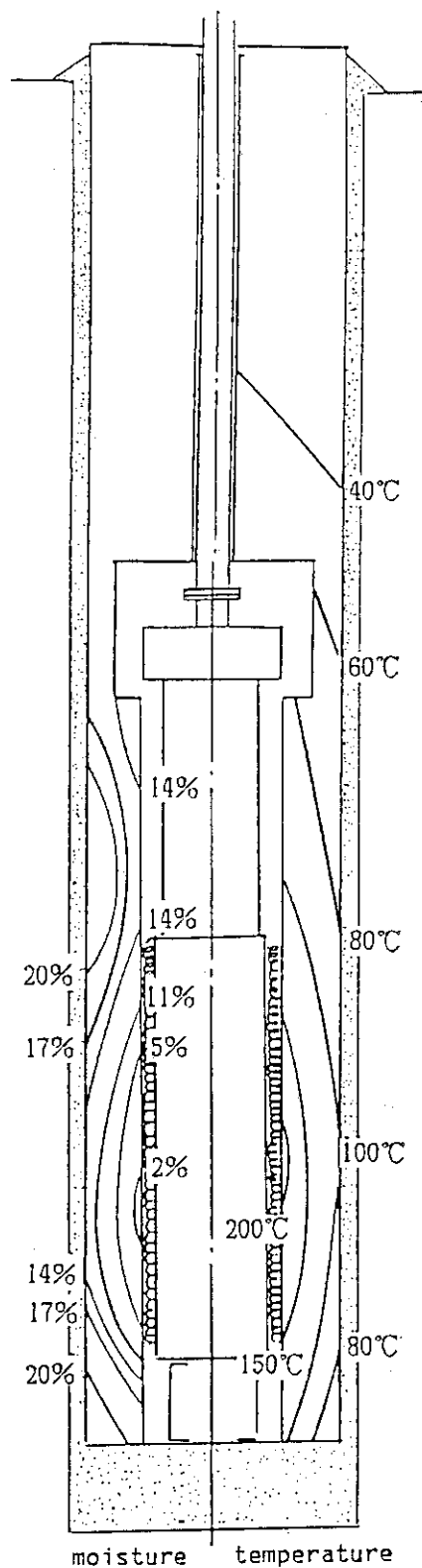


Fig. 4 Moisture and temperature distributions in the hole (at 1800 hours heating)

## (2) In-situ corrosion test

S. Muraoka

In the geological disposal of high-level waste, the canister and/or the overpack is one of the most important engineered barriers. The in-situ stress corrosion cracking (SCC) test for 10 kinds of metal, as shown in Table 1, has been carried out from Dec. 1984 for sensitized specimens by double U bend method in an experimental room at the Inada quarry. The results of 1.5 years experiment show the susceptibility of type 304 L stainless steel and Hastelloy C to SCC among 10 alloys.

Fig. 1 summarizes the patterns of crack growth of the notched specimens of these materials. According to the results of ground water analysis, the aqueous concentration of  $\text{Cl}^-$  and  $\text{SO}_4^{2-}$  in the test holes were 3.5 ppm and 3 ppm respectively. It is difficult to rank the susceptibility to SCC of candidate materials only from these results. In the range of this experimental condition it decreases in the order of type 304L stainless steel, Hastelloy C, type 304EL stainless steel, Inconel 600, Inconel 625 and Incoloy 800.

It is important to perform this kind of test for a long period in the durability evaluation point of view. As for such materials as 304L stainless steel and Hastelloy C which cracked in the early stage of the test, the cause should be analysed in detail to understand the mechanism of crack propagation. It is also important to carry out the tests by using of a lot of specimens to evaluate its life statistically. We are now carrying out the SCC test under gamma-ray irradiation simulating the disposal condition as described in 2.2.1. As a next step, the test should be performed in the underground condition to evaluate the corrosion behavior in the real repository condition.

Table 1 Chemical composition and heat treatment

Alloy	Element (%)										Heat treatment
	C	Si	Mn	P	S	Ni	Cr	Fe	Mo	others	
SUS 304 ss	0.075	0.52	0.95	0.010	0.024	9.2	18.22	bal.	—	—	700°Cx100min→A.C. →500°Cx24h→A.C.
SUS 304L ss	0.035	0.46	0.96	0.032	0.004	8.52	18.11	bal.	—	—	
SUS 304EL ss	0.015	0.59	1.50	0.034	0.003	10.20	18.16	bal.	—	—	
SUS 309S ss	0.14	0.56	1.53	0.023	<0.005	14.30	23.76	bal.	—	—	1050°Cx30min→W.C. →700°Cx100min→A.C. →500°Cx24h→A.C.
Incoloy 825	0.003	0.34	0.68	0.020	0.002	40.66	22.41	bal.	3.00	Cu;2.0 Ti;0.8 Al;0.10 Al;0.16	
Inconel 600	0.050	0.33	0.50	0.004	0.001	bal.	15.37	6~10	—	Cu;0.5max Nb;3.65	
Inconel 625	0.05	0.25	0.25	0.007	0.008	61.0	21.5	3.89	9.00	Ti;0.2 Al;0.20	1100°Cx30min→W.C. →700°Cx100min→A.C. →500°Cx24h→A.C.
Hastelloy C*	0.1	0.7	0.7	—	—	57	16	5	17	W;4	
Ti code 12*	0.012	—	—	—	—	0.84	—	0.09	0.34	Ti;98.9	
Ti	0.045 Fe, 0.069 O, 0.0026 H, 0.0045 Ni, 99.88 Ti										700°Cx100min→A.C. →500°Cx24h→A.C.

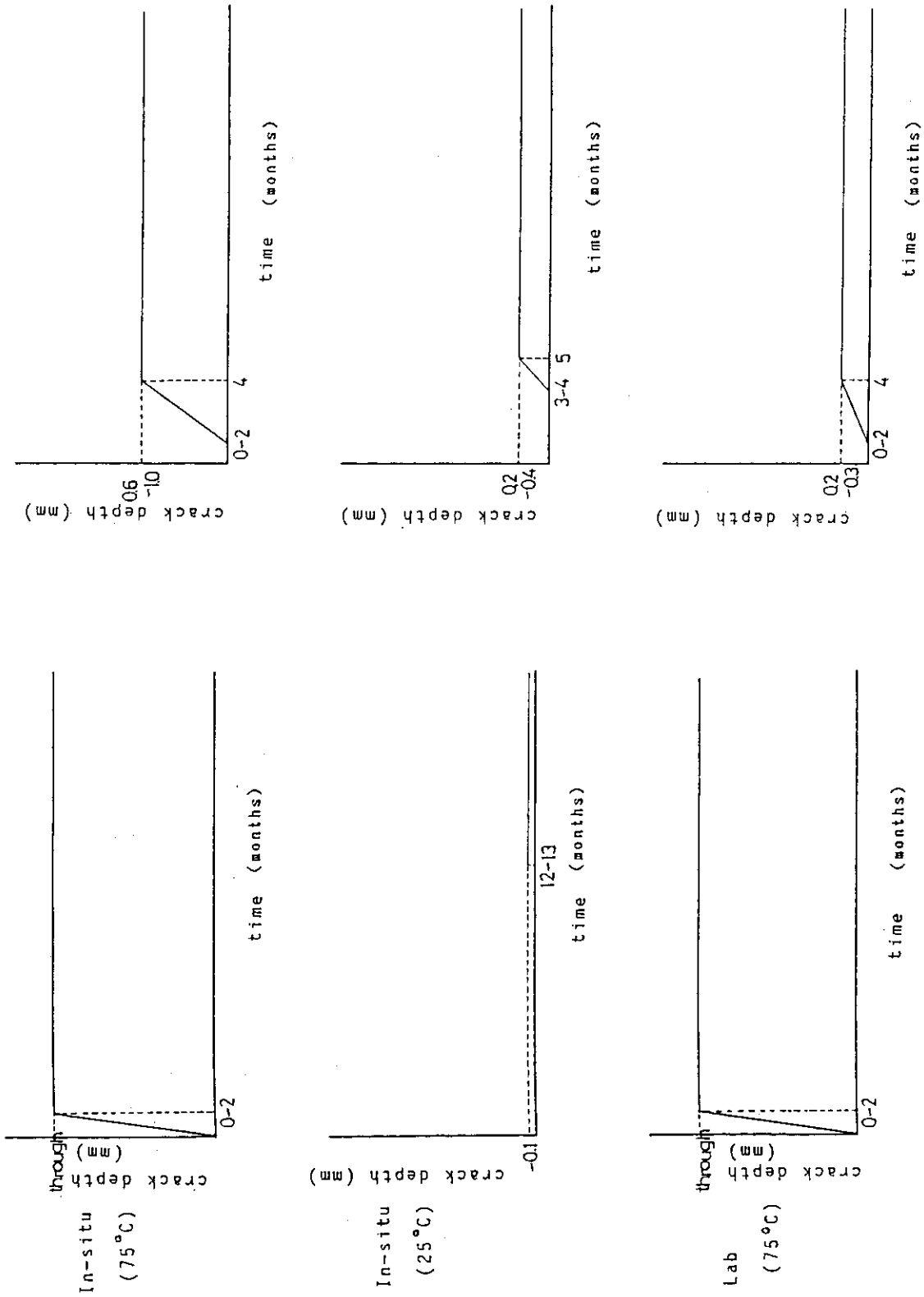


Fig. 1 Crack growth patterns of two alloys during in-situ

stress corrosion cracking test

( right: type 304 ss, left: Hastelloy C )

## 2.3 Nuclide migration experiment

### (1) Diffusion of "non-sorbing" ions in rock pores

H. Kita

#### [Introduction]

In a safety assessment of the high-level waste disposal in deep geological formations, it is generally recognized that radionuclides are transported to the biosphere by groundwater flows through the fracture networks within the rock body.

Besides the radionuclide transport with moving groundwater, the importance of radionuclide diffusion in pores and micro-fissures in rock matrix must be recognized. In the case of no groundwater flow or a very little flow in no-fractured rock matrix, diffusion is a main mechanism of radionuclide migration. Even in the case of considerable groundwater flow in fractured rocks, diffusion coefficient of radionuclide through the pore of rock matrix is one of basic parameters of radionuclide retardation in the perpendicular direction to the main fracture.

Measurements of diffusion coefficients of an "non-sorbing" ion were conducted on granite and tuff samples, which were selected as typical igneous and sedimentary rocks in Japan, using iodide anion as a tracer.

#### [Experimental]

Diffusion experiment was carried out at ambient temperature using an acrylic resin cell divided into two compartments by a disc rock sample of 30 mm in diameter and 5 mm thick (Fig. 1).

The rock samples having no oriented major fissures were sealed into acrylic resin holders. These holders were screwed on the center cell walls and the sealing between the holders and cell walls were provided by "o" rings and silicon sealant.

One compartment provided a reservoir of diffusing species, and the other a measurement cell. The measurement cell was filled with 600 ml of distilled water and the reservoir cell was filled to an equal depth with 1 M KI solution. Prior to experiments, the rock samples were saturated with distilled water by immersing them for several days.

Iodide concentration in the measurement cell was measured as a function of time, using an ion selective electrode directly into the measurement cell.

## [Results and Discussion]

Fig. 2 shows the concentration of iodide anions which have diffused through pieces of a granite sample from Inada and a tuff sample from Izu, as a function of time. The curves can be fitted to straight lines by the asymptotic solution of the diffusion equation (Bradbury, 1982; Shagius and Neretnieks, 1986):

$$C_2 = (D_e C_1 A / V l) t - \alpha A l C_1 / 6 C_2 V$$

where  $D_e$  is the effective diffusion coefficient,  $C_1$  the concentration in the reservoir,  $C_2$  the concentration in the measurement cell (with  $C_2 \ll C_1$ ),  $A$  the cross-sectional area of the rock sample,  $l$  the sample thickness,  $V$  the volume of distilled water in the measurement cell,  $t$  the time. The rock capacity factor  $\alpha$  is defined here by

$$\alpha = \epsilon + \rho R_d$$

with the porosity  $\epsilon$ , the density of rock  $\rho$  and the distribution ratio  $R_d$ .  $D_e$  and  $\alpha$  can be obtained respectively from the slope and the intercept of the fitted straight line.

The diffusion results for the granite and tuff samples are given in Table 1. A good agreement of two values of  $D_e$  determined by two different runs for the granite sample can be noticed. However there is a difference of a factor of about 2 for the  $D_e$  values obtained by a duplicate run for the tuff sample.

$\alpha$  is the sum of a physical contribution such as porosity and a chemical contribution such as sorption, but the present experiment only yields an apparent value of  $\alpha$  and so the each contributions of the porosity and the sorption cannot be separated. If the iodide anion has no sorption on rocks ( $R_d=0$ ) then  $\alpha = \epsilon$ . It seems that the  $\alpha$  values for the granite samples are larger than the porosity for no-fissured granites (about 0.01 in this case). It could be explained by a sorption of the iodide anion on these rocks. It is difficult to measure the distribution ratio for weakly sorbed species, so an independent measurement of the porosity is needed to estimate values of  $R_d$ .

$D_e$  is derived independently of  $\alpha$ . This means that diffusivity can be determined by this technique, with an accuracy of at least an order level, although further detailed studies of contributions of  $\alpha$  are required.

The  $D_e$  values of two rock types show that the diffusivity of iodide anion is much larger in the tuff sample than in the granite sample. This



fact can be understood by the difference of their porosities (0.2 for the tuff sample and 0.01 for the granite sample).

[References]

Bradbury, M.H., Lever, D., and Kinsey, D., 1982. Aquous Phase Diffusion in Crystalline Rock, in Scientific Basis for Nuclear Waste Management V. vol. 11, pp. 569-578, Elsevier, New York.

Skagius, K., and Neretnieks, I., 1986. Porosity and Diffusivities of Some Nonsorbing Species in Crystalline Rocks, Water Resources Research, vol. 22, No. 3, pp.389-398.

Table 1 Results of the diffusivity and  $\alpha$  value determinations.

	$D_e$ ( $m^2/s$ )	$\alpha$
Granite	$2.2 \times 10^{-12}$	0.31
	$2.6 \times 10^{-12}$	0.09
Tuff	$5.3 \times 10^{-11}$	0.20
	$9.3 \times 10^{-11}$	0.33

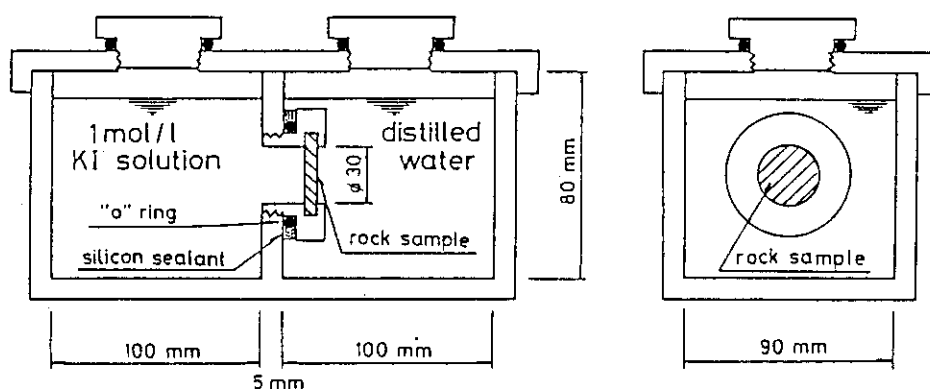
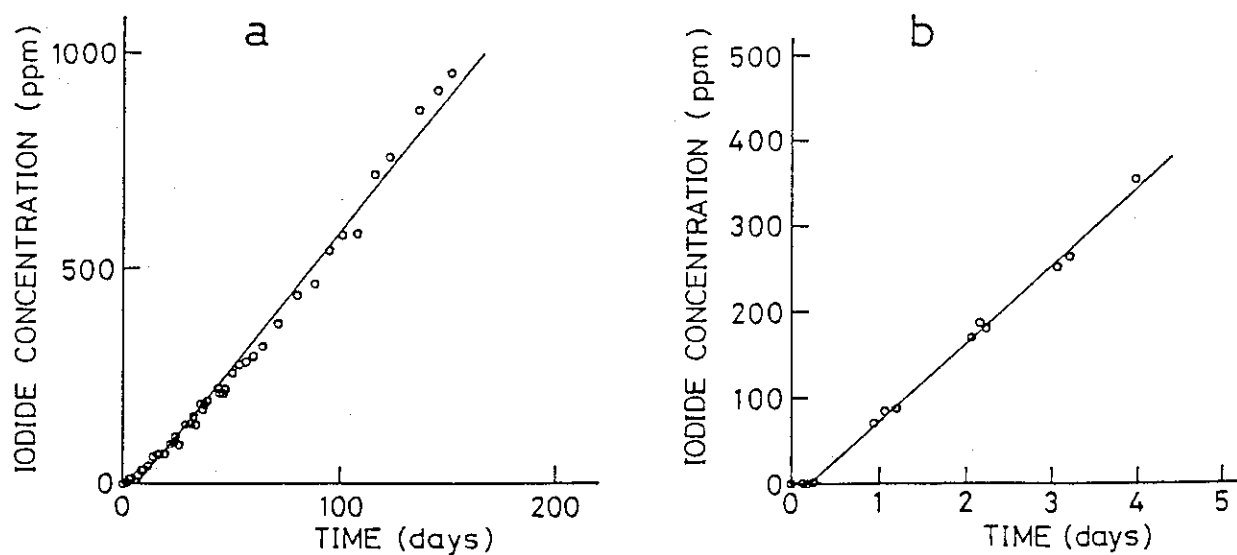


Fig. 1 Description of the diffusion cell.

Fig. 2 The diffusion of iodide anion through rock discs.  
a):granite, b):tuff.

## 2.4 Natural analogue

### (1) Red coloration of a granitic rock along fractures

S. Nakashima

#### 1) Introduction

Application of natural phenomena to the safety evaluation of radioactive waste disposal has many approaches covering various disciplines. Among many aspects of this "natural analogue" study, a) elucidation of mechanisms of trace element migration-fixation processes in geosphere which might also work for waste radionuclides, and b) evaluation of their quantitative aspects in a geological time scale, are of primary importance.

Study of microphases in minerals and rocks, which are supposed to play an important role in radionuclide migration-fixation, is now in progress. The characterization of microphases in minerals such as micro-inclusions, crystal defects, crystal boundaries and metamict minerals by means of microanalytical devices will provide useful informations on possible sites for radionuclide fixation and on the long-term stability of fixed radionuclides in these sites. An example of this approach is presented below.

#### 2) Fixation of groundwater elements in crystalline phases

##### (a) Red coloration of feldspars along fracture

Occurrence of red feldspars are common in alteration zones of feldspar-bearing rocks, especially granitic rocks. This phenomenon can be considered to be a clear evidence of groundwater-rock interaction. The origin of red color of these altered feldspars has been considered to be the presence of iron, but its chemical form in feldspars has not yet been well established. Iron can be present in the crystal structure, as iron-bearing microcrystals such as hematite(1) or as iron staining on the grain boundaries and cleavage planes (2).

##### b) Microphase characterization in minerals

Scanning electron microscopy equipped with energy dispersive X-ray analyzer (SEM-EDX) was applied to characterize the microphases in a red feldspar from altered granitic rock from Northwest Kyushu, Japan. Red feldspars are observed only in alteration zones along fractures (Fig. 1). Among feldspars of this altered zones, white feldspars are also recognized together with red feldspars.

SEM-EDX analyses of these altered feldspars having both whitish and reddish parts indicate that potassium rich parts correspond to the whitish parts. The reddish parts appear to correspond to the Na-Ca rich parts (Plagioclase molecule:  $\text{NaAlSi}_3\text{O}_8$ - $\text{CaAl}_2\text{Si}_2\text{O}_8$ ). Iron is found to be present in a part of these Na-Ca rich parts in the order of 20  $\mu\text{m}$ , while no iron was detected by this SEM-EDX technique in plagioclase feldspars from less altered zone. Quantitative analyses of these Fe rich phases in red altered feldspars reveal that they are epidote group minerals  $[\text{Ca}_2(\text{Al}, \text{Fe}^{3+})_3\text{Si}_3\text{O}_{12}(\text{OH})]$ , which contains generally  $\text{Fe}^{3+}$  replacing  $\text{Al}^{3+}$  of the crystal structure. But these minerals have greenish, yellowish or greyish colors and do not show pink or red colors except for the presence of  $\text{Mn}^{2+}$  in Ca site, which is not the case here. We should then look for submicron iron containing microphases in order to elucidate the origin of the red color of these altered feldspars.

Transmission electron microscopy equipped with energy dispersive X-ray analyzer (TEM-EDX) was used to search for submicron phases in red altered feldspars. This technique reveals the presence of iron minerals in the order of 0.5  $\mu\text{m}$ . We are now trying to characterize these microcrystals by means of electron diffraction technique in order to know if they are iron oxides such as hematite ( $\text{Fe}_2\text{O}_3$ ) or iron hydroxides such as goethite ( $\text{FeO}\cdot\text{OH}$ ).

A tentative explanation of the red color in the altered feldspars studied here is the presence of iron containing submicron microphases such as hematite in plagioclase feldspars. These irons, which can be supplied by groundwaters during alteration of iron bearing minerals (for instance, hornblende in this study), might be precipitated as iron oxides or hydroxides into favorable sites in minerals. Similar phenomena can be supposed for some dissolved radionuclides in groundwater.

Trace element fixation in the form of microinclusions in minerals can be the main mechanism of water-rock interaction in the present case. On the other hand, it should be noted also that calcium sites in rocks can be one of the possible sites for the fixation of dissolved metal cations, having higher valence states and larger ionic radii. In fact, rare-earths, U and Th are commonly found to be present in Ca-containing natural minerals such as allanite. The close exchange relationship between Ca and U in the course of water-rock interaction has been already noticed (3). The calcium sites in minerals, together with microinclusions, grain boundaries and crystal defects, are then considered to play an

important role in the radionuclide immobilization.

These results suggest applications of microphase characterization techniques to the study of trace element migration and fixation in rocks, as a natural analogue to the radioactive waste disposal.

(c) Water in altered minerals

A first trial of the application of infrared microspectroscopy to the characterization of minerals is in progress (a). The infrared spectra of  $20 \times 20 \mu\text{m}$  area of the above mentioned feldspars were measured. Red altered feldspars appear to have higher content of molecular water (peak around  $3630 \text{ cm}^{-1}$ ) than less altered white feldspars (Fig. 2). This result shows an evidence of hydrolysis of feldspars along groundwater paths. Analyses of spatial distribution of water (OH and  $\text{H}_2\text{O}$ ) by means of infrared microspectroscopy can be then useful in evaluating spatial distribution of influence of groundwater which is related to alteration front.

(d) Alteration front in rocks

The studied red coloration of feldspars in granitic rocks are limited to only a few centimeters width from the fracture (Fig. 1). This width of red colored zone can be considered to be an example of spatial limit of groundwater-rock interaction : alteration front.

A numerical model for the evaluation of this alteration front was applied recently by FUJIMOTO (1987) to explain spatial distributions of natural alteration zones of rocks (5). The author employed the term  $\rho V/Ak$  as an indicator of the alteration width, based on the following one dimensional mass balance equation in the case where the diffusion of an element in water is negligible compared with the water velocity:

$$\frac{\partial C_i}{\partial t} = -V \frac{\partial C_i}{\partial x} + \frac{Ak}{\rho} (C_{ieq} - C_i) \quad (1)$$

$C_i, C_{ieq}$  : concentration of species i in water and that in equilibrium state.

$\rho, V$  : density of water and water penetration velocity

$A$  : contact area of rock and water

$k$  : rate constant of a first-order reaction such as dissolution and precipitation

t : time

x : distance from the starting point of rock column.

This kind of approach can be used in evaluating quantitatively the spatial limit of water-rock interaction.


#### REFERENCES


1. DEER W.A., HOWIE R.A. and ZUSSMAN J. (1966). An introduction to the rock forming minerals. Longman, London.
2. ISSHIKI N. (1958). Notes on rock-forming minerals (3) Red coloration of anorthite from Hachijo-jima. J. Geol. Soc. Japan, 64, 644-647.
3. NAKASHIMA S. and IIYAMA J.T. (1983). Behavior of uranium during the formation of granitic magma by anatexis (II). Influence of major element cations on the mobility of uranium. C.R. Acad. Sci. Paris. t.296, serie II. p.1425-28. (in French)
4. NAKASHIMA S. (1987). Infrared microspectroscopy of minerals: a new microphase characterization technique in earth sciences. NIHONDENSHI News, 27, 1-2, 12-17. (in Japanese)
5. FUJIMOTO K. (1987). Factors to control the width of a partially altered zone. Mining Geology, 37.1, 45-54. (in Japanese)




Fig.1 Schematic drawing of a red altered granitic rock sample from Northwest Kyushu, Japan.

F : fracture filled with prehnite:  $\text{Ca}_2(\text{Al}, \text{Fe}^{3+})_2\text{Si}_3\text{O}_{10}(\text{OH})_2$

: feldspars with dots representing schematically the density of reddish color

: quartz

: black to greenish black minerals such as hornblende and chlorite.

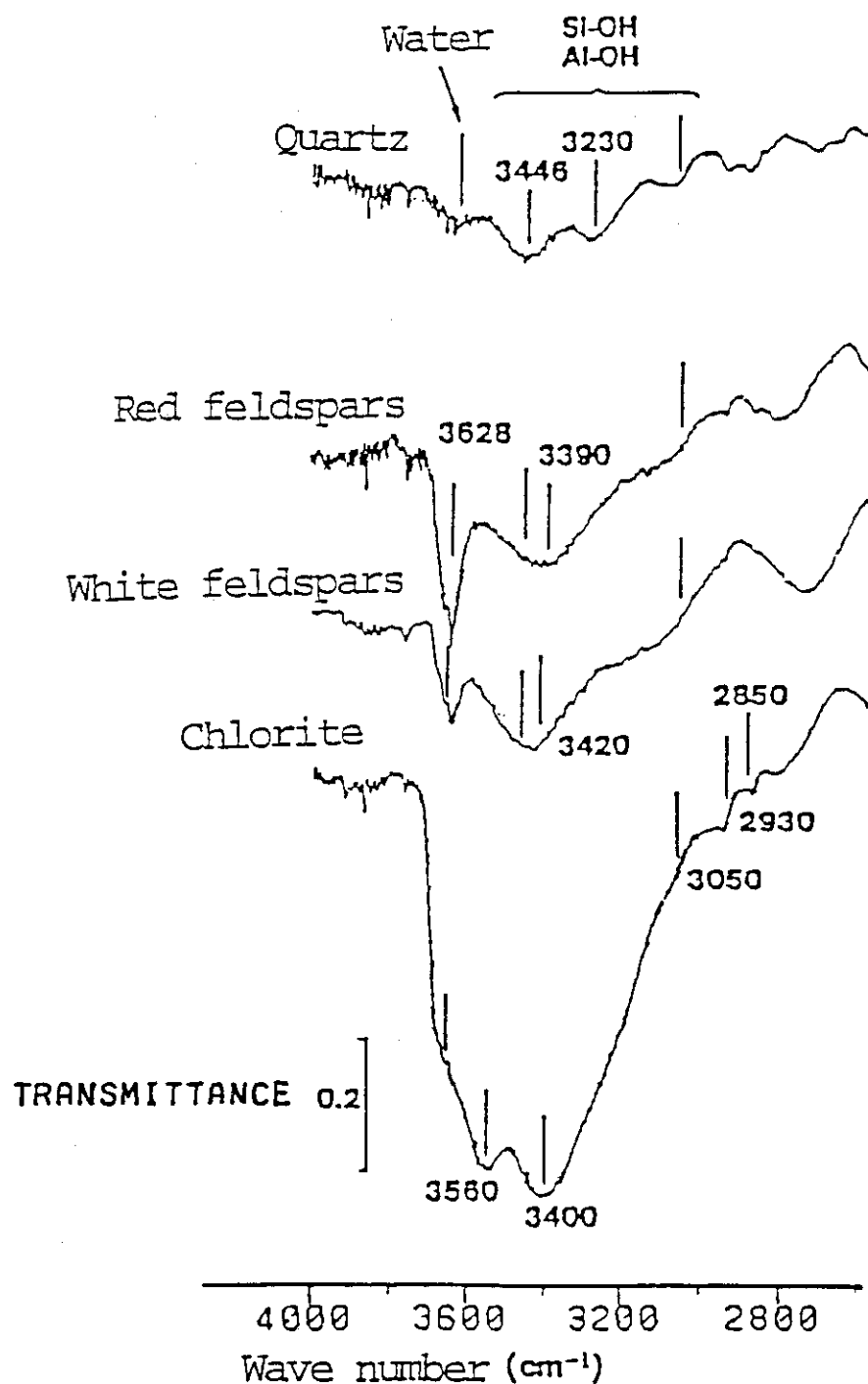


Fig.2 Infrared spectra of 20 x 20  $\mu\text{m}$  area of minerals in the red altered granitic rock. Broad bands at 3000–3500  $\text{cm}^{-1}$  can be attributed to OH groups bound to Si and Al, while a sharp band at 3628  $\text{cm}^{-1}$  can be due to molecular water in minerals.



## 2.5 Subseabed disposal

S. Nakashima

Subseabed disposal of high-level radioactive wastes is considered to be an alternative future option for the radioactive waste disposal. This option has been evaluated internationally by many investigators under the organization of OECD/NEA. After having studied main properties of deep-sea sediments by an international cruise for deep-sea drilling-penetrating programs, OECD/NEA organized another project for evaluating hole closure characters after the penetrator input (HOCUS: Hole Closure Experiments in Sediments). We participated in this HOCUS project by sampling and analyzing sea floor sediments before and after the penetration at Antibes site in the North-west French Mediterranean continental shelf during November 1986. Our main purpose of the participation is to know if the sediment characters are disturbed by the penetration in the light of the distribution of redox-sensitive elements.

- (1) Distribution of redox-sensitive elements in undisturbed and disturbed sea floor sediments at Antibes site, France taken during HOCUS project.

S. Nakashima

### [Introduction]

The redox environment in the sediments causes the redistribution of several redox-sensitive trace metals such as U, Mn, Cu, Ni and V (BONATTI et al., 1971). The distribution of these elements are closely related to the presence of organic matter and the redox processes resulted in concentration peaks of these elements at the same depth in the depth profile (COLLEY et al., 1984). Consequently, the concentration peaks of these elements can be taken as certain key beds in sea floor sediments.

In order to study the hole closure state after the penetration of several penetrators in sea floor sediments, aiming the safety assessment of the seabed disposal of radioactive wastes, vertical distribution of several redox-sensitive elements were investigated on the uppermost 200cm of the two sediment cores: one from the undisturbed part and another from the penetrated part. The vertical distribution of these elements will provide informations on sediment mixing, caused by the hole closure during and after the penetration.

## [Methods]

The Antibes site is situated at about 5 km from Antibes in the North-west French Mediterranean Sea.

One of the undisturbed sediment cores (K5) was taken from the clayish sediments at the water depth of 266 m. The disturbed sediment core (No.3) was taken inside the BRE penetrator hole. The BRE penetrator has a diameter of 35.6 cm, a length of 300 cm and a weight of 1500-1600 kg. This penetrator was launched from the ship CASTOR 02 and the depth of penetration in the sediments from the tail of the penetrator is 6.5 m. A 6 m core was taken inside this penetrator hole. The position of this core is about 150 m east-southeast from the core K5. The water depth is about 266 m, which is about the same depth as that of the core K5. The appearance of the sediments is just the same as that of the core K5.

Subsampling of the sediments were made on land by using a plastic box of 2 cm cube on these two cores every 20 cm from the top of the cores downward to 200 cm.

The subsamples were dried at 110°C and ground in agate. Organic carbon and carbonate contents were determined using an induction furnace and hydrochloric acid decomposition treatments. Transition metal elements were analyzed by ICP on the solution prepared by an acid decomposition of sediments. Uranium content was determined on the sample solution by a colorimetry using Arsenazo III.

## [Results and Discussion]

## Undisturbed sediments

Depth profiles of the element contents on a dry sediment basis in the undisturbed sediments (core K5) are presented in Fig. 1. The carbonate content as CO<sub>2</sub> wt % is homogenous around 16 %, reflecting a homogenous feature of the sediments throughout 200 cm.

The redox front can be set in the depth profiles of U, Mn and organic carbon contents of the sediments by a concentration peak of U which is accompanied by an increase of organic carbon content and by a decrease of Mn content (WILSON et al., 1985). Though this type of redox front is not so clear in the present case, it can be tentatively set around the depth of 40 cm.

The organic carbon content shows higher values at 20 cm, 60 cm and 120-160 cm. This pattern appears to have no correlation with U and Mn

contents. On the other hand, Cu, Ni and V contents have their peaks at similar depths (20 cm, 80 cm and 120-140 cm) to that of organic carbon. This fact suggests some associations of these transition elements with organic matter. The present sediment core can be considered to have three layers enriched in organic carbon, Cu, Ni and V at depths of 20 cm, 60-80 cm and 120-160 cm.

#### Disturbed sediments

Depth profiles of the element contents on a dry sediment basis in the disturbed sediment core No.3 (C3) is presented in Fig. 2. The carbonate content appears to have a homogeneous feature around 16 % just as the case of the undisturbed sediment core.

The redox front is difficult to determine in this case because of an absence of a decrease of Mn content in the uppermost part of the core. However, a peak of U content can suggest the redox front around 40 cm, which is similar to that of the undisturbed sediments.

The organic carbon content is high at 5 cm, 85 cm and 165 cm, while those of Cu, Ni and V have their peaks around 5 cm, 85 cm and 125 cm. Despite some difference at the deeper part between the peak positions of organic carbon and those of Cu, Ni and V, the sediments can be considered to have three layers rich in organic carbon, Cu, Ni and V in the 200 cm core around 5 cm, 85 cm 125-165 cm. The positions of these layers are very similar to those of the undisturbed sediments.

The vertical distribution of U in this core has somewhat inverse feature comparing with that of organic carbon. This fact suggests that most of U may not be bound directly to organic matter. This opposite distribution between U and organic carbon can be explained by a hypothesis that a part of organic matter can be consumed directly to precipitate U from pore waters by a reduction process during sediment diagenesis. The direct uranium reduction capacity of some types of organic matter has been already noticed (NAKASHIMA et al., 1984). The U content profile shows a different distribution pattern, especially at the deeper part of the cores, between undisturbed and disturbed sediments. An increasing feature downward to 200 cm in the undisturbed sediments is opposed by a decreasing feature in the disturbed sediments. This fact leaves a possibility of a drag, by the penetrator, of the sediments at the deeper part of the core. However, the depth profiles of other elements do not confirm this hypothesis, except for that of organic carbon.

## [Conclusions]

All these results suggest that the surface sediments disturbed by the penetrator show no significant change in vertical distribution of several redox-sensitive elements, except for U and organic carbon at the deeper part, during the penetration and the hole closure. No dramatic vertical mixing of the uppermost sediments during the hole closure can be then supposed. However, it should not be neglected that dissolved oxygens introduced by the penetration may alter the redox environment resulting in the decrease in barrier properties, in terms of reduction processes, for the radionuclides originating from radioactive wastes disposed by penetrators in seabeds.

## [References]

- BONATTI E., FISHER D.E., JOENSUU O. and RYDELL H.S. (1971). Post-depositional mobility of some transition elements, phosphorous, uranium and thorium in deep sea sediments. Geochimica et Cosmochimica Acta, 35, 189-201.
- COLLEY S., THOMSON J., WILSON T.R.S. and HIGGS N.C. (1984). Post-depositional migration of elements during diagenesis in brown clay and turbidite sequences in the North East Atlantic, Geochimica et Cosmochimica Acta, 48, 1223-1235.
- NAKASHIMA S., DISNAR J.-R., PERRUCHOT A. and TRICHET J. (1984). Experimental study of mechanisms of fixation and reduction of uranium by sedimentary organic matter under diagenetic and hydrothermal conditions. Geochimica et Cosmochimica Acta, 48, 2321-2329.
- WILSON T.R.S., THOMSON J., COLLEY S. HYDES D.J., HIGGS N.C. and SORENSEN J. (1985). Early organic diagenesis: The significance of progressive subsurface oxidation fronts in pelagic sediments. Geochimica et Cosmochimica Acta, 49, 811-822.

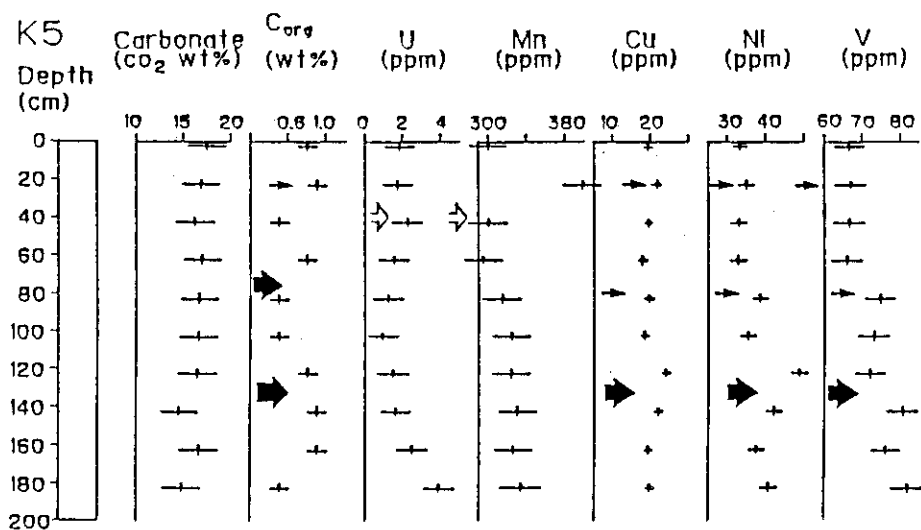


Fig.1 Solid phase concentration-versus-depth profiles for carbonate (as CO<sub>2</sub>), organic carbon, U, Mn, Cu, Ni and V for the undisturbed sediment core K5. Their concentrations are expressed in wt % or ppm on a dry sediment basis.

→: possible layers rich in organic carbon, Cu, Ni and V  
 ↪: possible redox front.

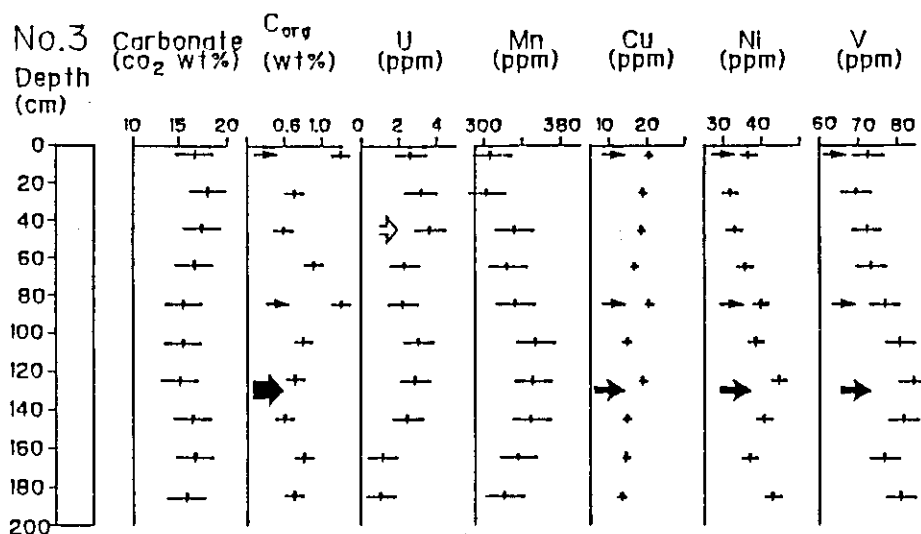


Fig.2 Solid phase concentration-versus-depth profiles for carbonate (as CO<sub>2</sub>), organic carbon, U, Mn, Cu, Ni and V for the disturbed sediment core taken inside the penetrator hole C3 (No.3). Their concentrations are expressed in wt% or ppm on a dry sediment basis.

→: possible layers rich in organic carbon, Cu, Ni and V  
 ↪: possible redox front.

## 2.6 Model for safety assessment

H. Kimura

## (1) Numerical model of radionuclide migration

Computer code MIG2DF was developed to quantify radionuclide migration from the radioactive waste repository to the biosphere. MIG2DF finite element code can handle radionuclide transport and saturated-unsaturated groundwater flow in the two dimensional porous medium. In this model, the fluid properties are assumed to be independent of concentration of nuclide, and the adsorption reaction is described by linear isotherms. The radionuclide convective and dispersive transport equations are solved by using Upstream Finite Element Method to eliminate the oscillation of numerical solutions when convective transport dominates the dispersive one.

The governing equation describes the convective-dispersive transport, radioactive decay and retardation by the adsorption of nuclide:

$$R_k \frac{\partial C_k}{\partial t} = \text{div}(\underline{D} \text{grad } C_k) - \text{div}(C_k \vec{u}) - \lambda_k R_k C_k + \lambda_{k-1} R_{k-1} C_{k-1} + Q_k \quad (1)$$

where  $R_k$  is the retardation factor of radionuclide  $k$ ,  $C_k$  is the concentration of radionuclide  $k$ ,  $\underline{D}$  is the dispersion coefficient tensor and is given by

$$D_{ij} \equiv D_T |\vec{u}| \delta_{ij} + (D_L - D_T) \cdot \frac{u_i u_j}{|\vec{u}|} + D_d \tau \delta_{ij} \quad (2)$$

$D_T$  is the transverse dispersion coefficient,  $D_L$  is the longitudinal dispersion coefficient,  $D_d$  is the molecular diffusion coefficient,  $\tau$  is tortuosity,  $\vec{u}$  is the Darcy velocity,  $\lambda_k$  is the decay constant of radionuclide  $k$  and  $Q_k$  is the source term of radionuclide  $k$ . This equation is discretized in space using Bubnov-Galerkin method and discretized in time by Crank-Nicholson method. The non-linear equation is solved by a kind of successive substitution method.

We calculated one dimensional radionuclide migration problems to verify MIG2DF code, and got good agreements with the analytical solutions.

## (2) HYDROCOIN study

HYDROCOIN (International project for studying groundwater hydrology modelling strategies) level-2 study deals with validation of models using field and laboratory experiments and comprises five cases. We calculated four cases (case 1, 3, 4, 5) of level-2 study using 2D-SEEP and 3D-SEEP code, and got reasonable agreements with experimental data.

Calculated result of level-2 case 4 problem, a three dimensional regional groundwater flow in low permeability rocks of Piceance Basin, Colorado, USA (Figure 1) is shown as the representative of these studies. The areal extent of the region is about 70-80 km, and the geological formation of this basin is divided into five layers. There are rainfall recharges at the top surface, and drainages along the southern boundary. Figure 2 shows the vertical view of finite element mesh used in the 3D-SEEP code, and figure 3 shows calculated hydraulic heads and heads obtained by kringing from measured values along a straight line in layer 4.

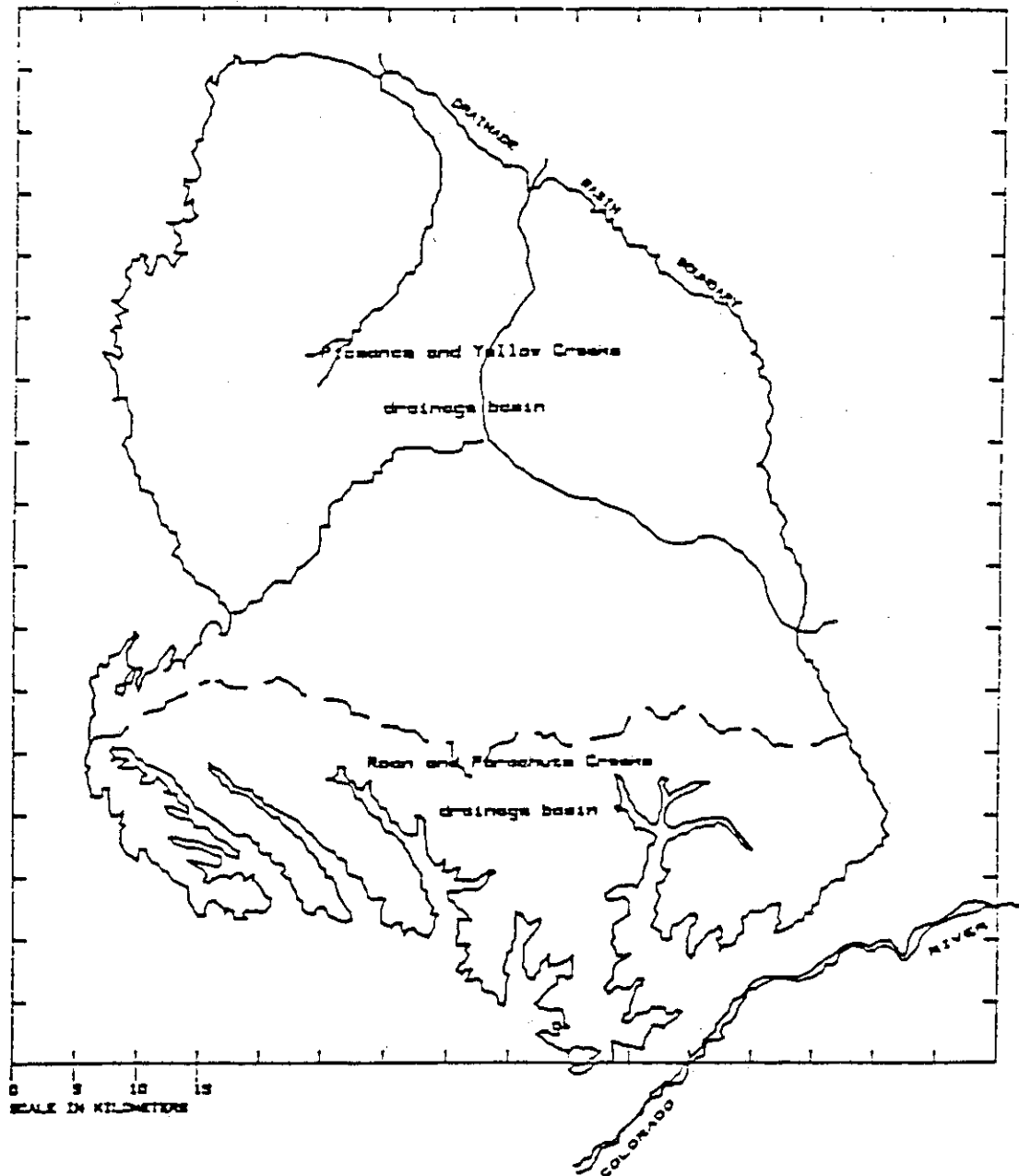


Fig. 1 Map of Piceance Basin, Northwestern Colorado.



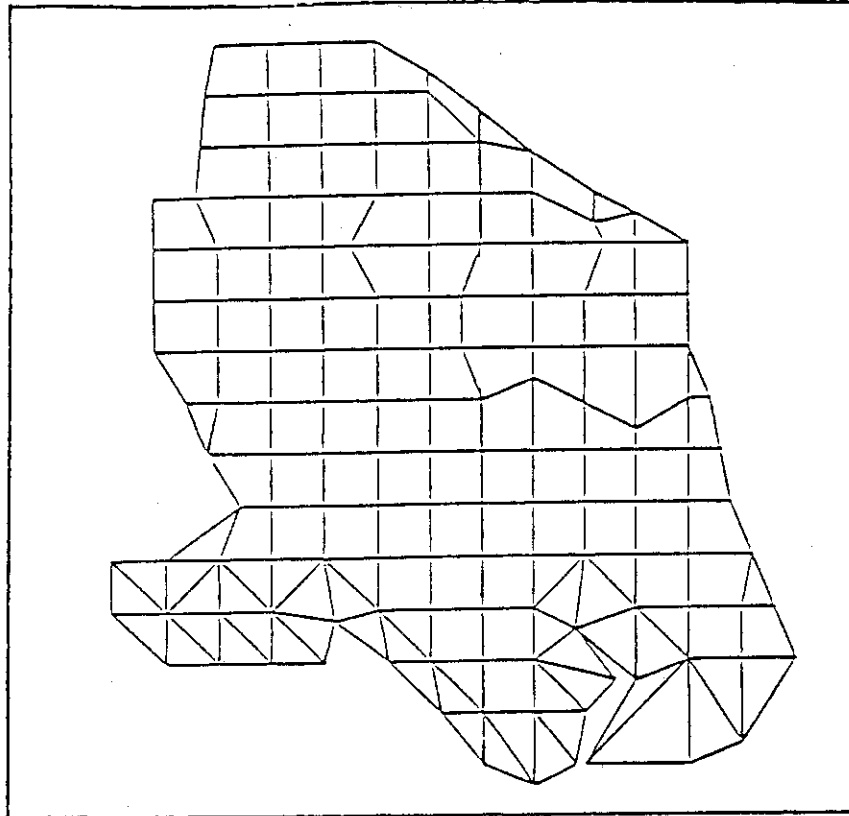


Fig. 2 Finite element mesh

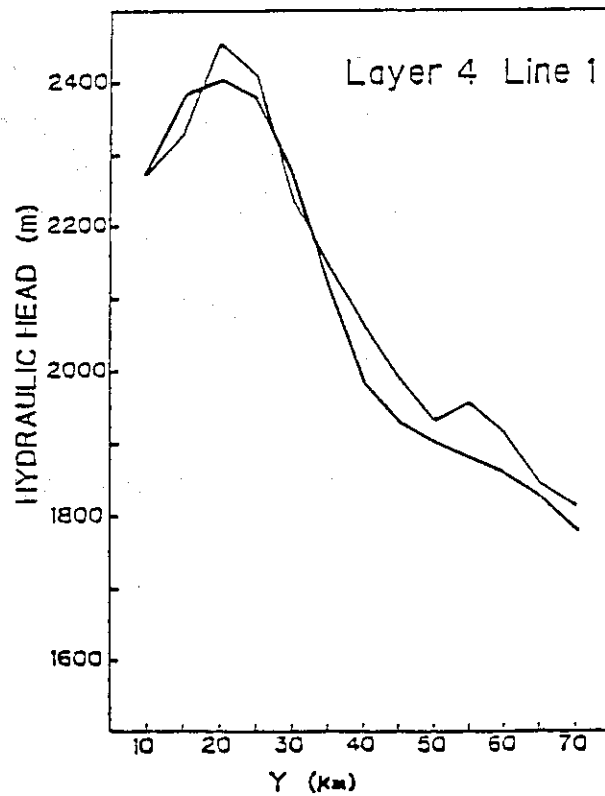


Fig. 3 Predicted heads (thick curves) and heads obtained by kriging from measured values along a straight line in one of the layers.

## 2.7 Conceptual design of repository for safety assessment in the preclosure period

H. Nakamura

Dose to man at accidents in preclosure period can not be neglected even if the probability is very small, because potential radioactivity causing the dose will be high due to the wastes existing near the working area. Examination of possible accidents and development of safety assessment method have been started as five years programme.

Concepts of repository to be discussed in the programme were taken as the first task. The concepts in various projects such as STRIPA, Project Gewähr, Concept in Canada and Basalt project in Hanford, were reviewed and informations on safety designs of underground facilities such as hydroelectric power stations and tunnels were surveyed by contracting the works with a general construction company. A meeting of experts on geology, hydrology and corrosion of metal was held for recommendations.

Potential disposal sites and any designs of disposal facilities have not yet been proposed in Japan. Therefore, various options were considered and their weights of consideration were discussed as follows.

### 1) Length of preclosure period

- 1 Non-monitoring
- 2 Monitoring for short period necessary to confirm the safety designs, especially heating effects on properties of rock mass
- 3 Long-term storage for leaving enough time for the development of new technologies and/or for obtaining much more public acceptance of the disposal options

The order of consideration will be 2 > 1 > 3 .

### 2) Counterplan for water leakage in preclosure period

- 1 Pumping out
- 2 Grouting in order to be no leakage

Option 1 will be mainly considered.

### 3) Packaging for the transport to underground facilities

- 1 Canister
- 2 Canister with metal overpack
- 3 Canister with metal overpack and buffer material

The order will be  $2 > 1 > 3$ . Contact handling together with non-contact one will be considered for 2 and 3.

#### 4) Site

- 1 Mountain -- Hard rock -- deep underground
- 2 Plain -- Soft rock -- non-deep underground
- 3 Continental shelf -- soft rock -- non-deep underground

There are no logical reasons in above combinations, which are selected to reduce cases to be assessed. The order will be  $2 > 1 > 3$ .

#### 5) Shape of disposal tunnel

- 1 Plain type -- Fig. 1-(a)
- 2 Block type -- Fig. 1-(b)
- 3 Silo type -- Fig. 1-(c)

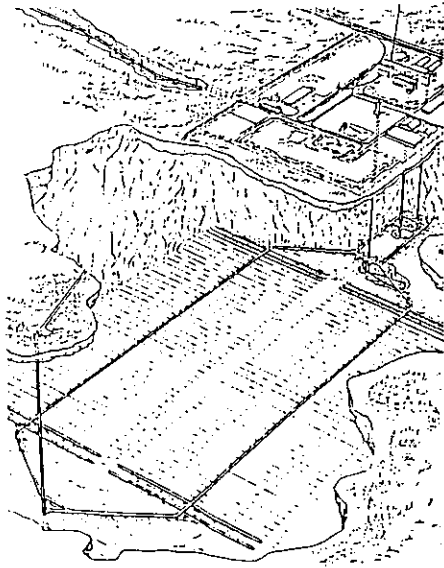
The order will be  $1 > 2 = 3$ . 2 and 3 should be considered more in Japan than others, because the desirable rock mass is available only in a small region.

#### 6) Enplacement position

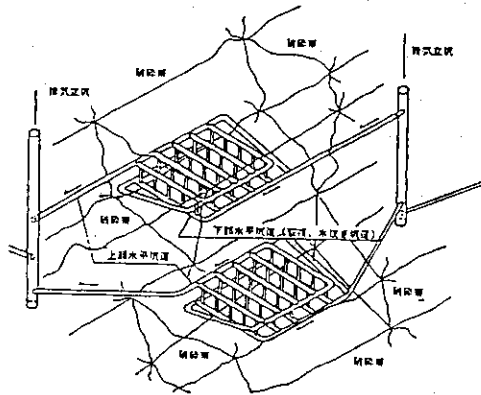
- 1 Center of the tunnel
- 2 Well in the tunnel floor
- 3 Horizontal or vertical tube between two tunnels

The order will be  $2 > 1 = 3$ , but the order will be changed due to other combined options. For instance, when a contact handling option of the waste package is used, 1 will be the desirable option.

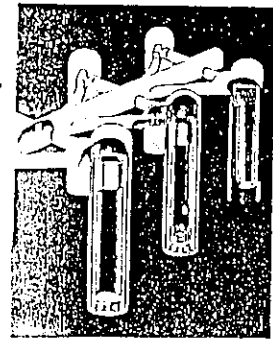
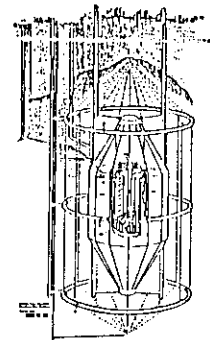
These options and the orders may be changed during further discussion on the programme of safety assessments of disposal facilities in preclosure period.



(a) Plain type



(b) Block type



(c) Silo type

Fig. 1 Shape of disposal tunnel

## 5. 結 言

JRR-2 における炉心の冷却能力低下に至る想定事故の 1 つである「重水流出事故」の解析、評価を行う際に用いる条件（配管破損の位置と規模）について検討し、次のような結果を得た。

- (1) 配管破損に加えて、安全系の 1 つである自然循環弁 DV-5 が故障した場合、結果が最も厳しくなる配管破損位置は、炉心正常水位の下方約 6.8 m にある耐食アルミニウム合金製の炉心入口管である。この配管においては、破損口の最大のもので、孔食によって生じる  $\pi t^2$ 、即ち約 3.4 cm<sup>2</sup> の貫通口を想定しておくのが妥当である。
- (2) 配管破損に加えて、安全系の 1 つである自然循環弁 DV-6 もしくは DV-7 のいずれかが故障した場合、結果が最も厳しくなる配管破損位置は、炉心正常水位の下方約 6.2 m にある SUS 304 製の主重水ポンプ出口管である。この配管においては、破損口の最大のもので、腐食疲労によって生じる  $\frac{1}{4}Dt$ 、即ち約 6.3 cm<sup>2</sup> の貫通き裂を想定しておくのが妥当である。

なお、ここで想定したような破損口が生じた場合においても、「炉心は冠水が維持され、燃料芯材最高温度はブリスト発生温度に比べ十分低く、炉心は大きな損傷に至ることがなく、かつ、十分な冷却が可能である。また、十分に厳しい結果を与える仮定をしても、トリチウムの大気への放出量は小さく、周辺の公衆に著しい放射線被爆のリスクを与えることはない。」との解析、評価結果が得られている。

## 謝 辞

本報告書に示した JRR-2 で想定すべき配管破損の位置と規模についての検討は、JRR-2 原子炉設置許可申請書の変更作業の一環として行われたものであり、同変更作業に携わった多くの人々の御協力を頂いた。とりわけ、燃料工学部長近藤達男氏、燃料工学部材料工学研究室長中島甫氏、研究炉管理部長二村嘉明氏、研究炉管理部 JRR-2 管理課長角田準作氏、研究炉管理部 JRR-2 原子炉主任技術者小金沢卓氏の各位には、多くの御尽力を頂いた。ここに深く感謝の意を表する。

## 付録 研究炉の配管破損解析に関する調査

本報で示した、JRR-2 の配管破損解析と対照させるため、国内及び海外で行われている研究炉の配管破損解析に関する調査を行った。調査結果を付表 1, 2<sup>17)~25)</sup> に示す。この調査結果からわかるように、研究炉の配管破損の形態や規模に関して、本報で示した程度に詳細な検討を行った例は見当たらない。

## 3. Safety Examination of Vitrified Forms in the Hot Cells of WASTEF

S. Tashiro

The WASTEF (Waste Safety Testing Facility) has continued studies on performance and long-term durability of vitrified forms and other materials to be used for high-level waste management.

In the fiscal year, seven vitrified products were made with radioactive simulated wastes for the examinations as listed in Table 1. Preparedness for actual waste treatment, MCC-4 type leaching apparatus, in-cell Synroc apparatus, plutonium adsorption behaviour onto leach container and volatilized radioactive cesium behaviour are described here as main activities at WASTEF.

Behaviour of volatilized radioactive ruthenium, migration behaviour of leached radioactive substances in rocks and accelerated alpha radiation stability tests under beta and gamma irradiation have been also made at WASTEF and such results will be reported in the next year.

Co-operative programs with USNRC and ANSTO (previous AAEC) have also continued in the WASTEF work. Co-operative program with PNC on leaching method of vitrified forms has been finished and will be continued as a new subject on alpha radiation effects in the following year.

In order to take steps to meet expanded subjects at WASTEF, two sets of glove-box were installed connecting to the already used glove-box line. The safety examination of the competent authorities has been cleared.

Table 1 Specification of Vitrified Forms

Serial Number	Volume	Radionuclides in the Forms	The Purpose of Vitrification
H86001	1 l	FP ( 2 mCi)	Preparation of actual waste test
H86002	8.3ml	Np-237 (0.27mCi)	Leachability examination
H86003	8.3ml	Np-237 (0.27mCi)	Leachability examination
H86004	8.3ml	Np-237 (0.27mCi)	Leachability examination
H86005	1 l	FP (4.3 mCi)	Preparation of actual waste test
H86006	1 l	Cs-134 (950 mCi)	Radioactivity balance test
H86007	1 l	Ce-144 ( 4.5 Ci)	Radioactivity balance test

### 3.1 Preparedness for the actual waste treatment

S. Kikkwa and T. Tuboi

It is planned at WASTE F to produce glass samples using actual wastes and carry out the various characterization tests in the next fiscal year of 1987. The actual waste (total volume; 15 liter, specific activity; 300 Ci/liter) will be transported in a Cendrillon container from the PNC Reprocessing Plant. Prior to the treatment of actual wastes at WASTE F, appropriate preparedness has been done for the transportation work between the cask and the receiving vessel in the No. 2 cell, and for the denitration process in the vitrification apparatus. This report describes the results and the future subjects.

#### 1) Transportation work of actual wastes to the receiving vessel in the No. 2 cell using a Cendrillon container

The cask which contains actual wastes will be carried on a trailer into the loading dock of WASTE F and then craned into the isolation room to connect to a pipe line on the back shielding wall of the No. 2 cell using a transportation bridge. Then the liquid waste will be transported into the vessel by a steam ejector which is installed in the No. 2 cell (Fig. 1). To make a series of the work sure, a transportation practice was performed using a simulated liquid waste containing 800 mCi of cerium-144.

During the practice radiation streaming from the bridge pipe line, operation control rode etc. and air tightness of the container were measured.

Table 1 shows the radiation dose rate at various locations during the transportation of radioactivity. It could be estimated based on the result that the radiation dose rate at the handling and the exhaust filter will be approximately 300 mrem/hr and 400 mrem/hr respectively in the case of actual wastes. This needs additional shieldings or other methods for radiation control. Regarding the air tightness test of the container using helium, the leak rate was  $5 \times 10^{-8}$  and this value is sufficiently below the criteria of  $1 \times 10^{-6}$ . It could promise safe transportation of actual wastes.

#### (2) Denitration process with the vitrification apparatus

The actual liquid waste is subjected to be denitrated prior to vitrification with the vitrification apparatus at WASTE F. The process

is performed by addition of nitrous acid and formic acid, and heating up to 100°C. For the preparedness the diagrams of the heating and addition of formic acid were confirmed.

Consequently 20 mole of nitric acid in 10 liter of simulated liquid waste was decomposed by addition of 0.4 mole of nitrous acid and 2.26 liter of formic acid (85%) in 2 liter/hr of flow rate resulting pH 1.4 of the acidity in 2 hours. It is concluded that the result will be sufficient and the method will be preferable for the actual waste treatment.

Table 1 Radiation dose rate during transportation work

Location	Radiation level (mr/h)
A: Gap of operation handle	0.08
B: Upper Cendrillon container	B. G
C: Lower Cendrillon container	B. G
D: Shielding tray	B. G
E: Side bridge	B. G
F: Offgas filter	0.1



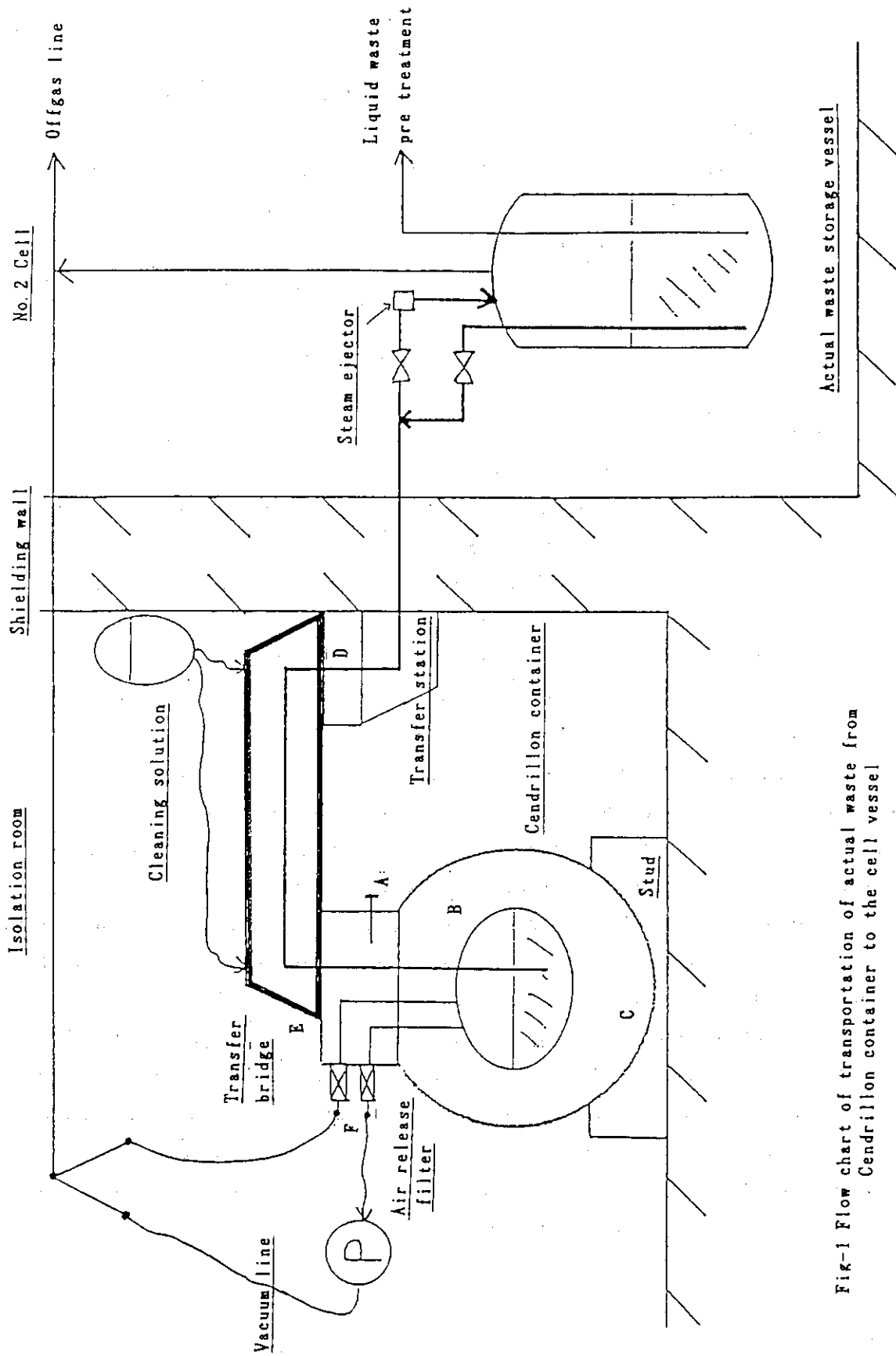


Fig-1 Flow chart of transportation of actual waste from Cendrilla container to the cell vessel

### 3.2 Cold tests with MCC-4 type low flow-rate leaching test apparatus

T. Sagawa

Low flow-rate leaching tests of HLW vitrified forms have been initiated at WASTE-F under the co-operative program with USNRC, using a cold simulated waste form and basalt brine to obtain reference data on the performance of the apparatus prior to the hot tests.

The apparatus has a design preferable to MCC-4 type test and composes of reserve tank, microtube pump, thermo-bath, receiver bottle, pipe line and control panel. The reserve tank of polyethylene provides Ar gas pouring through the cap to prevent the basalt brine from contacting with air. The microtube pumps, three sets of  $10^2$  ml/yr, seven sets of  $10^3$  ml/yr and three sets of  $10^4$  ml/yr, can transfer the leachant from the reserve tank to the leaching cells with a 10 % accuracy of each designed flow-rate. Two sets of the air bath are controlled upto 200 °C with SCR-PID controller. During the tests the temperature in the bath are measured with 10 sets of Pt resistant temperature measuring devices and automatically recorded. The leaching cell of stainless steel are composed of Type A and Type B. The Type A is for specimen of  $10^3 \text{ m}^{-1}$  SA/V. The Type B is for specimen of  $10^2 \text{ m}^{-1}$  SA/V and  $10^{-1}$  SA/V. Supporting stands are also made of stainless steel and the contact area with the glass specimen is smaller than 5 % of the total area of specimen surface. Sampling tube of stainless steel is attached with ribbon heater to keep the sampled leachate at the same temperature as in the leaching cell so that no component deposits to the inner wall of tube will be formed.

The cold tests were started in January 1987 and will end in July 1987. Two types of specimen are used. One is pineapple-sliced specimen for  $10^3$  and  $10^2 \text{ m}^{-1}$  SA/V, another is block specimen for  $10 \text{ m}^{-1}$  SA/V. The experimental parameters concerning the relationship between specimen and flow-rate are summerized in Table 1. The leaching temperature is kept at  $90 \pm 1$  °C. The acidity and the leached substance contents of sampled leachate are measured. Figure 1 shows boron concentration of leachate in relation with leaching time giving a reasonable result and proving good operation as an intermediate evaluation.

Table 1 Planned experimental parameters of the cold test

Test.no	Cell	Specimen	SA/V (m <sup>-1</sup> )	Pump rate (ml/year)	Sampling Frequency (days)	Feeding mode (Pulsed or continuous)	& Flow rate
1	Type A	Type A	* 10 <sup>3</sup>	1 0 0	6 5	P.	17.8ml/65days
2		Blank	—	1 0 0	6 5	P.	17.8ml/65days
3		Type A	* 10 <sup>3</sup>	1 0 0 0	2 0	C.	2.74ml/day
4		Type A	* 10 <sup>3</sup>	1 0 0 0	2 0	C.	2.74ml/day
5		Blank	—	1 0 0 0	2 0	C.	2.74ml/day
6	Type B	Type A	** 10 <sup>2</sup>	1 0 0 0	2 0	C.	2.74ml/day
7		Type A	** 10 <sup>2</sup>	1 0 0 0	2 0	C.	2.74ml/day
8		Type B	** * 10	1 0 0 0	2 0	C.	2.74ml/day
9		Tepe B	** * 10	1 0 0 0	2 0	C.	2.74ml/day
10		Type B	** * 10	1 0 0 0 0	Sampling on 4.8.16 and every 16days	C.	27.4ml/day
11	Type B	Type B	** * 10	1 0 0 0 0	〃	C.	27.4ml/day
12		Blank	—	1 0 0 0 0	〃	C.	27.4ml/day

\* e. g. Fifty 80mmOD×23mmID×3mmT glass slices. ~5.000cm<sup>2</sup> total SA  
in 500cm<sup>3</sup> synthetic basalt ground water leachate=1000m<sup>-1</sup> SA/V

\*\* e. g. Five 80mmOD×23mmID×3mmT glass slices in 500cm<sup>3</sup> leachate

\*\*\* e. g. One 50mmφ×7mmT glass block in 500cm<sup>3</sup> leachate

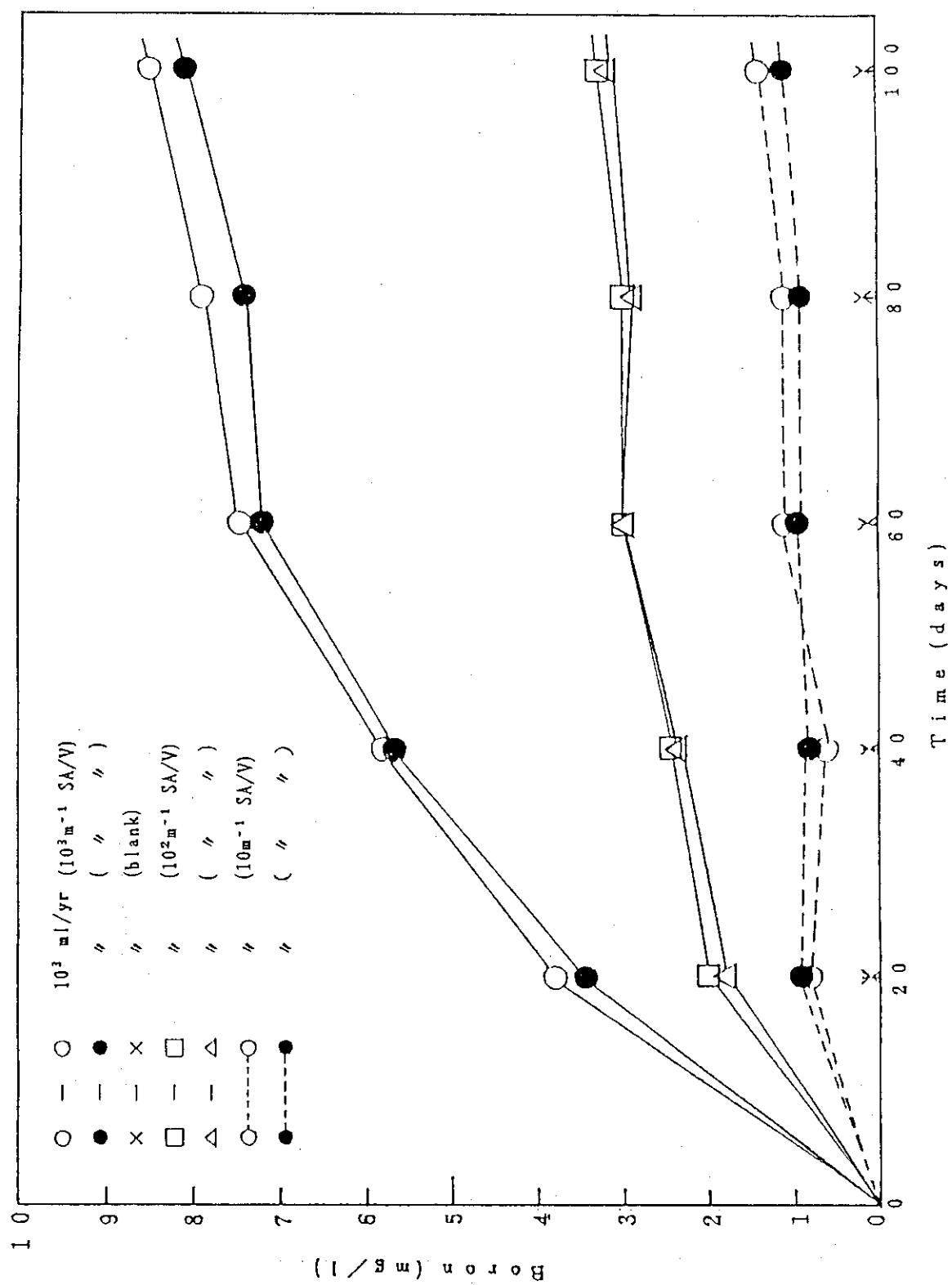


Fig. 1 Boron Concentration in the Sampled Solutions

### 3.3 In-cell Synroc solidification apparatus

S. Matsumoto

A program on Synroc development has been carried out as a future alternative of high-level radioactive waste solidification under co-operation with the Australian Nuclear Science & Technology Organisation (ANSTO). For the program a hot cell apparatus; In-cell Synroc Solidification Apparatus, was installed in the hot cell of WASTE-F to solidify actual waste and TRU element in Synroc. The apparatus consists of three parts; a pretreatment pot, a hot press and a system for off-gas treatment. Fig. 1 shows the flow sheet. The followings describe the details.

#### (1) Pretreatment pot

In the pot, slurry mixture of precursor and radioactive simulated wastes are adjusted in acidity finally to pH 9 by addition of aqueous ammonia, dried in flowing nitrogen atmosphere, then calcinated in reducing atmosphere by Ar-4%H<sub>2</sub> flowing, and then resulted in homogeneous calcine. (Fig. 2)

The pot of SUS 304L is attached with a heating furnace, a propeler, inlet/outlet of gas etc. and such attachments can be dismantled by cell crane and manipulator. The rotating propeler contacts lightly to the bottom of the pot with the self-weight. The rotating rate is controled continuously upto 200 rpm. temperature control in the pot is made by a temperature controller which is set in the operation area connecting a thermocouple in the rotating shaft. (Fig. 3)

Ar-H<sub>2</sub> gas flows through the bottom of the pot as cooling the rotating shaft and the pressure in the pot is kept at -30 ~ -100 mmH<sub>2</sub>O by a exhaust blower. The calcination temperature is 750 °C. The volume of pot is approximately 1000 ml (80 mm × 200 mmH) and the pot can produce 30 g of calcine a batch.

#### (2) Hot press

The calcine is mixed with titanium powder by a V-tyled mixer, and pressed and sintered at a high temperature to make to fine Synroc products. The heating unit with high frequency induction method can raise the temperature of the furnace to the operation temperature of 1200 °C in 30 minuts. The temperature is controled through a thermocouple which is set in a small hole near the specimen of graphite mold. The power to

the heater is supplied through a transistor AC to DC inverter which is set in the cell.

The hot press can press 20 mm specimen by  $300 \text{ kg/cm}^2$  using oil cylinder which is controled by an oil pump and a pressure control unit in the operation area. During operation nitrogen gas is purged through the bottom of specimen housing to keep reducing atomosphere and to prevent burning of graphite mold. (Fig. 4)

### (3) Off-gas treatment line

Vapour,  $\text{NO}_x$  and some volatilized radioactive substances are removed through a off-gas treatment unit which is attached to the pretreatment pot. The unit contains a condenser, two  $\text{NO}_x$  cleaners, a filter and an exhaust blower. The treated gas is wasted to the outlet of cell ventilation.

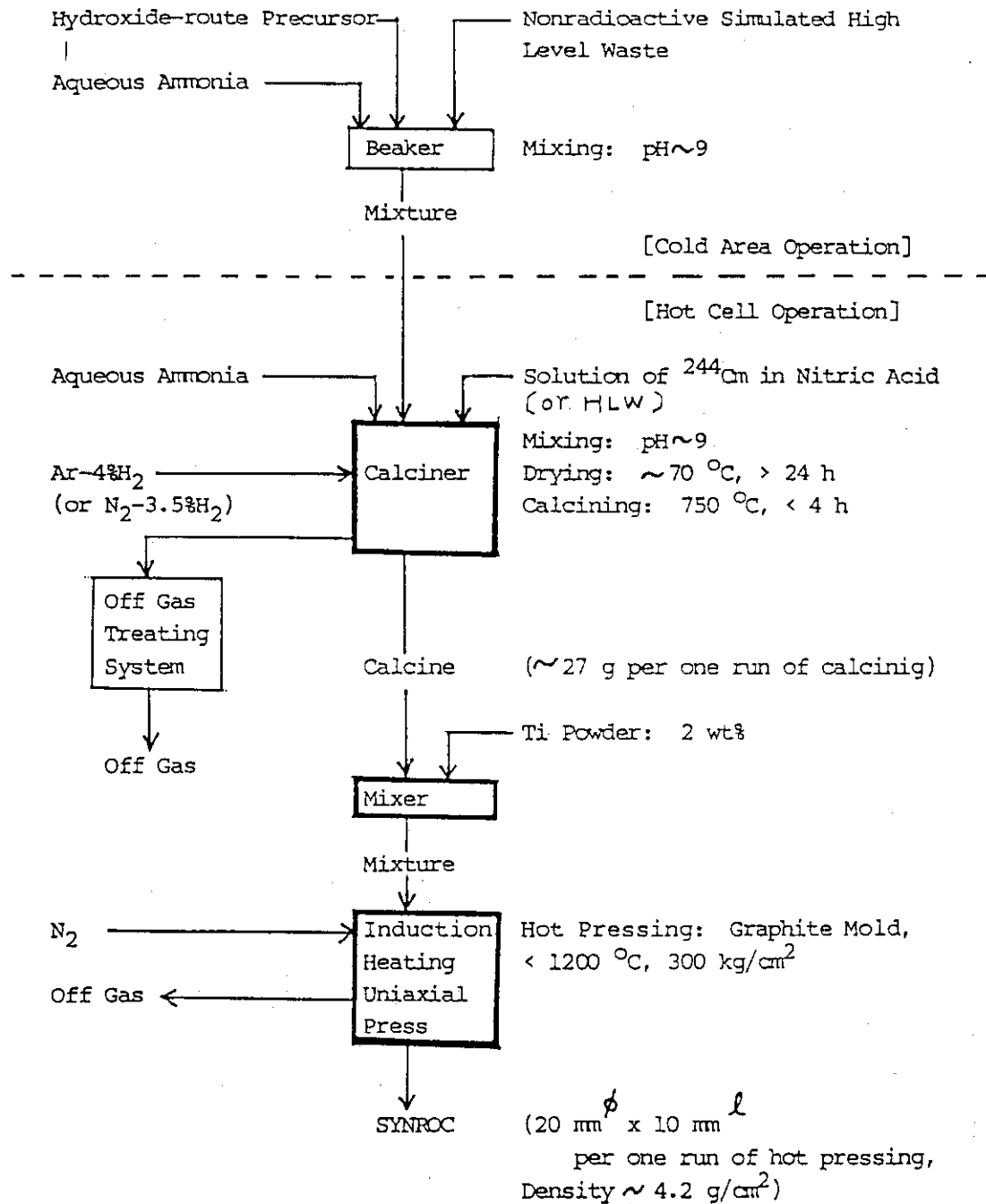
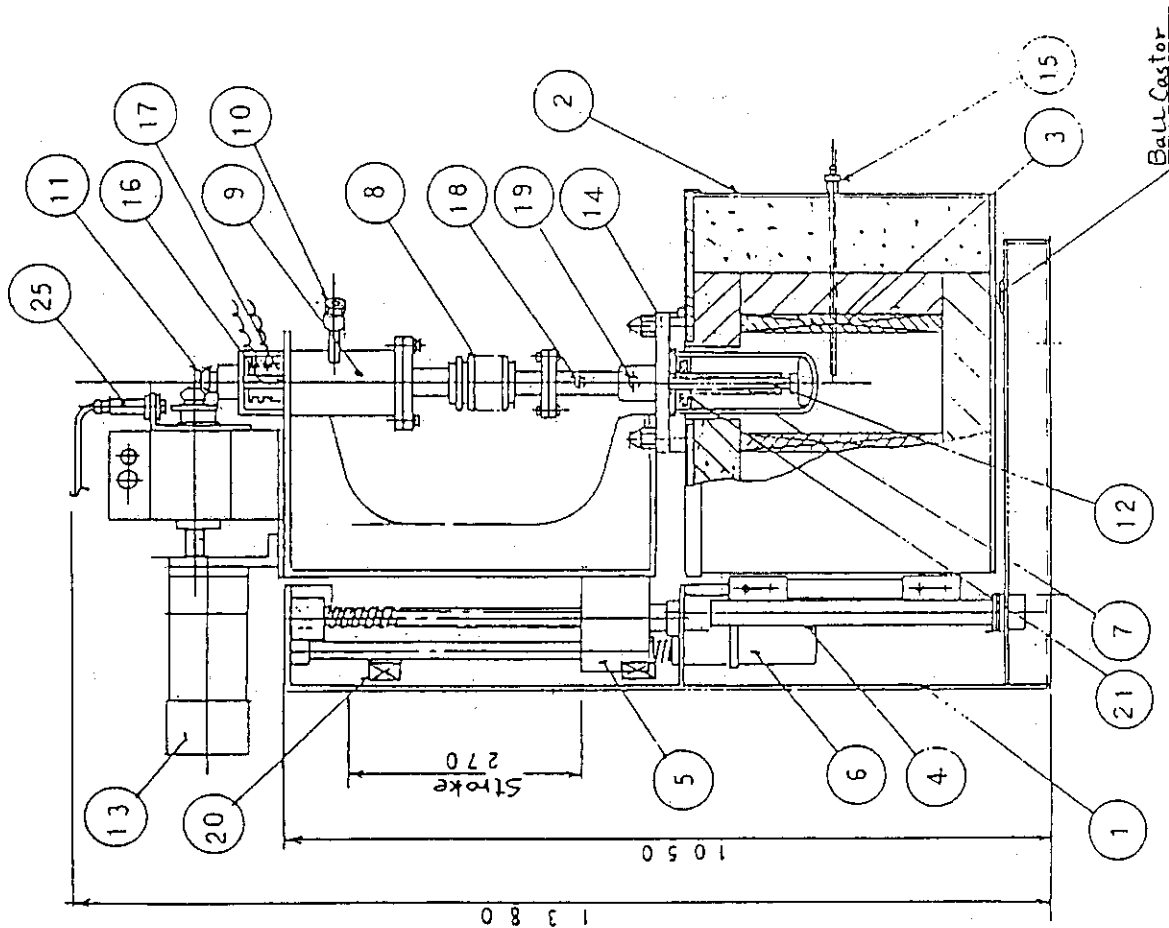


Fig. 1 Process Flow Diagram of Synroc Solidification at WASTE F



21	Buffer
20	Limit Switch
19	Nozzle for OFF-Gas
18	Nozzle for Ar-H <sub>2</sub> Gas
17	Slip-ring
16	Thermocouple
15	Thermocouple
14	Lid Flange
13	Motor for Mixer
12	Mixer
11	Driving Gear
10	Nozzle for Cooling Water
9	Mechanical Seal
8	Bellows
7	Pot for Drying and Calcining
6	Motor
5	Elevator
4	Pivot Shaft for Furnace
3	Heater
2	Casing of Furnace
1	Frame
No.	Name of Parts

Fig. 2 Calciner for Synroc Solidification



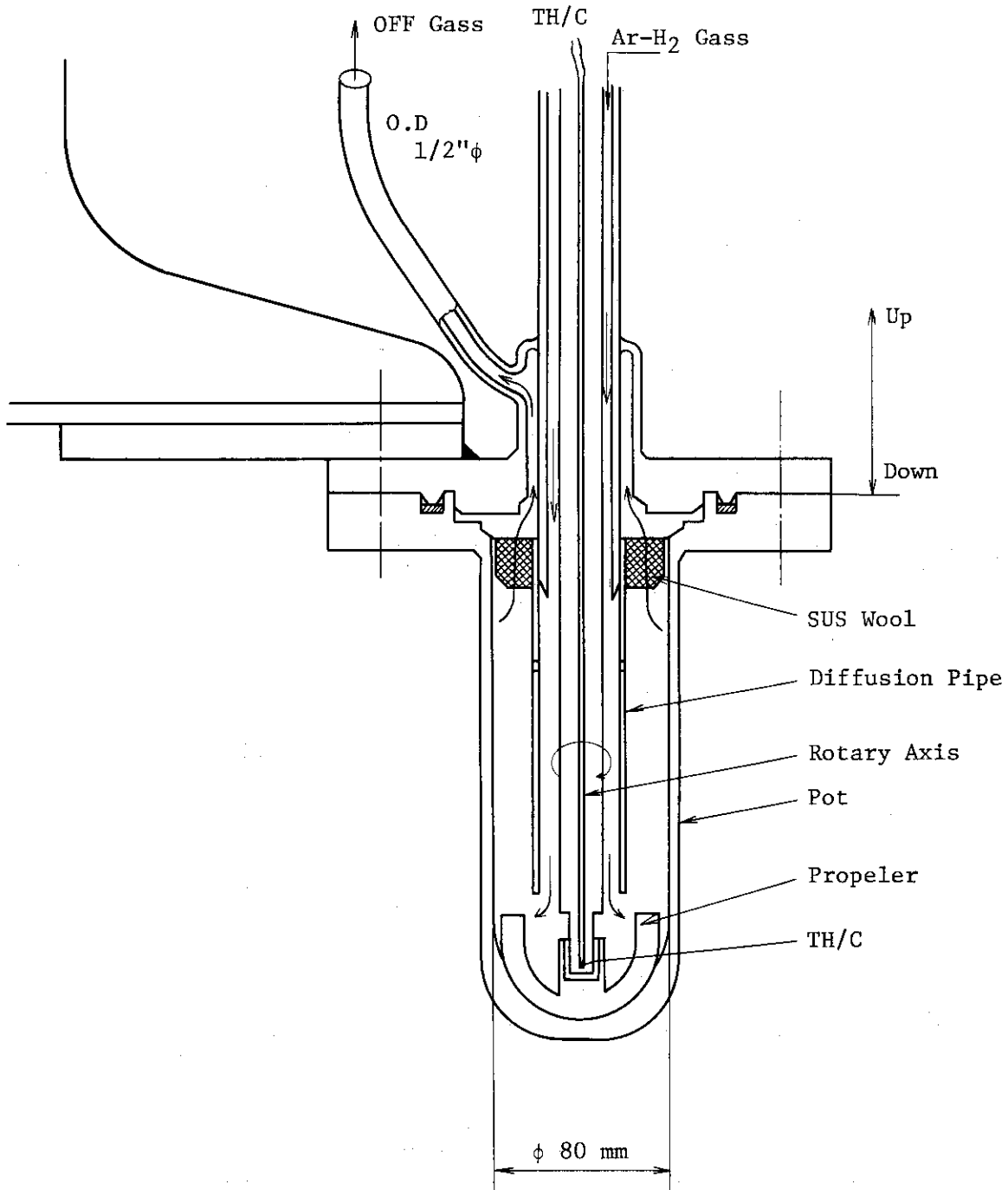
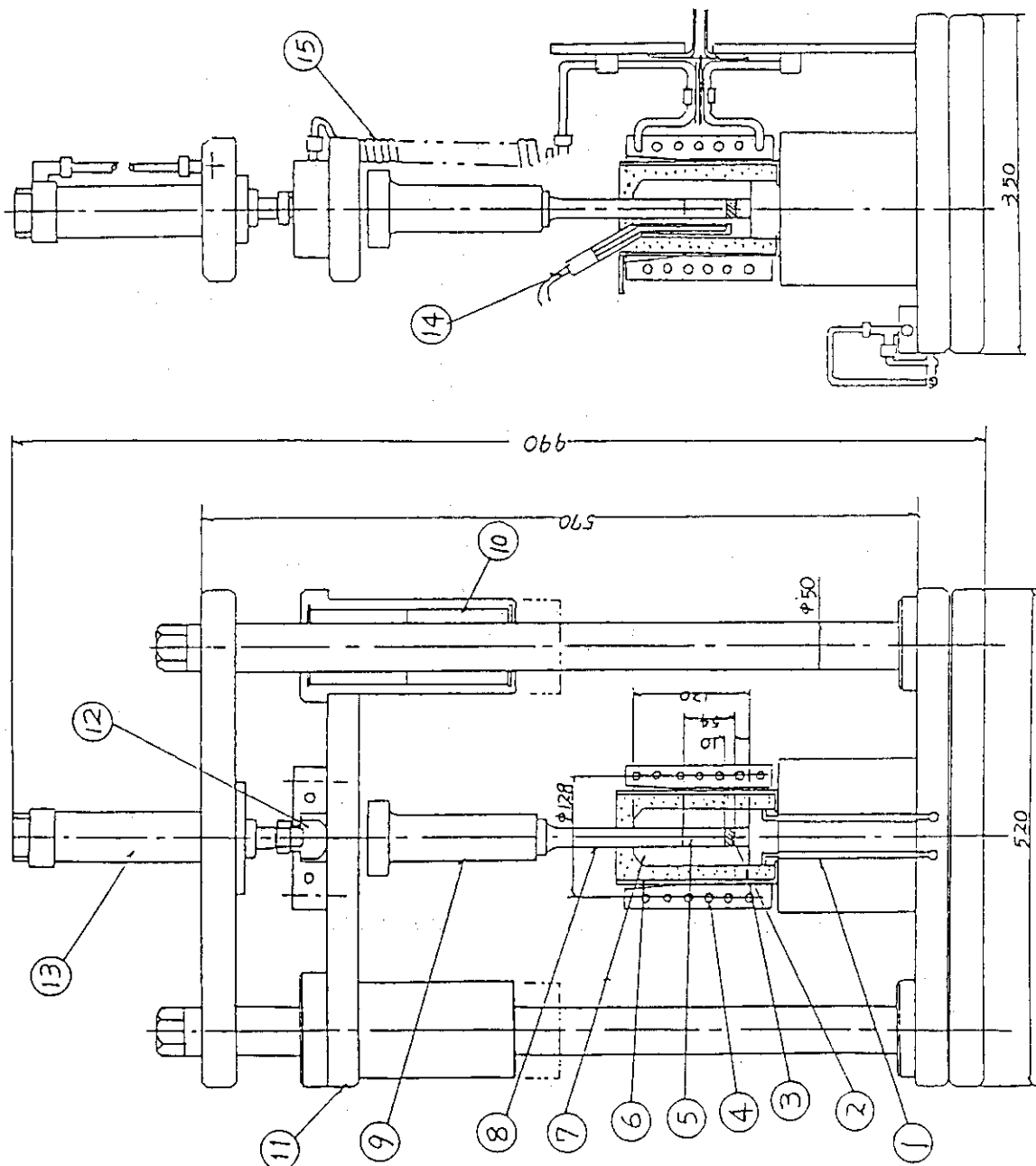


Fig. 3 Details of Pretreatment Pot



15	Curing Hose for Water
14	Thermocouple
13	Hydraulic Cylinder
12	Semiglobular Joint
11	Sliding Press-Plate
10	Ball Bushing
9	Alumina Rod
8	Graphite Rod
7	Graphite Mould
6	Quartz-Glass Container
5	SYNROC Sample Material
4	Induction-Heating Coil
3	Granulated Alumina Insulator
2	SYNROC Specimen
1	Feeding Hole for N <sub>2</sub> -Gas
No.	Name of Parts

Fig. 4 Hot Press

### 3.4 Contamination and decontamination behaviour of volatilized cesium from waste glass onto container materials

Y. Togashi

In a process of pouring molten glass containing high-level radioactive wastes into canisters, radioactive contamination might happen on the surface of canisters by volatile radioactive substances. Considering that the contamination could be a source term for accidental safety assessment of the storage facility, a demonstrative examination has been carried out to know the contamination and decontamination behaviour.

#### 1) Experimental

The apparatus for a sorption test of volatile radioactive substances is shown in Fig. 1. A glass product of simulated high-level radioactive waste containing about 1 mCi of  $^{137}\text{Cs}$  was molten in a crucible which was set in an electric furnace. Specimens were placed with a holder above a crucible. The surface of SUS 304L stainless steel which represents a canister material was exposed to the fume from the molten glass, then radioactivity on the surface of specimens was measured by a scintillation counter.

The contamination specimens were soaked for a given period in 10 % HCl solution and water at room temperature. Decontamination factor (DF) was calculated from the ratio of the activity of specimens before decontamination to that after it.

#### 2) Results and discussion

Fig. 2 shows the radioactivity of volatile radioactive substance on the surface of the specimen. The amount of volatile radioactive substances increases according to the exposure time. Fig. 3 shows results of decontamination tests using specimens which were exposed at 900 °C of fume temperature and for 60 minutes. DF was settled at the first one minute of soaking time, and was constant with respect to soaking time. HCl solution has an more ability on decontamination than water.

Fig. 4 shows results of decontamination tests using specimens which were exposed at 900 °C of temperature and for 4 hours. In this case, HCl solution and water have nearly the same ability on decontamination, and have smaller ability on decontamination in comparison with former results.

So far, the general situation of decontamination and decontamination tests has been outlined. Even if we use the same decontamination solution, DF differs depending on the contamination conditions of specimens. Especially, it is necessary to examine detailed decontamination tests.

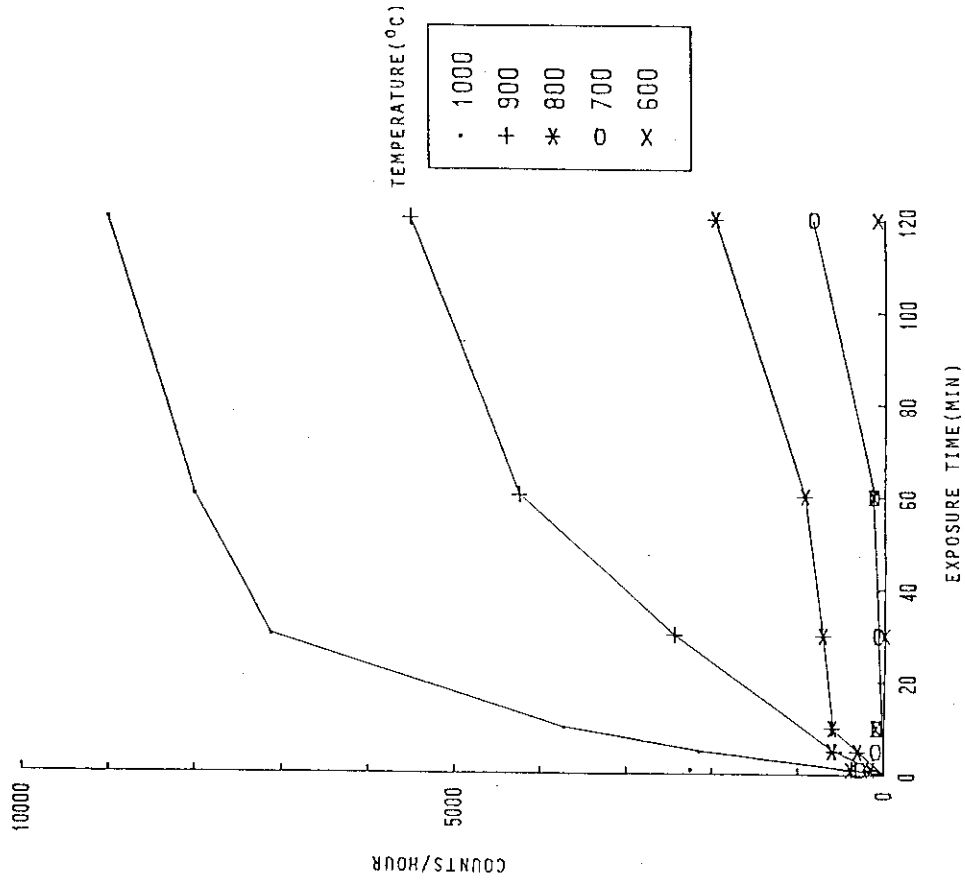


Fig.2 Increase with time of sorption of a volatilized radioactive substance ( $^{137}\text{Cs}$ ) on the surface of SUS 304L specimens.

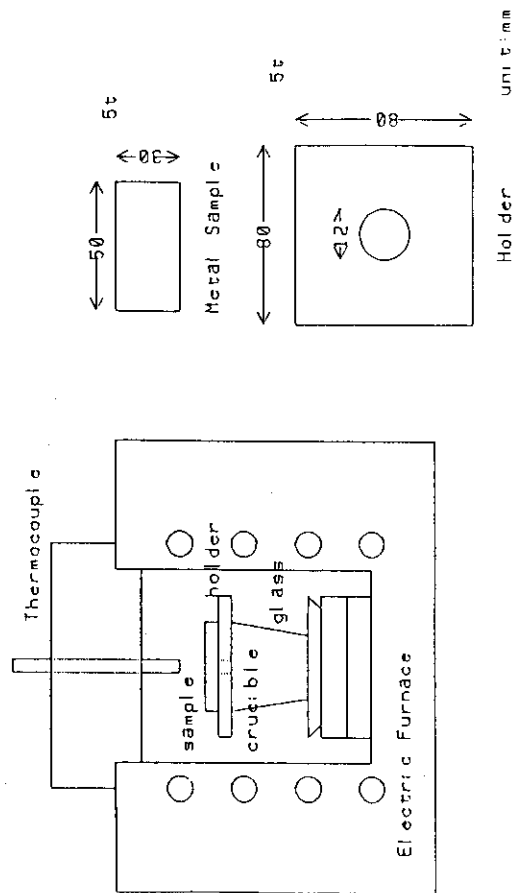


Fig.1 Apparatus for sorption tests of volatilized radioactive substances from waste glasses.

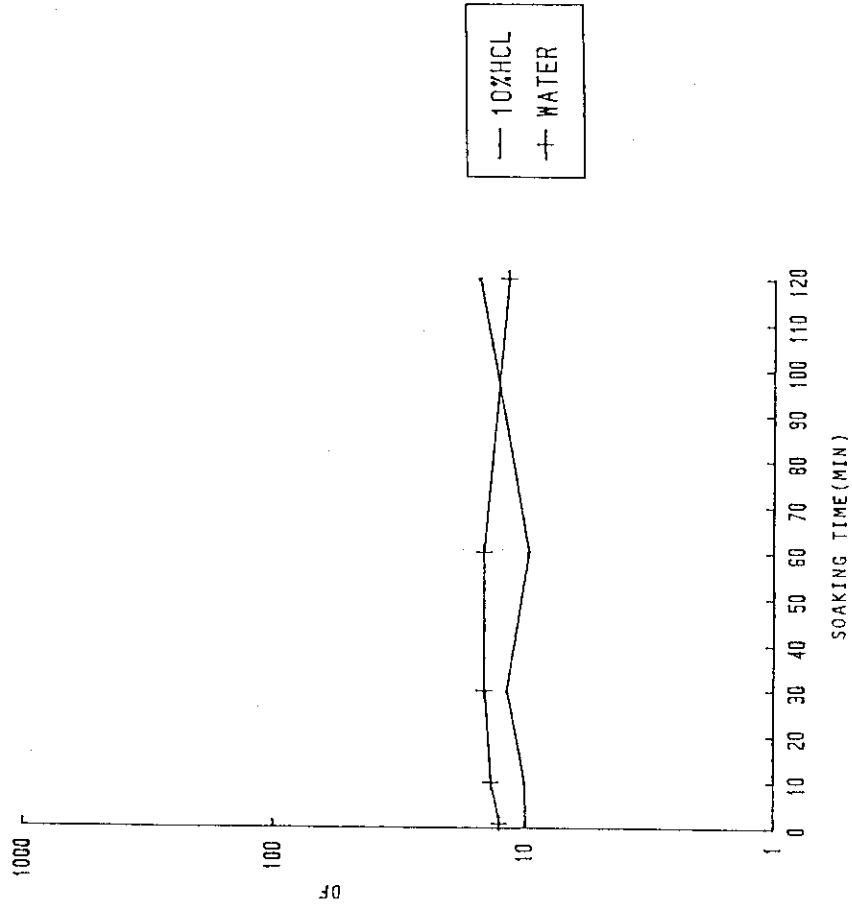


Fig.3 Decontamination effect of 10 % HCl solution and water for specimens which were exposed at 900 °C of fume temperature and for 60 minutes.

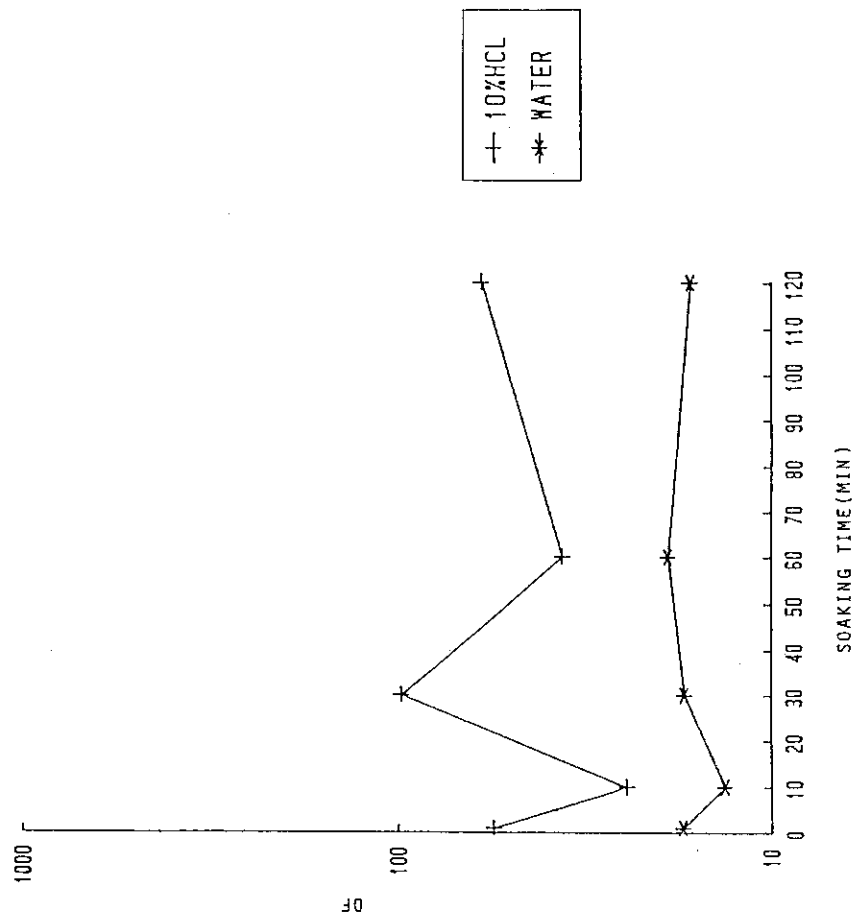


Fig.4 Decontamination effect of 10 % HCl solution and water for specimens which were exposed at 900 °C of fume temperature and for 4 hours.

### 3.5 Adsorption of plutonium and curium leached from waste glass on various materials for leach-container

T. Banba

The adsorption tendency of leached-out radionuclides on the surface of leach-containers, during the leaching experiment of high-level waste glasses, was studied. A flow sheet of experimental procedures is shown in Fig. 1. The test pieces of silica glass, PFA teflon, gold and stainless steel, which are candidates for a leach-container, were immersed in deionized water with the waste glass containing Pu-238 or Cm-244 in a Pyrex glass container at 100°C. Fig. 2 shows the results of the adsorption and desorption of plutonium and curium on the test pieces. The silica glass was found to have the smallest contamination of Pu-238 and Cm-244 and can be decontaminated with dilute nitric acid. Measurement of radioactivity and observation by alpha autoradiography were made on both contaminated and decontaminated test pieces. Adsorption and desorption of curium and plutonium were discussed in relation with difference of materials, time dependence and acidity of leachate. Curium, which has been previously leached out from waste glasses, showed a relatively simple adsorption and desorption behavior. In the case of plutonium, the colloidal species would take a large part in the adsorption and desorption processes. The relationship between the ratio of the colloidal to the ionic species of plutonium and the adsorption-desorption behavior was discussed. The observation of alpha autoradiographs elucidated that the ionic adsorption was desorbed more easily than the colloidal one.

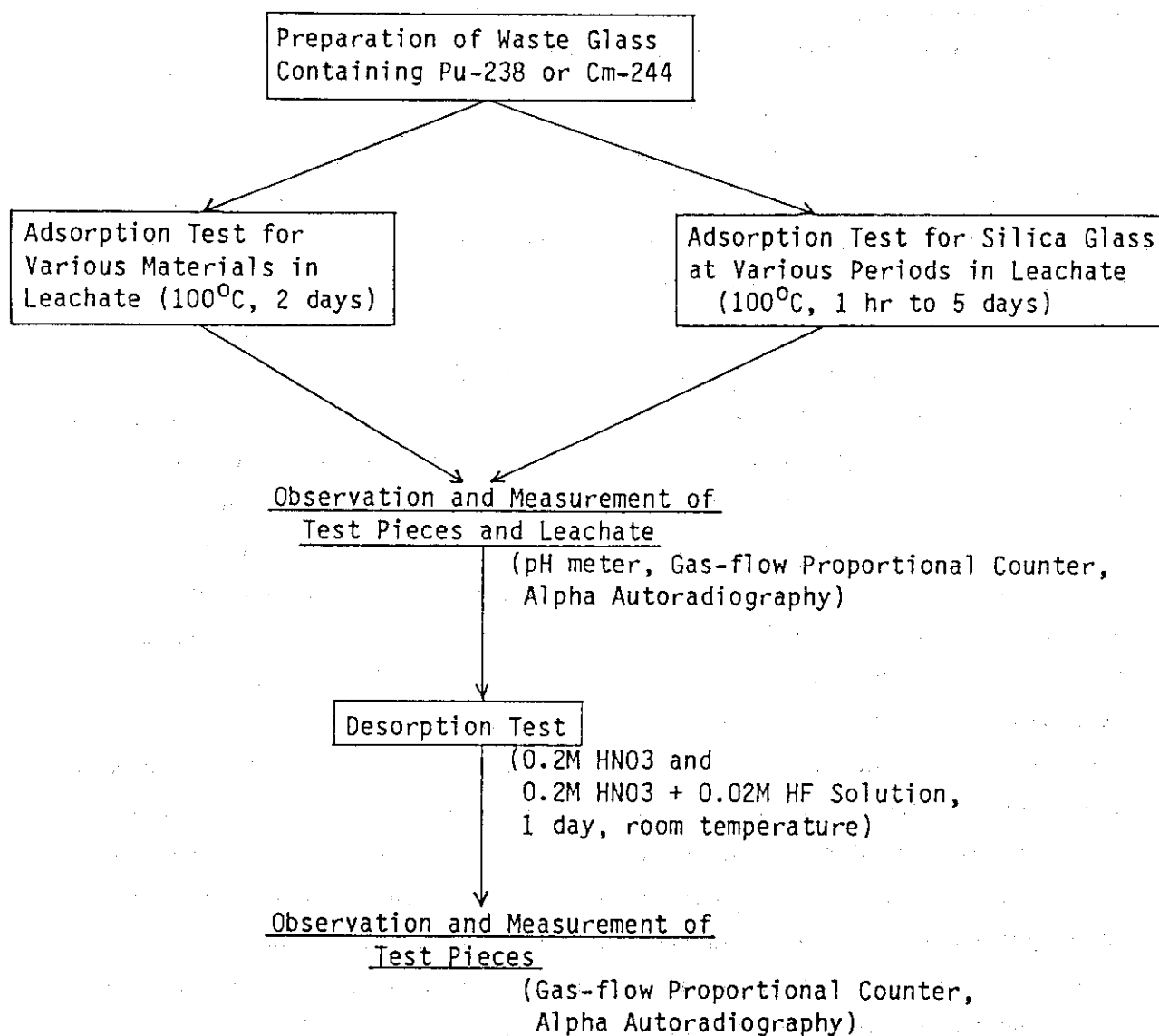


Fig. 1 Flow sheet for experimental procedure.



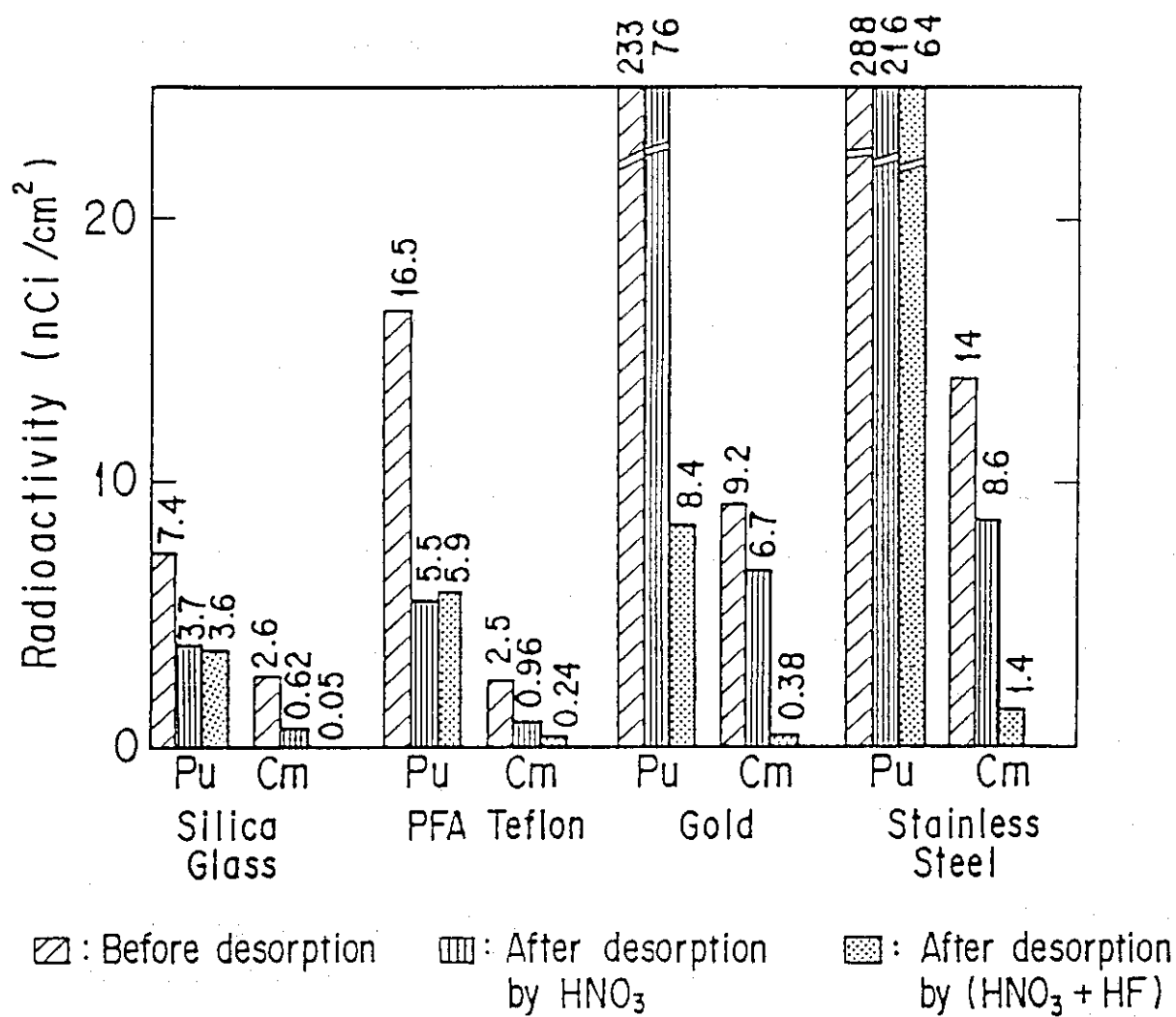


Fig. 2 Radioactivity of Pu-238 and Cm-244 adsorbed on various materials in leachates and remaining after the treatment of desorption.

## 3.6 Cs migration by column test

T. Iwai, S. Amagai and K. Shimooka

## [Introduction]

Multi-barrier system which consists of natural barriers and engineered barriers is expected to retard the migration of radionuclides leached out from the vitrified wastes.

In order to know the important retardation mechanism for the radionuclides in the rock formation, hot column tests has been carried out using the  $^{134}\text{Cs}$  solution prepared from a nuclear waste glass through columns of fresh and weathered granite samples.

A cold column test using non-radioactive nuclide ( $\text{Cs}^+$ ) and batch sorption tests were carried out as preliminary tests in order to compare the distribution coefficient ( $K_d$ ) determined with these two methods.

The hot column tests were then conducted and concentration profiles of  $^{134}\text{Cs}$  in the columns were measured. Retardation factors and distribution coefficients obtained by these tests were compared with those determined above.

## [Apparatus and experimental]

Column test apparatus is shown in Fig. 1. It consists of  $1.9\phi \times 47$  cm column, inlet valve for spike injection method, roller pumps and a fraction collector. The flow rate in the column is controlled and kept constant at a value from 0.16 to 1.6 ml/min by the roller pumps.

Experimental conditions in the preliminary tests and the hot column test are the followings.

## 1) Preliminary test

## i) Cold column test

Rock sample	: Inada fresh granite 3.5 - 4.0 mesh
Specific gravity of the granite	: 2.62
Porosity of the column	: 50.0 %
Density of the column	: $1.81 \text{ g/cm}^3$
Flow rate	: 0.17 ml/min (0.11 cm/min)
Concentration	: 10 ppm ( $\text{Cs}^+$ ), pH = 7.0

10  
 11  
 12  
 13

Concentration : 7.81 ppm ( $\text{Cs}^+$ )    pH = 7.0

Carrier solution was spiked with 1  $\mu$ l of  $^{137}\text{Cs}$  (2.8  $\mu\text{Ci}/\mu\text{l}$ ) and the

## Hot column test

Simulated nuclear waste glass: weight 161.7g,  $^{134}\text{Cs}$  0.137 mci/g

Leaching solution: ground water(sampled at Lake Kasumigaura)  
 volume 10.0 liter  $8.99 \times 10^{-7}$  mci/ml pH 5.6  
 before experiment  $1.01 \times 10^{-6}$  mci/ml pH 6.4 (Gf)  
     $1.27 \times 10^{-6}$  mci/ml pH 6.4 (Gw)

Rock sample: Inada fresh granite(Gf)

Inada weathered granite(Gw) mesh 3.5-4.0

Specific gravity : Gf 2.59 Gw 2.42

Porosity of the column : Gf 49.1%                      Gw 45.7%

Density of the column : Gf 1.81 g/cm<sup>3</sup> Gw 1.77 g/cm<sup>3</sup>

Effluent time : Gf 24.0 hour Gw 43.6 hour

Flow rate : Gf 0.17 ml/min Gw 0.17 ml/min

Velocity of solution : Gf 0.125 cm/min Gw 0.132 cm/min

Concentration of  $^{134}\text{Cs}$  in the column was measured by a NaI scintil-

## [Results and discussion]

The results of retardation factors(Rf) and distribution coefficients (Kd) obtained from each method are shown in Table 1.

Experimental breakthrough curve of the cold column test is shown in Fig. 3. A nuclide transport equation in one dimension considering advection and dispersion is adopted to simulate the  $\text{Cs}^+$  migration. By a curve fitting of the experimental results in Fig. 3, the following parameters were obtained.

$$\begin{aligned} D \text{ (hydrodynamic dispersion coefficient)} &= 3.056 \times 10^{-6} \text{ m}^2/\text{sec} \\ R_f \text{ (retardation factor)} &= 8.77 \\ K_d \text{ (distribution coefficient)} &= 4.33 \text{ ml/g} \end{aligned}$$

Distribution coefficient(Kd) derived from the cold column test was calculated from the nuclide retardation factor(Rf) by the following equation.

$$R_f = 1 + \rho \frac{1-\theta}{\theta} K_d \quad (1)$$

where  $\rho$  is the density of the rock and  $\theta$  is the porosity of the column.

Another way to determine Rf and Kd values is to use the ratio of the travel time of the nuclide(1050 min) to the travel time of water (250 min) for the Rf value (4.2). The Kd value can be then calculated by equation (1) to be 1.2 ml/g.

In the batch test, the study on distribution ratios (Rd) as a function of time might suggest the important role of the sorption kinetics. The relation between Rd and time for the fresh granite is shown in Fig. 4. Rd values then reached equilibria giving Kd values, for the fresh and weathered granite, of 25 ml/g and 219 ml/g (elapsed time 118 hours), respectively.

In the hot column test, radionuclide retardation can be evaluated by measuring activity profiles of the effluent solution and/or residual activity profiles in the column itself. In this paper the results on the activity profile of the latter are shown in Table 1 and Fig. 5, 6. In future the hot column test for the former will be reported.

The Rf and Kd values of Cs by this hot column test agree well with these determined by the travel times during the cold column test. This

fact indicates that the concentration profiles of the column can be also effective to estimate  $R_f$  and  $K_d$  values.

[Reference]

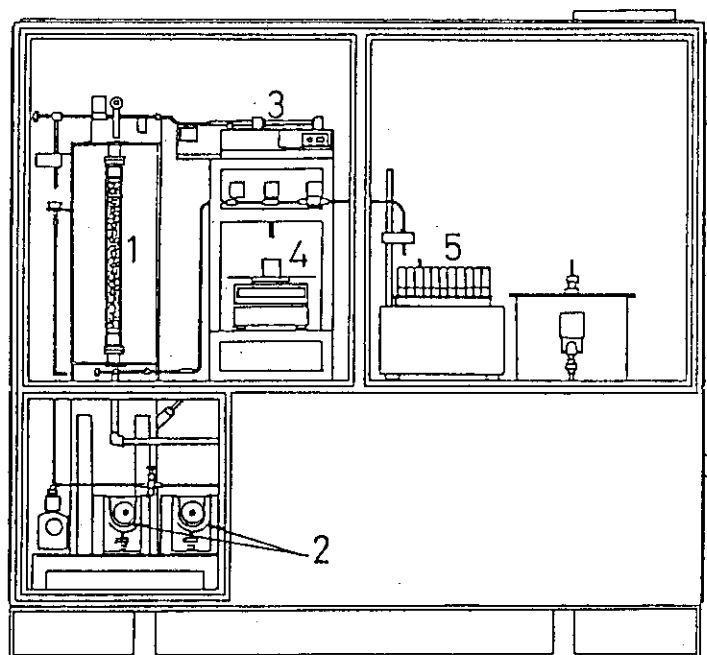
- 1) R.J. Serne, J.F. Relyea (1982), The Status of Radionuclide Sorption - Desorption Studies Performance by the WRIT Program, PNL Battelle Memorial Institute
- 2) OECD NEA (1983), SORPTION - Modelling and Measurement for Nuclear Waste Disposal Studies, summary of an NEA workshop held in Paris

Table 1 Retardation factor(Rf) and distribution coefficient(Kd) values obtained on granite samples by three different methods

Method	Rock sample	Kd(ml/g)	Rf
Batch	Gf	25.84	-
	Gw	219.02	-
Cold column	Gf <sup>1</sup>	2.99	8.77
	Gf <sup>2</sup>	1.20	4.20
Hot column	Gf	1.02	3.75
	Gw	4.46	13.80

1: determined by a curve fitting of the data in Fig.3 by a nuclide transport equation

2: determined by the data on travel times of Cs and water



1. column      2. roller pump      3. spike injection  
4. balance      5. fraction collector

Fig.1 Column test apparatus

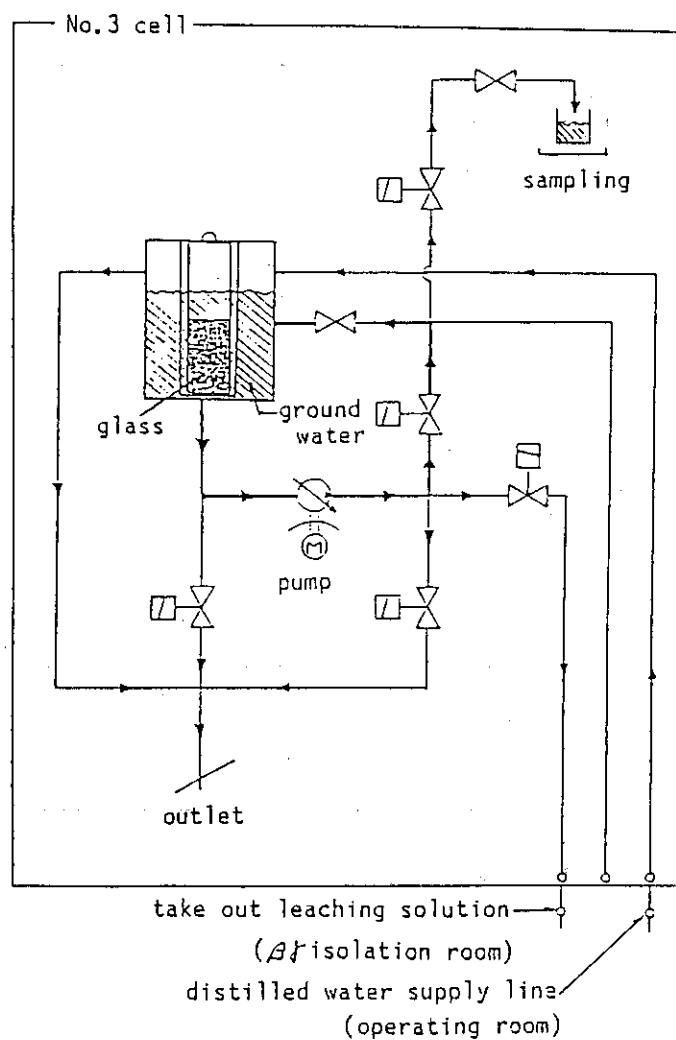


Fig.2 Leaching solution making apparatus

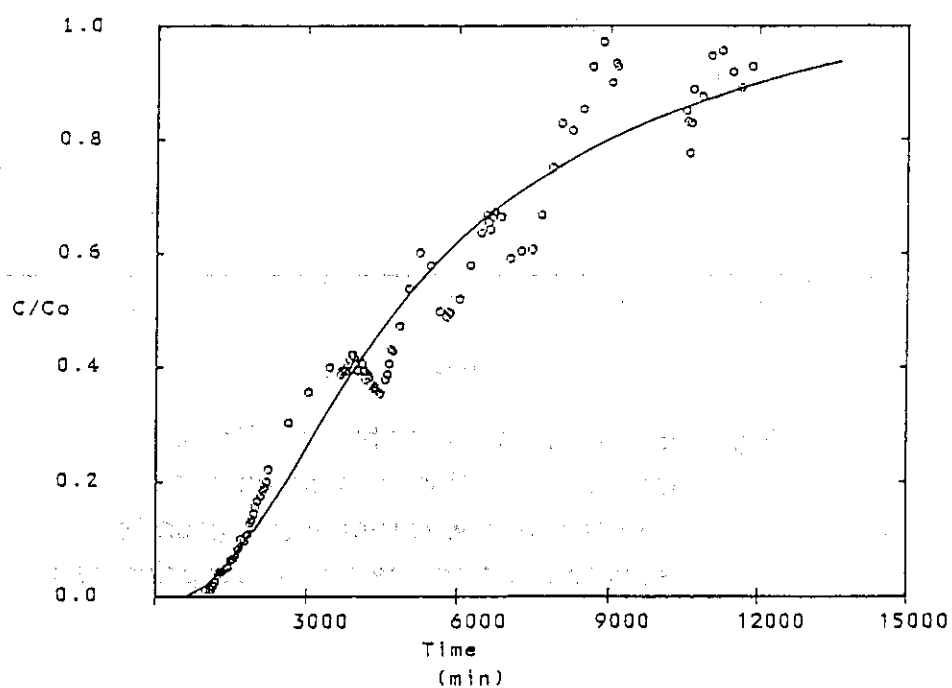


Fig.3 Experimental breakthrough curve for cesium

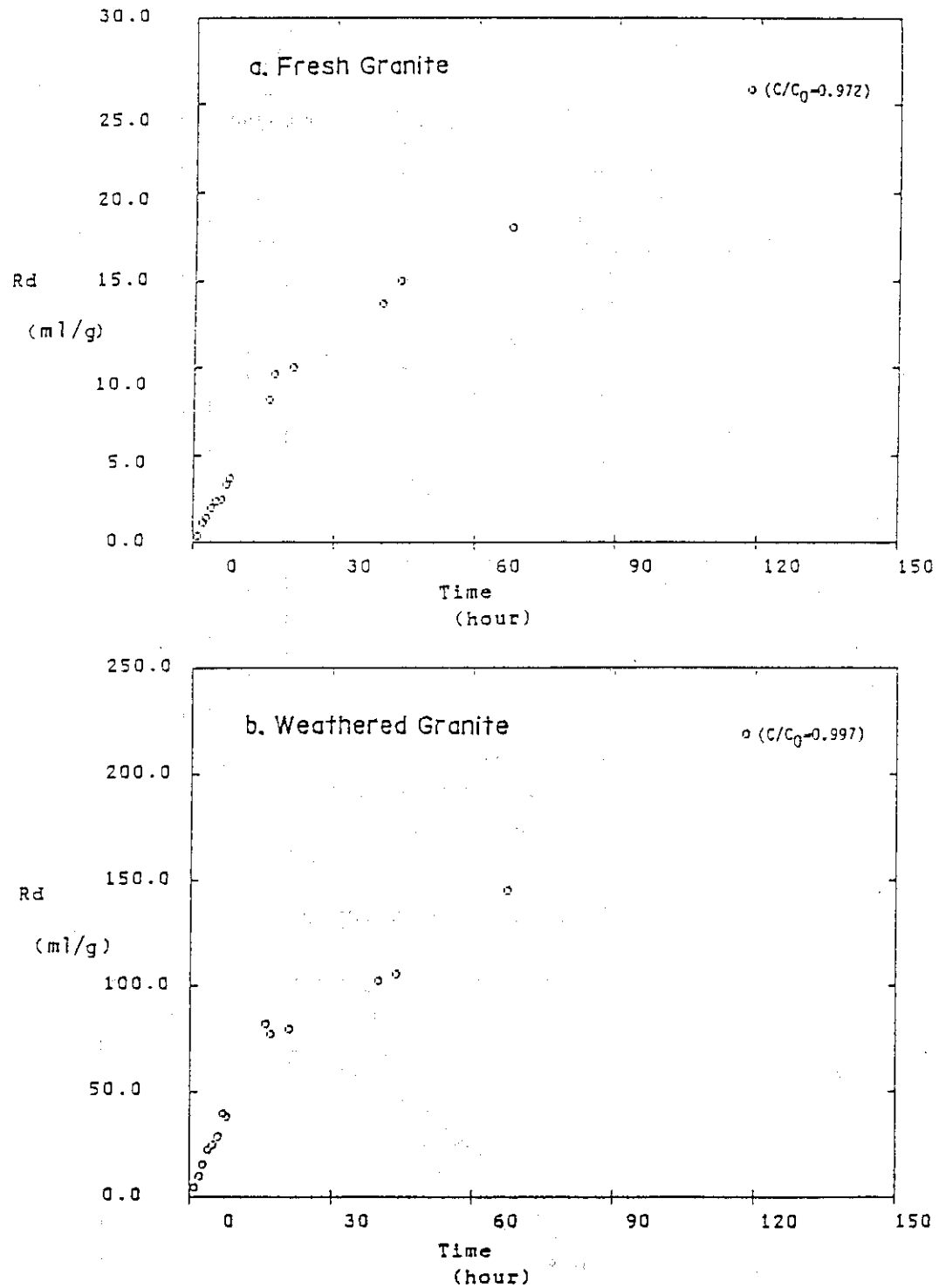


Fig.4 Evolution of distribution ( $R_d$ ) of Cs as a function of time, on the fresh(a) and weathered(b) granite samples during the batch sorption test



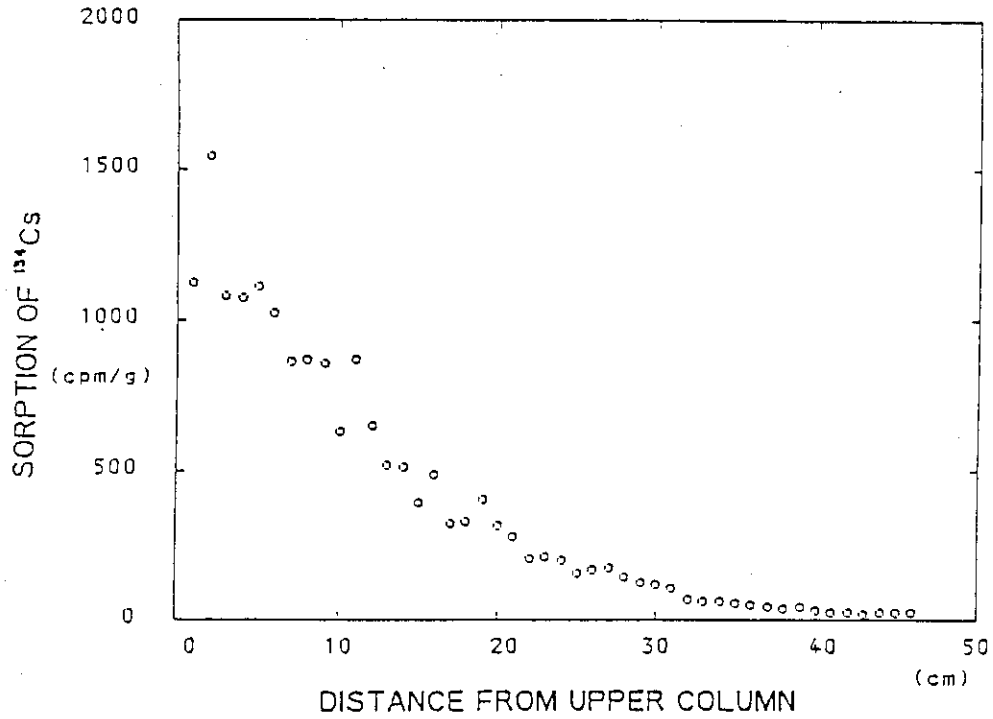


Fig.5 Sorption of Leached out  $^{134}\text{Cs}$   
from The Vitrified Wastes for Fresh Granite

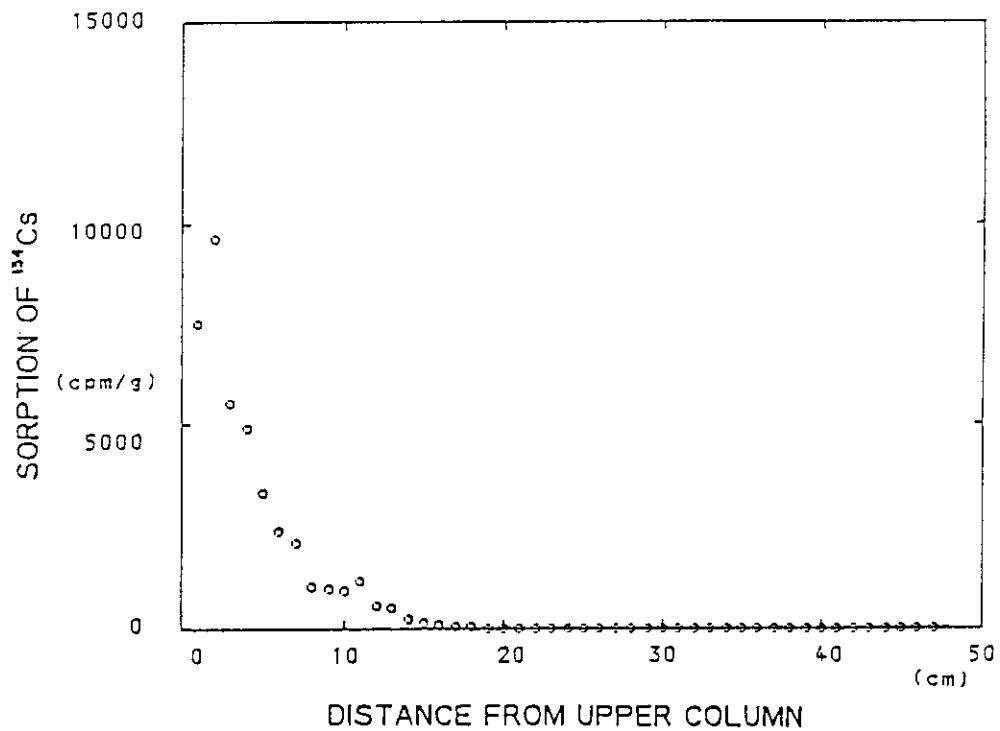


Fig.6 Sorption of Leached out  $^{134}\text{Cs}$   
from The Vitrified Wastes  
for Weathered Granite of Fracture Zone